Does pyroptotic cell death contribute to anthracycline-induced cardiotoxicity?

Thesis submitted by Dr Handi Yuwono Salim

MBChB MRCP (UK)

For the degree of Doctor of Philosophy

University College London, UK

The Hatter Cardiovascular Institute
Institute of Cardiovascular Science
University College London
67 Chenies Mews
London WC1E 6HX, United Kingdom

Declaration

I, Handi Yuwono Salim, confirm that the work presented in this thesis is my own. Where information has been derived from other sources, I confirm that this has been indicated in this thesis.

Abstract

Background:

Anthracyclines are widely used as effective chemotherapeutic agents. However, research has found that anthracycline-induced cardiotoxicity (AIC) causes significant morbidity and mortality. While the precise mechanism of AIC remains elusive, apoptosis has long been suspected as a key player. The precise mechanism of AIC remains elusive, although apoptosis has long been suspected as a key player. In recent studies, pyroptosis, a programmed lytic cell death pathway, was also found to contribute to AIC potentially. Most studies have focused on evaluating AIC in the myocardium, but emerging evidence suggests that AIC may also affect vascular cells. Furthermore, the relative toxicity of doxorubicin (DOX) or its supposed active metabolite, doxorubicinol (DOXOL), has not been widely investigated in cardiac vascular cells.

Purpose:

This thesis examines the hypothesis that pyroptosis plays a role in AIC. Specifically, this thesis investigates DOX and DOXOL cytotoxicity in H9c2 immortalised rat cardiac myoblasts, two types of human cardiac endothelial cells, a human breast cancer cell line MCF-7, and a human monocytic acute myeloid leukaemia cell line THP-1. Subsequently, this thesis evaluates the expression of a pore-forming protein Gasdermin D (GSDMD) and its N-Terminal domain (GSDMD NT), caspase 3 and its cleaved product as the key executioner of pyroptosis and apoptosis, respectively; this being investigated in the above cells treated with DOX and DOXOL.

Methods:

In vitro experiments were conducted to ascertain dose-dependent death response in H9c2, and cardiac endothelial cells following an 18-hour 0-10 μM DOX or DOXOL treatment.

Morphological changes were observed with Annexin V and Propidium Iodide (PI) following DOX or DOXOL treatment compared to known inducers of pyroptosis (LPS & Nigericin).

Western blot experiments were conducted to study the expression of full-length GSDMD, GSDMD-NT, caspase 3 and cleaved caspase 3, following DOX or DOXOL.

Results:

My data suggest that dose-dependent cell death following DOX treatment was greater compared to DOXOL in H9c2 and both cardiac endothelial cells. When treated with DOX, these three cell types underwent apoptotic changes (intracellular granulations, cell shrinkage and blebbing) with more severe effects at higher concentrations. In contrast, DOXOL caused milder effects, with these cells undergoing early apoptosis. Despite detecting of GSDMD and caspase 3 protein bands in the Western blot experiment with DOX or DOXOL, the respective cleaved proteins, GSDMD-NT or cleaved caspase 3 protein, were not detected.

In MCF-7 cells, DOX-induced apoptotic changes were observed in the absence of caspase 3, but no changes were observed following DOXOL treatment.

Interestingly, in THP-1 cells, DOX exerted predominantly apoptotic cell death, whereas DOXOL predominantly exerted pyroptotic cell death (nuclei and membrane swelling, membrane rupture). This was accompanied by the detection of full-length caspase 3 and GSDMD with its cleaved proteins in DOX and DOXOL, respectively.

Conclusion:

My data show that DOX and DOXOL primarily induce apoptotic cell death in H9c2 cardiomyocytes and cardiac endothelial cells. In MCF-7 cells, DOX induced apoptotic changes. Interestingly, THP-1 cells can be driven towards apoptotic or pyroptotic cell death induced by DOX or DOXOL, respectively.

These findings suggest that pyroptosis is not likely to play a major role in anthracycline-induced cytotoxicity. Instead, anthracycline-induced cytotoxicity is likely to be due to apoptotic injury.

Impact statement

The clinical success of anthracyclines in cancer treatment comes at a significant cost: irreversible cardiotoxicity. While the precise mechanisms remain elusive, apoptosis has long been suspected as a key player in anthracycline-induced cytotoxicity. However, recent research suggests pyroptosis might also contribute to anthracycline-induced cytotoxicity.

The research in this PhD thesis seeks to investigate whether pyroptosis plays a role in anthracycline-induced cardiotoxicity. This thesis provides an insight into cytotoxicity caused by doxorubicin and its supposed active metabolite, doxorubicinol. As will be discussed in the relevant chapter, only a limited number of studies investigated doxorubicin and its metabolites.

Furthermore, studies have hypothesised whether apoptosis or pyroptosis drives anthracycline-induced cardiotoxicity. However, these studies tend to investigate apoptosis and pyroptosis in isolation. This thesis assessed apoptosis and pyroptosis together and therefore contributes to further our knowledge of the mechanism of action related to anthracycline-induced cytotoxicity.

Part of my research has been presented as a poster presentation at a national cardiovascular conference. I hope to publish my research in peer-reviewed cardiovascular journals to disseminate my research findings in the future.

Acknowledgement

Undertaking this PhD has been a life-changing journey full of intellectual curiosity, patience, and perseverance. Throughout this journey, I have met many people to whom I would like to express my eternal gratitude for their encouragement, friendship, and support.

I would like to express my deepest gratitude to my supervisors, Professor Derek Yellon and Professor Sean Davidson. Professor Derek Yellon has been a father figure to me at the Hatter Cardiovascular Institute. He believes that I have the potential to succeed and deliver my PhD at times when I doubted myself. I thoroughly enjoy listening to his wisdom and sharing ideas with him. Professor Davidson has been instrumental throughout my journey for his guidance and encouragement in my research. I am grateful for the fruitful discussions, review of works and invaluable feedback on my thesis. I am also grateful to HCA Healthcare UK, for entrusting me with the Hatter-Wellington scholarship, taking me under the tutelage and giving me an incredible opportunity to pursue my PhD at UCL.

I would like to extend my gratitude to Dr Lim Ven Gee, my friend and former Hatter PhD fellow, who introduced me to Professor Yellon and the Hatter family. I am also grateful to Mrs Jill Jarvis and Mrs Sara Giesz, the secretaries of Prof Yellon, whose housekeeping ensures that I am not running out of lab consumables and I can keep abreast with current research by attending meetings, seminars and conferences. Thank you to Dr Robert Bell for his constructive feedback during my PhD upgrade viva, and Dr Petros Syrris for his support as my Postgraduate Research Tutor.

I would like to express my gratitude to the past and present research team at the Hatter Cardiovascular Institute. Dr Miroslava Katsur has played a major role in patiently teaching me the laboratory techniques necessary for my research, along with Dr Sapna Arjun, and Dr Pelin Golforoush. Thank you to my fellow Hatter-Wellington scholarship awardees Dr Ali Rauf, Dr Osman Najam, and Dr Hibba Kurdi for their company and support. Thank you to my laboratory colleagues, Dr David He, Dr Siavash Beikoghli, Dr Lucie Pearce, Dr David Matthews, Dr Ahmed Chilmeran, and Elias for their support. Special thanks to my fellow doxorubicin researcher, Dr Alex Byrne. I believe that all the discussions we had have been invaluable to our research.

I would like to further express my heartfelt gratitude to Alhanoof, Liyana, and Lea, whose company and support led to endless laughter in the lab and long-lasting friendships.

My heartfelt appreciation goes to my close friends, Andrew, Ibnu, Destry, Shendy, Sarah, and Tom. Thank you for your never-ending support and encouragement.

Very importantly, special thanks must go to my parents (Darmajuwan Halim and Linawaty Tjhang), my parents-in-law (Sofyan Tan and Elinar), brothers and sisters for their faith in me. Their support has been invaluable to keep me going.

Any words of gratitude cannot fully express how I appreciate my wife, Tracey. I have been privileged to witness her accomplishment in pursuing her PhD. I am lucky for her to be by my side in every step of my journey. I have been forewarned that PhD journey can be arduous and of solitude. Despite the ups and downs I have encountered, never have I felt alone because of her. Tracey, thank you for your sacrifice, endless support, and warm embrace so that I never feel lonely and discouraged in this journey. This thesis is my humble appreciation to you.

This has been a chapter of my life that I will cherish forever!

Publication

National poster presentation and abstract journal publication

Salim H, Davidson SM, Yellon DM. BS82 Pyroptosis may not contribute to anthracycline doxorubicin and its metabolite doxorubicinol cytotoxicity in coronary artery endothelial cells. *Heart* 2023;109**:**A306.

Presented at the British Cardiovascular Society conference, 5th-7th June 2023, Manchester, UK.

Table of Contents

Figures

Tables

Abbreviations

ACEi	Angiotensin-Converting Enzyme inhibitors
AIC	Anthracycline-Induced Cardiotoxicity
AKT	Aldo-Keto Reductase
ANOVA	Analysis of Variance
APAF1	Apoptotic Protease-Activating Factor 1
ARB	Angiotensin Receptor Blockers
ASC	Apoptosis-associated Speck-like protein containing CARD
ATP	Adenosine TriPhosphate
ATTC	The American Type Culture Collection
BCA	Bicinchoninic Assay
BID	BH3 Interacting domain Death agonist
BH	Bcl-2 Homology
BME	Beta-Mercaptoethanol
BNP	B-type Natriuretic Peptide
BSA	Bovine Serum Albumin
CAR	Chimeric Antigen Receptor
CARD	Caspase Recruitment Domain
CARP	Cardiac Ankyrin Repeat Protein
CCSS	Childhood Cancer Survivor Study
DAMP	Danger-Associated Molecular Patterns
DIC	Doxorubicin-Induced Cardiotoxicity
DISC	Death Inducing Signalling Complex
DNA	Deoxynucleic Acid
DOX	Doxorubicin
DOXOL	Doxorubicinol
EDTA	Ethylenediaminetetraacetic Acid
FADD	Fas-associated Death Domain

FBS	Fetal Bovine Serum
FITC	Fluorescein Isothiocyanate
GSDMB	Gasdermin B
GSDMD	Gasdermin D
GSDMD-NT	N-Terminal of Gasdermin D
GSDME	Gasdermin E
GZMA	Granzyme A
GZMB	Granzyme B
HCAEC	Human Coronary Artery Endothelial Cells
HCMEC	Human Cardiac Microvascular Endothelial Cells
HER2	Human Epidermal growth factor Receptor 2
HO	Heme Oxygenase
hPSC-CM	Human Pluripotent Stem Cell-derived Cardiomyocyte
HR	Hazard Ratio
ICE	Interleukin-1β Converting Enzyme
INT	Tetrazolium salt
LAD	Left Anterior Descending artery
LDH	Lactate Dehydrogenase
LPS	Lipopolysaccharides
LV	Left Ventricle
LVEF	Left Ventricular Ejection Fraction
mRNA	Messenger RNA
miRNA	Micro RNA
mPTP	Mitochondrial Permeability Transition Pore
NAD(P)H	Nicotinamide Adenine Dinucleotide Phosphate Hydrogen
NETs	Neutrophil Extracellular Traps
NF-AT	Nuclear Factor of Activated T cells
NF-κB	Nuclear Factor Kappa B
NLRP	Nod-Like Receptor Protein

NO	Nitric Oxide
NOS	Nitric Oxide Synthase
PAMP	Pathogen-Associated Molecular Patterns
PARP	Poly-ADP Ribose Polymerase
PBS	Phosphate Buffer Saline
PCR	Polymerase Chain Reaction
PI	Propidium Iodide
PVDF	Polyvinylidene Difluoride
qRT-PCR	Quantitative Reverse Transcription PCR
RIPA	Radioimmunoprecipitation Assay
RNA	Ribo Nucleic Acid
ROS	Reactive Oxygen Species
SDS	Sodium Dodecyl Sulphate
SEM	Standard Errors of the Mean
SLE	Systemic Lupus Erythematosus
tBID	The caspase 8-activated BID
TBS	Tris Buffered Saline
TBST	Tween in Tris Buffered Saline
TINCR	Terminal Differentiation-Induced Non-Coding RNA
TKIs	Tyrosine Kinase Inhibitors
TLRs	Toll-Like Receptors
TME	Tumour Microenvironment
TNF-α	Tumour Necrosis Factor Alpha
TOP2	Topoisomerase 2
UK	United Kingdom
WHO	World Health Organization
XIAP	X-linked Inhibitor of Apoptosis Protein
ΔΨ	Trans-membrane potential

Chapter 1 Introduction

1.1 The burden of cancer

Cancer and cardiovascular disease, principally ischaemic heart disease and stroke, rank within the top 10 leading causes of death globally and in the United Kingdom (Vos *et al.*, 2020, Roth *et al.*, 2020).

There were an estimated 18.1 million new cancer cases worldwide, and about 10 million cancer deaths occurred in 2020 (Sung *et al.*, 2021). Furthermore, cancer incidence globally is projected to rise by 55% in 2040. The increasing impact of cancer on healthcare worldwide is also felt economically. The total cost of cancer in Europe, including the United Kingdom (UK), was €199 billion in 2018 (Hofmarcher *et al.*, 2020). This economic cost is projected to rise globally to $25.2 trillion in international dollars from 2020 to 2050 (Chen *et al.*, 2023).

In the UK, Cancer Research UK reported that there were 375,000 new cancer cases in the UK between 2016 to 2018. Breast, prostate, lung, and bowel cancer comprised over half of the new cases. In addition, there were 167,000 deaths from cancer reported in the UK between 2017 to 2019. This was equivalent to 460 cancer deaths every day. Almost half of all cancer deaths were from lung, bowel, prostate, and breast cancer. The total cost of cancer in the UK was reported to be €23 million in 2018 (Hofmarcher *et al.*, 2020). These statistics suggest that the burden of cancer is high in the UK.

1.2 Today's cancer survivors are tomorrow's cardiac patients

Despite the increasing cancer burden, cancer survival is improving with remarkable advances in cancer research, screening, diagnosis and treatment. As a result, the mortality rates for all cancers combined have decreased by 10% over the last decade in the UK. In England and Wales, half of the patients with cancer survive for ten years or more.

Chemotherapy, radiotherapy, and surgery comprise the core management in cancer patients. In the UK, between 2013-2014, chemotherapy was used in 28% of the management of all cancers (National Cancer Registration & Analysis Service and

Cancer Research UK, 2017). This number includes those who had chemotherapy alone or in combination with other forms of management.

Despite improved outcomes and survival from cancer, many patients paradoxically are exposed to cancer therapy's potential acute and chronic side effects. These sequelae may profoundly affect the quality of life and, eventually, the life expectancy of cancer survivors. Cardiovascular disease, or cardiotoxicity, is considered one of the severe side effects attributable to cancer treatments. Such cardiotoxicity could occur acutely or as late-onset, decades from the initial course of the treatment. It may manifest as hypertension, left ventricular systolic dysfunction, cardiomyopathy, arrhythmias, and coronary and valvular heart disease.

A retrospective population-control study conducted by Paterson *et al* in Alberta, Canada, found that their 224,000 participants with new diagnoses of cancers had hazard ratios (HRs) of 1.33 for cardiovascular mortality and HRs of 1.62 for heart failure, compared to participants without cancer during a median follow up period of 11.8 years (Paterson *et al.*, 2022). They further observed that cardiovascular risk was the highest in the genitourinary, gastrointestinal, thoracic, nervous system and haematologic malignancies. The risk of cardiotoxicity manifesting long after the cessation of cancer treatment was also evident in the Childhood Cancer Survivor Study (CCSS). The CCSS found that cardiac deaths accounted for 7% of deaths twenty five years after the first cancer diagnosis (Mertens *et al.*, 2008).

In view of such evidence, preventing today’s cancer survivors from becoming tomorrow’s cardiac patients has become the vision across the relevant multi-disciplinary professional communities from basic science and translational to clinical research. The collaborative drive to elucidate further knowledge and understanding of cardiotoxicity is underlined in the recent guidelines and position statements from professional bodies such as the European Society of Cardiology (Lyon *et al.*, 2020).

1.3 General introduction to common chemotherapy agents

The pharmacological innovation in cancer therapy results in an array of chemotherapeutic agents. Chemotherapeutic agents can be administered as a monotherapy. Alternatively, it is common to combine multiple chemotherapy agents into a regimen to achieve the intended anti-neoplastic effect and minimise the side

effects of each chemotherapy agent. This section will give a brief overview of the common chemotherapy agents used in the clinical setting.

1.3.1 Alkylating agents

Alkylating agents, such as cyclophosphamide, are nitrogen mustard derivatives that are used to treat various cancers, such as breast, lung, myeloma, and ovarian cancer. In addition, cyclophosphamide is used in transplant medicine as an immunosuppressant to prevent graft rejection.

Cyclophosphamide, an alkylating oxaphosphorine, requires hepatic bioactivation via the cytochrome P450 enzyme system to exert its cytotoxic effects. This metabolic process yields phosphoramide mustard, the active cytotoxic metabolite. Importantly, elevated intracellular concentrations of phosphoramide mustard are implicated in the development of oxaphosphorine-induced cardiocytotoxicity, increasing the production of free reactive oxygen species (ROS) (Ahlmann *et al.*, 2016).

Cyclophosphamide can induce cardiotoxicity in the form of arrhythmias and cardiomyopathy (Eisenhauer *et al.*, 1998). Recent research reveals that cyclophosphamide also induces vascular sclerosis and pulmonary hypertension (Soultati *et al.*, 2012).

1.3.2 Antimetabolites

Antimetabolites represent a diverse class of chemotherapeutic agents encompassing five primary categories: folate antagonists, pyrimidine antagonists, purine antagonists, sugar-modified analogues, and ribonucleotide reductase inhibitors. Each category disrupts essential metabolic pathways for DNA synthesis within proliferating cancer cells. Among these, pyrimidine antagonists, exemplified by 5-fluorouracil, are of particular interest in the context of drug-induced cardiotoxicity.

5-Fluorouracil exerts its anti-proliferative effect by inhibiting the synthesis of thymidine nucleotides through the disruption of thymidylate synthase activity. 5-Fluorouracil is metabolized to fluorodeoxyuridine monophosphate, a structural analogue of thymidine nucleotides. The catalyst thymidylate synthase is trapped by

the pseudosubstrate fluorodeoxyuridine monophosphate molecule at an intermediate step, blocking all DNA synthesis and thereby replication (Ivanetich *et al.*, 1988).

5-Fluorouracil is clinically used to treat solid malignancy, such as breast and colorectal cancer. 5-Fluorouracil can be administered via direct infusion or in the form of capecitabine, an orally bioavailable prodrug. Capecitabine undergoes enzymatic conversion within the body, releasing 5-Fluorouracil selectively to the tumour. However, both treatment modalities are associated with a risk of cardiotoxicity. The cardiotoxicity can manifest as arrhythmias, congestive cardiac failure, and myocardial ischaemia. In addition, vascular endothelial side effects have been reported in the form of angina, coronary artery spasm, and hypertension (Shiga *et al.*, 2020).

1.3.3 Taxoids

Taxoid-based chemotherapeutic agents, such as paclitaxel, work by interfering with the mitotic process in the cell. Taxoids-based agent exert their antitumor effects through a multifaceted mechanism. Primarily, they disrupt the mitotic spindle apparatus by promoting the stabilisation of microtubules. This impairs cell division and ultimately leads to mitotic arrest. Additionally, the migratory capacity of cancer cells is attenuated by interfering with key processes involved in cell motility, such as polarization and chemotaxis. Furthermore, taxoid-based treatment can contribute to the generation of reactive oxygen species (ROS) within cancer cells, potentially triggering apoptotic cell death pathways (Schiff *et al.*, 1979).

Taxoid treatment is associated with cardiotoxicity side effects. Arrhythmias have been reported, which include transient bradycardia to ventricular tachycardia (Rowinsky *et al.*, 1991). Myocardial infarction has been reported, while the combination of doxorubicin and paclitaxel has been documented to cause congestive cardiac failure (Eisenhauer *et al.*, 1998).

1.3.4 Tyrosine kinase inhibitors

Tyrosine kinase inhibitors (TKIs) can be broadly categorised into two main classes based on their target specificity: (i) small molecules targeting both receptor and non-receptor tyrosine kinases (e.g. imatinib, sunitinib); and (ii) monoclonal antibodies blocking the function of growth factor receptor tyrosine kinases (e.g. trastuzumab).

Imatinib exerts its targeted therapeutic effect in chronic myeloid leukaemia by inhibiting the Bcr-Abl tyrosine kinase. This action is achieved through competitive binding to the adenosine triphosphate (ATP)-binding pocket of the enzyme, effectively blocking its catalytic activity (Druker *et al.*, 2000). Consequently, Bcr-Abl-mediated downstream signalling pathways are disrupted, leading to energy depletion, compromised cellular proliferation, and ultimately, the induction of apoptosis in leukemic cells.

Sunitinib disrupts cellular signaling cascades by targeting a multitude of receptor tyrosine kinase implicated in both tumor angiogenesis and tumor cell proliferation, such as platelet-derived growth factor receptor and vascular endothelial growth factor receptor. This multi-pronged approach potently inhibits tumour neovascularization and triggers apoptosis (Wilhelm *et al.*, 2004).

The potency of TKIs not only affect neoplastic cells, but also non-cancer cells. TKIs cause cardiotoxicity side effects in the form of arrhythmias, such as QT-prolongation, cardiomyopathy, hypertension and acute coronary syndromes (Chu *et al.*, 2007, Small *et al.*, 2014)

Trastuzumab represents a targeted therapeutic approach for human epidermal growth factor receptor 2 (HER2)-positive breast cancer by directly inhibiting HER2 receptor signalling, a key driver of cancer cell proliferation (Shepard *et al.*, 1991). It is administered both as a monotherapy or in combination with other chemotherapeutic agents. Furthermore, trastuzumab has shown efficacy in treating uterine papillary serous carcinomas, another cancer type exhibiting HER2 receptor overexpression (Santin *et al.*, 2008).

The precise mechanism underlying trastuzumab-induced cardiotoxicity during cancer treatment remains elusive. However, evidence suggests that trastuzumab disrupts cardiomyocyte contractility, leading to cardiac dysfunction, rather than causing direct myocyte loss in breast cancer patients (Suter *et al.*, 2007).

1.4 General introduction to anthracyclines

1.4.1 A brief history of anthracyclines

Anthracyclines were first discovered in the 1950s as an antibiotic isolated from *Streptomyces Peucetius*, a microorganism found near the soil of the Adriatic Sea, at the Farmitalia Research Laboratories in Italy (Di Marco *et al.*, 1964, Ewer *et al.*, 2011).

Streptomyces Peucetius is a spore-producing species of Actinomycetota, and it produces a red pigment that expresses antibacterial properties. This pigment was further investigated and purified but was far too toxic to be antibacterial. Around the same timeline, DuBost *et al* at Rhone-Poulenc successfully isolated rubidomycin from *Streptomyces Coerubleorubidus (Dubost et al., 1963)*. These two compounds were found to have the same structure, and their original names were combined with daunorubicin, marking the dual discovery and the first generation of anthracycline.

The first anthracycline to be introduced clinically was daunomycin in the 1960s (Di Marco *et al.*, 1964). Di Marco *et al* reported that daunomycin showed remarkable cytotoxicity. Daunomycin was able to completely inhibit the mitotic activity of normal and neoplastic cells *in vitro* at a concentration range from 0.01 to 0.1 μg/mL.

A second anthracycline, a derivative of daunomycin, was identified as 14-hydroxydaunomycin or adriamycin, later renamed doxorubicin (DOX) (Di Marco, 1969). Despite the name change, the term adriamycin is still encountered in contemporary literature, but this refers to the initial generic name of the compound. Doxorubicin was shown to be a more potent antineoplastic agent than its predecessor (Arcamone *et al.*, 1969, Di Marco, 1969).

Anthracyclines nowadays are one of the most widely used and effective chemotherapy (Minotti *et al.*, 2004). Doxorubicin, or anthracyclines in general, remains the mainstay chemotherapy treatment of a wide variety of solitary tumour and haematological malignancies, such as breast cancer, acute myelogenous leukaemia, and lymphoma, to name a few (Minotti *et al.*, 2004). Indeed, the World Health Organization acknowledge the importance of anthracyclines in their list of essential medicine.

1.4.2 Anthracyclines structure

Anthracyclines' molecular structures comprise an anthracylinone core with quinones, phenolic groups, and other substituents on the ring structures A, B, and C and the saturated D ring (Figure 1.1) (Bachour, 2002). The water solubility is provided by mono- or multi-saccharide substitutions, usually at the carbon C7 position of ring A.

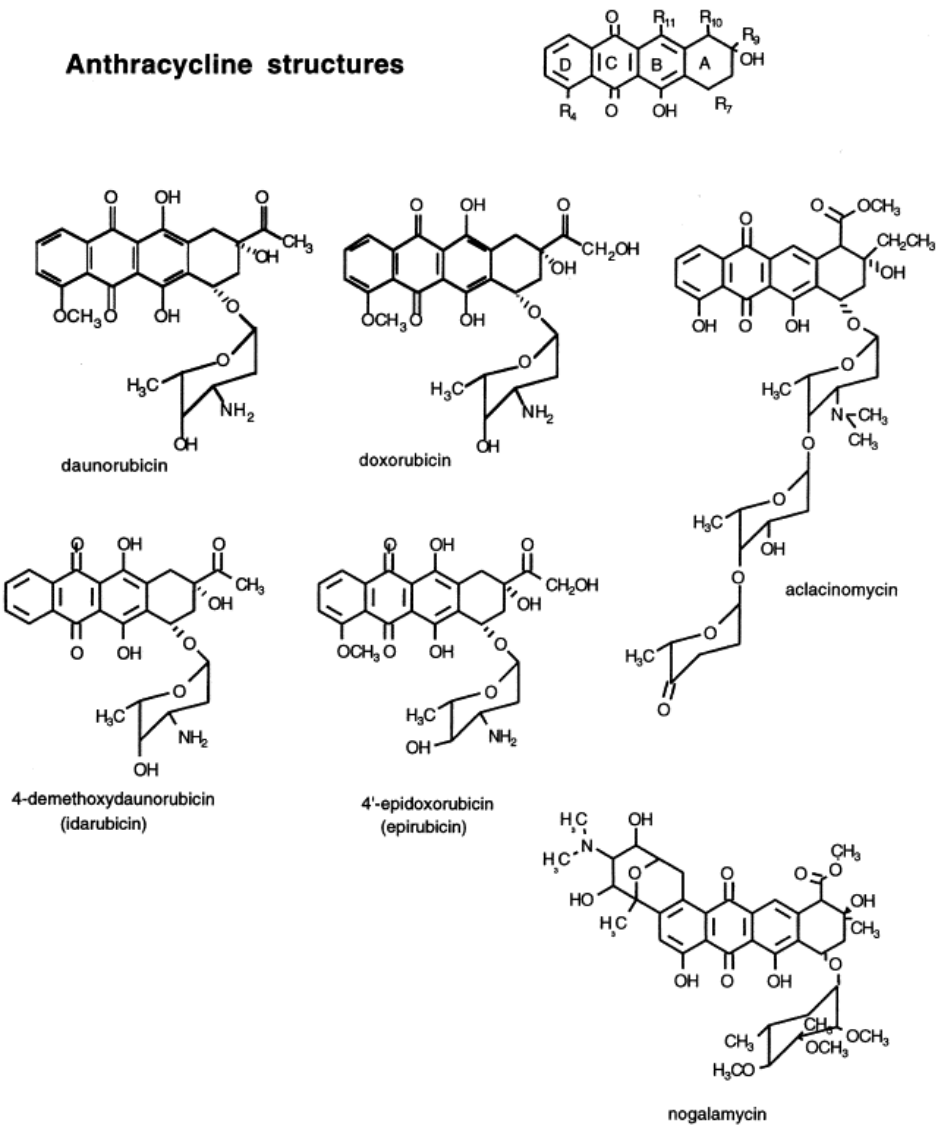

Figure 1.1 The chemical structure of anthracyclines. Figure taken from Bachour *et al*., 2002.

Looking at the chemical structure of doxorubicin in particular, the important structural characteristics are:

1. The planar anthraquinone ring system
2. Quinone group on the unsaturated rings

3. Stereochemistry of ring substitution at C9
4. The amino sugar daunosamine, which enhances water solubility and chemical frame for stabilising deoxynucleic acid binding

1.4.3 Brief overview of the pharmacokinetics of anthracyclines

The four most common anthracyclines are doxorubicin, daunorubicin, epirubicin, and idarubicin.

In the clinical setting, anthracyclines are administered via intravenous route. Following intravascular entry, rapid and extensive tissue penetration ensues, with a high affinity for tissues like the heart, muscle, liver, and kidneys. Anthracyclines do not pass the blood-brain barrier, except idarubicin.

The distribution of anthracyclines such as doxorubicin follows a multi-compartmental model (Methaneethorn *et al.*, 2023). After initial rapid distribution into the plasma (central compartment), an uptake by peripheral tissues occurs. The sheer volume of distribution reflects widespread tissue accessibility and relatively low plasma concentrations. Cellular binding, particularly to DNA, further contributes to the decline in plasma levels.

Doxorubicin undergoes extensive hepatic metabolism via three primary pathways: (1) one-electron reduction, (2) two-electron reduction, and (3) deglycosidation. Notably, approximately 50% of the administered dose is eliminated from the body unchanged (Mordente *et al.*, 2009). Among these pathways, the two-electron reduction pathway constitutes the dominant metabolic route. This process involves the enzymatic reduction of doxorubicin to doxorubicinol, a secondary alcohol metabolite, by various enzymes including alcohol dehydrogenase, carbonyl reductase, and aldo-keto reductase (see Figure 1.2).

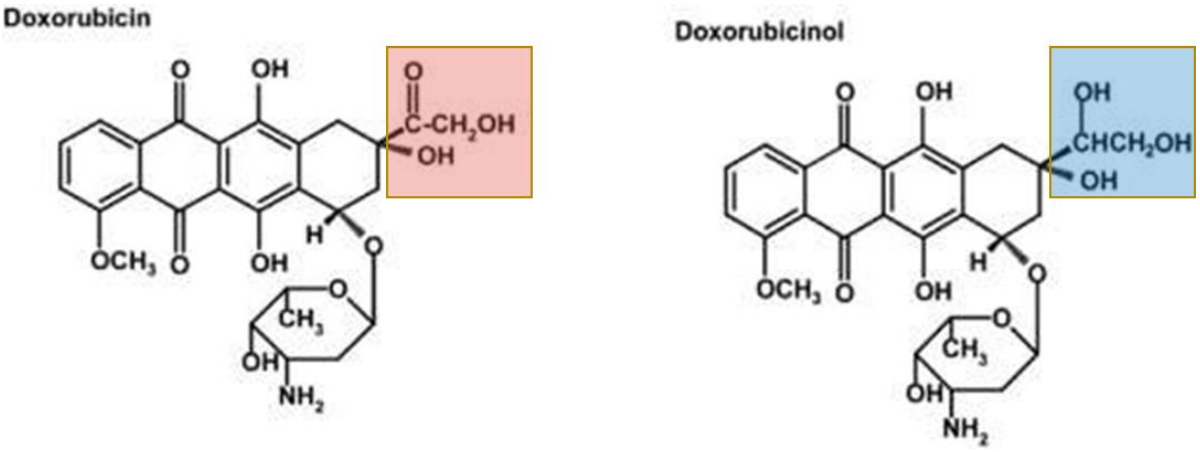

Figure 1.2 Comparison of the chemical structure of doxorubicin and doxorubicinol. Figure taken from Wang *et al*., 2001.

The one-electron reduction is mediated by several oxidoreductases, both cytosolic and mitochondrial, to form a doxorubicin-semiquinone radical. These enzymes include mitochondrial and cytosolic Nicotinamide Adenine Dinucleotide Phosphate Hydrogen (NAD(P)H) dehydrogenase, xanthine oxidase, and nitric oxide synthases. While the semiquinone metabolite can be reoxidized back to doxorubicin, this process is accompanied by the concomitant generation of reactive oxygen species (ROS), including hydrogen peroxide (Minotti *et al.*, 1998).

Meanwhile, doxorubicin deglycosidation constitutes a minor metabolic pathway, contributing only 1-2% to its overall metabolism (Mordente *et al.*, 2009). Within this pathway, cytoplasmic enzymes such as NAD(P)H quinone dehydrogenase, xanthine oxidase, and NADPH-cytochrome P450 reductase catalyse the transformation of doxorubicin into two aglycone metabolites: doxorubicin deoxyaglycone (via reduction) and doxorubicin hydroxyaglycone (via hydrolysis).

Biliary excretion accounts for about 50% of the administered doxorubicin dose, while renal elimination plays a minor role (<10%) (Mordente *et al.*, 2009). Doxorubicin undergoes a multi-phasic half-life with a terminal elimination half-life of approximately 30 hours, although its pharmacologically active lifespan is significantly shorter due to tissue binding and rapid distribution. The distribution half-life of doxorubicin is approximately 5 minutes.

Age, gender, and hepatic or renal function impact doxorubicin pharmacokinetics. Elderly patients or those with organ dysfunction may exhibit slower

elimination and heightened toxicity risk. Co-administered drugs can also alter metabolism or clearance, necessitating cautious monitoring for interactions.

1.5 Cardiocytoxicity of anthracyclines

Despite its important role as a chemotherapeutic agent, the administration of anthracycline can lead to cardiotoxic sequelae, for instance, in the form of heart failure.

The cardiotoxic potential of doxorubicin was recognised soon after its clinical introduction in 1979. Von Hoff *et al* noted clinical signs and symptoms of congestive heart failure in 2.2% of 4,000 patients receiving doxorubicin therapy (Von Hoff *et al.*, 1979). This landmark study established the cumulative dose as a key determinant of cardiotoxicity risk. Notably, the dose-dependent incidence of heart failure escalated from 3% and 7% at 400 and 500 mg/m², respectively, to a concerning 18% at 700 mg/m².

Early manifestation of anthracycline-induced cardiomyopathy was demonstrated in a recent seminal study (Cardinale *et al.*, 2015). With a population cohort of 2600 patients receiving anthracycline-based chemotherapy over a decade, the study employed serial echocardiography to monitor left ventricular ejection fraction (LVEF). Anthracyline-induced cardiomyopathy was defined echocardiographically as a >10% decrease in LVEF from baseline or LVEF <50%. This rigorous surveillance revealed a 9% incidence of anthracycline-induced cardiomyopathy within the cohort. Notably, 98% of these cases manifested within the first year of therapy, with some occurring as early as three months. These findings reinforce the association between anthracycline-induced cardiomyopathy and anthracycline dose, highlighting the potential risk for early-onset cardiotoxicity within the first year of treatment.

Once doxorubicin-induced cardiomyopathy manifests, its cardiotoxic effects become irreversible, characterized by a poor prognosis. A study utilising endomyocardial biopsies in doxorubicin-induced cardiomyopathy patients revealed a 50% mortality rate at two years (Felker *et al.*, 2000).

These findings, alongside other investigations, provided the scientific basis for the current clinical recommendation of limiting the lifetime cumulative doxorubicin dose to ≤450 mg/m² (Zamorano *et al.*, 2016, Cardinale *et al.*, 2016).

1.6 Potential mechanism of actions of anthracycline-induced cytotoxicity

The exact mechanism of action of anthracycline-induced cardiotoxicity (AIC) remains elusive and requires further studies. It is possible that AIC is multifactorial and targets multiple cell death mechanisms.

There are many mechanisms of AIC. The consensus is that doxorubicin targets cancer and non-cancer cells through two major mechanisms: (1) DNA intercalation and inhibition of topoisomerase-II-mediated DNA repair pathways, and (2) cytotoxic reactive oxygen species (ROS) generation leading to membrane damage, DNA oxidation, calcium dysregulation and oxidative stress induction, ultimately triggering apoptotic cascades (Thorn *et al.*, 2011).

1.6.1 DNA intercalation and disruption of Topoisomerase 2

Doxorubicin can translocate into the nucleus and exert its cytotoxic effect by intercalating into DNA and binding to topoisomerase 2 isozymes (Top2) (Champoux, 2001). This enzyme is ATP-dependent and functions by catalyzing the transient breakage of both strands within a single DNA duplex. Subsequently, it facilitates the passage of an intact duplex DNA segment through the generated break, followed by resealing the cleaved phosphodiester backbone. This coordinated activity alleviates torsional stress accumulated during essential cellular processes, including DNA replication and transcription (Yang *et al.*, 2014).

Topoisomerase 2 is expressed in two isozymes in humans, Top2α and Top2β (Wang, 2002). Doxorubicin's efficacy in cancer treatment stems from its ability to induce cytotoxicity in proliferating cells. This effect is primarily mediated by the inhibition of topoisomerase IIα, the predominant isoform expressed in rapidly dividing cells (See Figure 1.3). The detrimental side effect of doxorubicin on cardiac function arises from its deleterious influence on non-proliferative cardiomyocytes. Topoisomerase 2β, the dominant isoform in cardiomyocytes, is targeted by doxorubicin, leading to cellular damage and ultimately, cardiomyopathy (Tewey *et al.*, 1984).

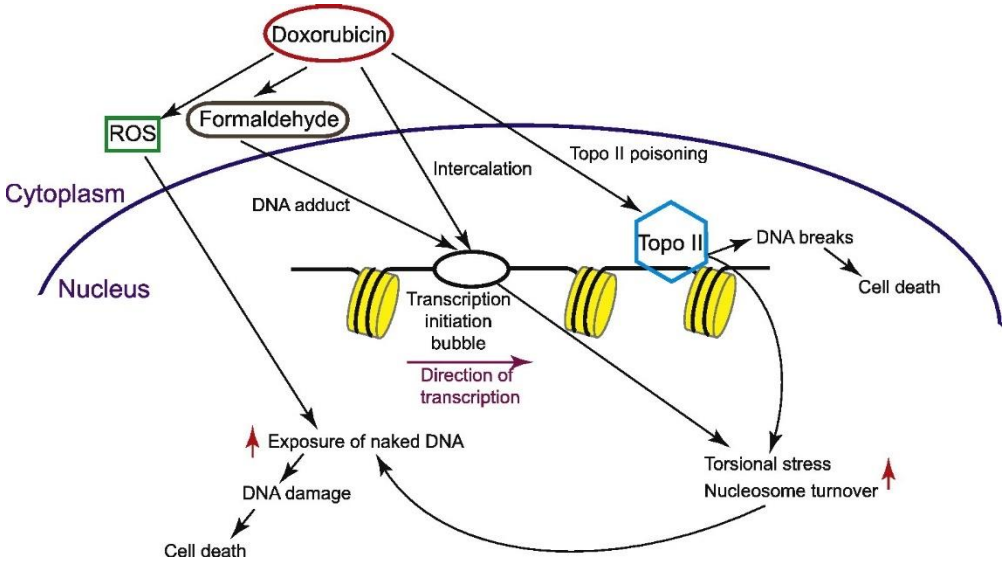

Figure 1.3 Simplified diagram of topoisomerase 2 damage induced by doxorubicin. Figure taken from Yang *et al*., 2014.

1.6.2 Role of Oxidative Stress

Free radical generation remains the most comprehensively elucidated mechanism underlying doxorubicin-induced myocardial injury. The heart's inherent susceptibility to oxidative stress has propelled this aspect to the forefront of research on doxorubicin cardiotoxicity (Myers, 1998). Our understanding of free radical generation and subsequent cardiac damage has progressed into a molecular-level comprehension of how enzymes, such as nitric oxide synthase and NAD(P)H oxidase, interact with doxorubicin to orchestrate oxidative stress (Montaigne *et al.*, 2010).

1.6.2.1 NOS-dependent ROS

Doxorubicin's interaction with endothelial nitric oxide synthase reductase disrupts the balance between superoxide free radicals and nitric oxide (NO) levels. This interaction decreases NO production while increasing superoxide levels, triggering a cascade leading to cardiotoxicity.

Supporting this mechanism, a study demonstrated that doxorubicin administration in bovine aortic endothelial cells upregulated NOS messenger RNA (mRNA) and protein expression, promoting redox-dependent activation and subsequent apoptosis (Drummond *et al.*, 2000). Interestingly, antisense NOS mRNA treatment dampened caspase 3 activity, suggesting a cardioprotective role against doxorubicin-induced cell death. Further evidence comes from animal models, where

transgenic mice with overexpressed NOS showed exacerbated cardiac ROS production upon doxorubicin exposure, while NOS knockout mice displayed mitigated levels (Kalivendi *et al.*, 2001).

These findings collectively implicate that NOS plays a role in doxorubicin-induced oxidative stress and subsequent cardiac injury.

1.6.2.2 NAD(P)H-dependent ROS

In myocardial cells, the reduction of anthracyclines by NAD(P)H dehydrogenase in mitochondrial respiratory complex I forms a semiquinone radical that can react with molecular oxygen to form the superoxide radical (Volkova *et al.*, 2011). This non-enzymatic pathway causes a redox cycle to be established, resulting in the accumulation of superoxide anions. These ROS mediate diverse cellular insults, including lipid peroxidation, DNA double-strand breaks, and protein oxidation, culminating in apoptotic cell death.

The significance of the NAD(P)H oxidase complex in doxorubicin-induced cytotoxicity has been demonstrated through pharmacological *in vitro* studies. Notably, cultured cell lines treated with NAD(P)H inhibitors exhibited enhanced cell survival, providing functional evidence for the complex's involvement in doxorubicin-mediated cytotoxicity (Gilleron *et al.*, 2009).

1.6.2.3 Mitochondrial-dependent ROS

Anthracyclines exhibit affinities for mitochondrial DNA, potentially inhibiting crucial mitochondrial functions involved in cellular energy generation.

This vulnerability may be attributed to the cationic nature of doxorubicin, which facilitates its retention within the mitochondrial inner membrane through the formation of an irreversible complex with cardiolipin protein. Mitochondrial respiratory chain proteins rely on proper cardiolipin binding for optimal function. Doxorubicin's interference with the cardiolipin-protein interface has been postulated to contribute to increased superoxide (O_2^-) production (Chen *et al.*, 2020). This disruption is plausibly implicated in impaired mitochondrial, and consequently cellular, metabolism, considering that mitochondria generate over 90% of the ATP utilised by cardiomyocytes (Ventura-Clapier *et al.*, 2004).

Furthermore, doxorubicin impairs the oxidation of long-chain fatty acids within cardiac mitochondria, while promoting glucose metabolism, thereby shifting the metabolic state from an aerobic to an anaerobic state. This metabolic shift, potentially triggered by oxidative stress, may contribute to cardiac dysfunction, characterised by impaired contractility and relaxation. In a Langendorff ischemia-reperfusion model of doxorubicin stress, inhibiting mitochondrial division mitigated contractile dysfunction and infarct size observed in rat hearts during the reperfusion stage (Gharanei *et al.*, 2013). This finding suggests that doxorubicin directly induces mitochondrial structural damage, prompting compensatory increased division attempts by the mitochondria.

Beyond alterations in mitochondrial biogenesis and function, anthracyclines have been shown to impact the structure and transmembrane potential (ΔΨm) of cardiac mitochondria. Doxorubicin exposure for just 60 min significantly reduces ΔΨm in isolated rat hearts (Montaigne *et al.*, 2010). This doxorubicin-induced ΔΨm collapse is specifically prevented by inhibiting the mitochondrial permeability transition pore (mPTP), independent of the calcium uptake uniporter and sodium-calcium exchanger (Solem *et al.*, 1994).

The mitochondrial permeability transition pore (mPTP) is a multi-protein complex embedded in the mitochondrial membranes implicated in the induction of apoptotic or necrotic cell death (Hausenloy *et al.*, 2002). The mPTP is postulated to be a multimeric channel spanning both the outer and inner membranes, acting as a non-selective pore critical for maintaining the inner membrane's permeability barrier. In the "closed" state, the inner matrix is impermeable to most solutes and ions, including Ca^{2+} and hydrated inorganic ions. However, various factors, including excessive oxidative stress (ROS accumulation), low pH, Ca^{2+} overload, and phosphate buildup, can trigger an irreversible transition to the "open" state. This transition drastically increases permeability, allowing for the diffusion of molecules under 1.5 kDa. This influx of solutes, coupled with mitochondrial matrix swelling, cristae unfolding, and outer membrane rupture, leads to the nonspecific release of intermembrane-space proteins, including cytochrome c, into the cytosol, ultimately inducing apoptosis or necrosis (Kroemer *et al.*, 1998). Using a rat heart's Langendorff ischaemia reperfusion model, it was demonstrated that doxorubicin exacerbates myocardial injury by opening mPTP (Gharanei *et al.*, 2013).

Doxorubicin also affects mitochondrial GATA-4 gene expression leading to the suppression of mitochondrial synthesis and their metabolism, resulting in apoptosis (Suliman *et al.*, 2007). This effect was mitigated by exposing the mice to low-dose carbon monoxide inhalation, which activated the genes responsible for mitochondrial biosynthesis and upregulated nuclear-encoded heme oxygenase (HO) levels (Piantadosi *et al.*, 2008). These findings suggest that doxorubicin also exerts disruptive effects on both nuclear and mitochondrial transcriptional regulation.

1.6.2.4 Fe-DOX complex

Doxorubicin, due to its cationic nature, exhibits a strong electrostatic interaction with the negatively charged phospholipid bilayer of the plasma membrane, facilitating membrane interactions and potential cellular uptake. This inherent positive charge also contributes to Doxorubicin's high affinity for iron, leading to the formation of Fe-DOX complexes. These complexes disrupt iron homeostasis, altering normal cellular iron metabolism (McGowan *et al.*, 2017). Additionally, Fe-DOX complexes can interact with free oxygen, promoting the generation of reactive oxygen species (ROS) (Ichikawa *et al.*, 2014).

Under normal physiological conditions, the limited availability of free iron prevents sufficient interaction with doxorubicin, precluding the development of cardiomyopathy (Minotti *et al.*, 2004). Studies suggest that doxorubicin's impact on iron metabolism may not be solely driven by direct Fe-DOX complex formation, but rather through its interactions with intracellular iron-binding proteins. One such mechanism involves the doxorubicinol metabolite. By forming complexes with the Fe-S cluster in cytoplasmic aconitase/IRP-1 (iron regulatory protein), doxorubicinol enhances the stability of transferrin mRNA, thereby suppressing the translation of iron-sequestration proteins (Minotti *et al.*, 1998). The subsequent downregulation of IRP-1 results in a corresponding increase in free intracellular iron. This enriched pool of free iron can perpetuate the cycle of reactive oxygen species generation. Thus, dysregulation of iron homeostasis contributes to the pathogenesis of doxorubicin-induced cardiomyopathy.

Miranda *et al* demonstrated significantly enhanced susceptibility to DIC in mice with depleted iron regulatory gene HFE, a genetic defect leading to hereditary hemochromatosis in humans (Miranda *et al.*, 2003). This observation was further

corroborated by another finding in rats model, where iron-rich dietary supplementation for 10-14 weeks markedly exacerbated DIC severity (Panjrath *et al.*, 2007). These studies highlighted the important role of iron in doxorubicin-induced cardiotoxicity.

Close monitoring of iron status is crucial in cancer patients undergoing chemotherapy due to a complex interplay of factors affecting iron homeostasis. Cancer itself, combined with chemotherapeutic regimens, can induce abnormal blood losses and nutritional deficiencies, potentially necessitating blood transfusions and iron supplementation (Ichikawa *et al.*, 2014). This was observed in paediatric and adult leukaemia patients, where increased iron overload was detected during chemotherapy (Barton *et al.*, 2000).

Regardless of the source, myocardial accumulation of excessive reactive oxygen species (ROS) poses a significant threat. Apart from overwhelming the enzymatic defence of cardiomyocytes, ROS can exert detrimental effects through various mechanisms, including altering gene expression by interacting with regulatory proteins. Notably, ROS can disrupt the function of membrane-bound proteins such as G-proteins via lipid peroxidation (Octavia *et al.*, 2012). Additionally, ROS can modify a protein's tertiary structure through the oxidation of disulfide bonds (S-S bonds). Perhaps most critically for the myocardium, ROS can trigger the release of Ca^{2+} ions, potentially leading to contractile dysfunction and cell death (Dhalla *et al.*, 2000).

1.6.2.5 Intracellular calcium dysregulation

Doxorubicin-induced cardiotoxicity is intricately linked to disrupted intracellular calcium (Ca^{2+}) homeostasis. This dysregulation manifests as elevated Ca^{2+} levels, but paradoxically, it also acts as a driving force for the generation of ROS.

Reactive oxygen species (ROS) and hydrogen peroxide (H_2O_2) generated through the aforementioned mechanisms exert detrimental effects on calcium homeostasis in a variety of muscle cell types. This disruption primarily stems from their impact on the sarcoplasmic reticulum (Octavia *et al.*, 2012). ROS and H_2O_2 can impede normal sarcoplasmic reticulum function by two mechanisms. First, by inhibiting the Ca^{2+} ATPase pump. This can occur through mechanisms like reducing the expression levels of SERCA2a mRNA, leading to impaired Ca^{2+} reuptake into the sarcoplasmic reticulum (Arai *et al.*, 2000). Second, ROS and H_2O_2 can directly activate

ryanodine calcium-release channels. This process bypasses the normal regulatory mechanisms and leads to uncontrolled Ca^{2+} release from the sarcoplasmic reticulum into the cytosol (Saeki *et al.*, 2002).

Doxorubicin has also been shown to inhibit the sodium-calcium exchanger channel in the sarcolemma (dos Santos *et al.*, 2018). Conversely, doxorubicin has been implicated in enhancing the activity of the L-type calcium channel, leading to increased Ca^{2+} influx into the cell (Keung *et al.*, 1991). Notably, inhibition of doxorubicin-mediated ROS production and subsequent apoptosis can be achieved through the use of Ca^{2+} chelators (Kalivendi *et al.*, 2005).

Elevating intracellular Ca^{2+} during oxidative stress, particularly in doxorubicin-treated cardiomyocytes, activates calpains, calcium-dependent proteases linked to sarcomere protein degradation and cardiomyocyte apoptosis. Specifically, increased Ca^{2+} store in the sarcoplasmic reticulum leaks and triggers calpain-mediated cleavage of caspase 12, an initiator of apoptosis (Jang *et al.*, 2004). This proteolytic cascade, further evidenced by titin degradation, contributes significantly to Doxorubicin-induced cardiomyopathy. Titin is the largest protein and a principal component of the heart sarcomere. Interestingly, calpain inhibition appears to offer cardioprotective effects by depleting cardiac ankyrin repeat protein, CARP, a negative regulator of cardiac genes that promotes sarcomeric stability (Lim *et al.*, 2004).

In summary, doxorubicin-induced cardiotoxicity is characterised by a multifaceted dysregulation of calcium homeostasis, culminating in apoptosis. This dysregulation is driven by doxorubicin ability to elevate intracellular free Ca^{2+} levels, which in turn activates Ca^{2+}-dependent signalling pathways leading to cell death.

1.6.3 Apoptosis

Apoptosis plays pivotal roles in shaping tissues during development and maintaining cell homeostasis by eliminating infected, injured, or aged cells in adult organism.

Triggered by diverse stimuli, apoptosis is executed in a tightly regulated manner, characterised by distinct biochemical and morphological hallmarks such as cellular shrinking, chromatin condensation, membrane blebbing, apoptotic body formation, and DNA fragmentation (Elmore, 2007, Häcker, 2000, Saraste *et al.*, 2000).

This active, controlled process stands in contrast to necrosis, characterised by uncontrolled cell lysis and inflammation.

It is understood that there are two central pathways mediating apoptosis: the extrinsic pathway, reliant on cell surface death receptors, and the intrinsic pathway, involving the mitochondria and endoplasmic reticulum (McIlwain *et al.*, 2013).

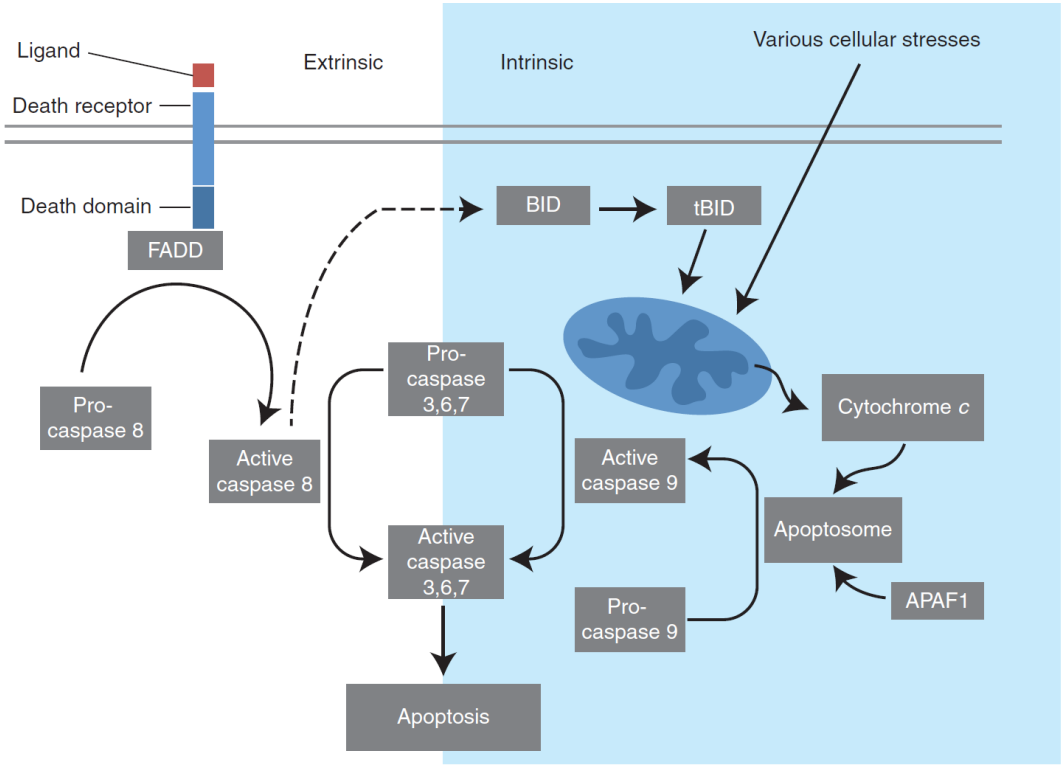

Figure 1.4 Simplified schematic of the extrinsic and intrinsic pathway of apoptosis. Figure taken from McIlwain *et al.*, 2013. APAF1 = apoptotic protease-activating factor 1, BID = BH3 interacting-domain death agonist, tBID = the caspase 8-activated BID, FADD = Fas-associated death domain.

1.6.3.1 The extrinsic pathway

The extrinsic pathway of apoptosis relies on interactions between death ligands such as FasL, tumour necrosis factor alpha (TNF-α) and their respective death receptors (Movassagh *et al.*, 2008). Ligand-receptor interaction, for example, with Fas, remodels inactive Fas complexes into active signalling platforms. This triggers the recruitment of specific adaptor proteins like Fas-associated death domain (FADD). These proteins serve as docking sites for procaspase 8 or 10, ultimately assembling the death-inducing signalling complex (DISC) (Kischkel *et al.*, 1995). This

subsequently results in autoproteolytic processing of these caspases by induced proximity and the release of their processed active proteases.

Processed caspase 8 exhibits cell-type specific activities in the extrinsic apoptotic pathway. In some cells, it directly cleaves downstream effector caspases, triggering the execution phase. In others, however, caspase 8 initiates an amplification loop by cleaving pro-apoptotic BID, a Bcl-2 family member. This triggers BID-mediated release of mitochondrial pro-apoptotic factors, effectively linking the extrinsic pathway to the intrinsic pathway for complete apoptotic execution (Luo *et al.*, 1998, Li *et al.*, 1998).

Although the FasL gene remains transcriptionally inactive in most cells, it can be activated by multiple factors like nuclear factor Kappa B (NF-κB), apoptotic protease-activating factor 1 (APAF1), nuclear factor of activated T cells (NF-AT), and p53 (Kasibhatla *et al.*, 1998). Upon ligand binding, the precise and critical interaction between death domains on FasL and Fas enables the assembly of the DISC, initiating the extrinsic apoptotic cascade. Fas signalling exhibits context-dependent versatility. While promoting apoptosis in most cases, Fas can trigger necrosis which requires FADD and Fas-interacting serine/threonine kinases receptor-interacting protein, but not caspase 8 (Holler *et al.*, 2000). Additionally, Fas surprisingly demonstrates pro-proliferative effects in specific cell types, highlighting its multifaceted signalling capabilities (Siegel *et al.*, 2000).

1.6.3.2 The intrinsic pathway

While the extrinsic pathway utilises specific death ligands at the cell surface, the intrinsic pathway acts as a comprehensive sensor for diverse stressors, including lack of survival signals, toxins, radiation, hypoxia, oxidative stress, and DNA damage, ultimately leading to apoptosis. Downstream signalling details differ, but all extrinsic and intrinsic apoptotic pathways converge on the intrinsic pathway, driven by central death machinery in mitochondria and the endoplasmic reticulum.

Within the mitochondria, mitochondrial outer membrane permeabilisation (MOMP) marks a pivotal step in apoptosis. This irreversible event facilitates the release of pro-apoptotic factors ("apoptogens") residing in the intermembrane space into the cytoplasm. Notably, MOMP frequently coincides with the dissipation of the

mitochondrial inner transmembrane potential (ΔΨm), suggesting a potential link between opening of mPTP in the inner membrane and the triggering of MOMP.

A distinct second mechanism for MOMP involves the interplay of Bcl-2 family proteins at the outer mitochondrial membrane. This family, with Bcl-2 as its prototypical anti-apoptotic member, critically regulates cell survival in the intrinsic pathway. Bcl-2 family members, such as pro-apoptotic proteins Bax and Bak, share Bcl-2 homology (BH) domains, promoting MOMP through conformational changes, oligomerisation, and mitochondrial translocation. This activation triggers the release of cytochrome c from the intermembrane space, a key step in apoptotic execution.

Caspases are cysteine-dependent aspartate directed protease. Caspases recognise specific peptide sequences and cleave solely after aspartic acid residues (McIlwain *et al.*, 2013). This precision contributes to the controlled execution of apoptosis, bypassing indiscriminate protein degradation. Their targeted cleavages, often altering protein function, encompass downstream caspases for cascade progression, apoptosis inhibitor such as Bcl-2, and proteins promoting cell disassembly. Caspase involved in apoptosis can be further classified by their functions, such as initiator caspases and executioner or effector caspases.

Initiator caspases like caspase 8, 9, and 10 exist as inactive procaspase monomers that are activated by dimerisation, not by cleavage. The induced proximity model postulates that while pro-caspases are inherently latent due to low abundance, upstream signalling events induce caspase dimerization, enabling intermolecular autoproteolysis and activation (Shi, 2004). This principle is exemplified by the ability of a caspase-9/caspase-8 chimera to be activated by the apoptosome, further supporting the model (Pop *et al.*, 2006). Subsequent to initiator caspase activation, a proteolytic cascade ensues, leading to downstream activation of effector caspases like caspase 3.

Caspases, unlike other modifiable cellular components, rely on irreversible proteolytic processing for activation. Therefore, they exist as latent pro-caspases within cells, minimising their lethal potential. This cautious approach is further reinforced by inhibitory proteins like X-linked inhibitor of apoptosis protein (XIAP), which maintain a strict threshold for active caspase levels. Consequently, achieving cell death necessitates not only triggering pro-apoptotic pathways but also overcoming

inhibitory pathways, such as XIAP neutralisation, to push the cell towards apoptosis (Movassagh *et al.*, 2008).

1.6.3.3 Role of anthracyclines in apoptosis

Targeting intrinsic and extrinsic apoptotic pathways is a lethal strategy employed by cancer drugs like doxorubicin (Kalyanaraman *et al.*, 2002, Rawat *et al.*, 2021).

Doxorubicin can activate intrinsic pathway by triggering caspase 3 and 9, the opening of mitochondrial permeability transition pore (mPTP) and subsequent release of cytochrome c into the cytosol (Ma *et al.*, 2020). Additionally, doxorubicin upregulates Fas and FasL expression, promoting ligand binding and subsequent caspase 3 activation via the CD95L death receptor pathway (Rawat *et al.*, 2021). Activation of effector caspases, such as caspase 3, 6, and 7, results in apoptotic cell death. Interestingly, doxorubicin-induced apoptosis exhibits early mitochondrial dysfunction in cardiomyocytes, marked by increased pro-apoptotic/anti-apoptotic protein ratio, DNA damage, and p53 activation (Sandhu *et al.*, 2014).

1.6.4 Pyroptosis

The advent of pyroptosis research arose in 1986 when Friedlander observed rapid cell death and content release in mouse macrophages treated with anthrax lethal toxin (Friedlander, 1986). Building upon this, the discovery of Interleukin-1β Converting Enzyme (ICE, later known as caspase 1) in 1989 established its role as an inflammatory caspase responsible for processing precursor IL-1β into its mature form (Cerretti *et al.*, 1992, Thornberry *et al.*, 1992). In 1992, Zychlinsky *et al* stumbled upon pyroptosis in Shigella-infected macrophages, initially misconstrued as apoptosis due to shared features like caspase dependence, DNA damage, and nuclear condensation (Zychlinsky *et al.*, 1992). Finally, in 2001, Cookson *et al* coined the term "pyroptosis" (derived from the Greek word "pyro" for fire and "ptosis" for falling), differentiating it from non-inflammatory apoptosis and solidifying its identity as a distinct, pro-inflammatory program of cell death (Cookson *et al.*, 2001).

Pyroptosis primarily manifests in macrophages during pathogen infection, serving as a critical mechanism for pathogen clearance. Morphologically, it is characterised by cellular swelling and subsequent plasma membrane rupture, leading

to the release of pro-inflammatory cytokines, notably IL-1β and IL-18, alongside cellular contents into the extracellular space, triggering the inflammatory response.

Our understanding of pyroptosis induction has grown to encompass four distinct pathways. Notably, pyroptosis can be triggered in both inflammasome-dependent and inflammasome-independent manners. The inflammasome-dependent pathways include the well-characterized canonical and non-canonical pathways, while the inflammasome-independent pathways involve activation via caspase 3 or granzyme proteases (Tan *et al.*, 2021).

1.6.4.1 The canonical pathway

The canonical pathway serves as a key platform for pyroptosis. In brief, inflammasome assembly, triggered by diverse inflammatory insults, engages Nod-Like Receptor Protein 3 (NLRP3) and orchestrates caspase-1 activation. This ultimately results in Gasdermin D (GSDMD) cleavage, pore formation in the plasma membrane, and subsequent cell rupture with release of pro-inflammatory cytokines.

The NLRP3 inflammasome is an essential component of pyroptosis and it relies on two independent steps, priming and triggering (Toldo *et al.*, 2021). The NLRP3 inflammasome is a large, multi-protein complex that is assembled in response to Pathogen-Associated Molecular Patterns (PAMPs), Danger-Associated Molecular Patterns (DAMPs), and other inflammatory insults.

Priming signals from PAMPs and DAMPs stimulate inflammatory receptors such as the Toll-Like Receptors (TLRs). These activate the nuclear factor kappa-light-chain-enhancer of activated B cells (NF-κB) and initiate the transcription of the components of the inflammasomes consisting of NLRP3, pro-caspase 1, pro-IL-1β, pro-IL-18, and ASC (apoptosis-associated speck-like protein containing a caspase recruitment domain (CARD)).

Primed cells exposed to diverse "trigger" factors, including mitochondrial reactive oxygen species and dysfunction, initiate NLRP3 inflammasome assembly. This complex, comprised of NLRP3 and ASC, activates caspase-1 via proteolytic cleavage, which subsequently cleaves pro-IL-1β, pro-IL-18, and GSDMD into their mature forms. GSDMD-NT oligomerizes on the plasma membrane, forming pores that

facilitate the release of mature IL-1β and IL-18, ultimately leading to pyroptosis (Rauf *et al.*, 2019, Toldo *et al.*, 2021).

1.6.4.2 The non-canonical pathway

The non-canonical inflammasome pathway bypasses NLRP3 and relies on a direct interaction between intracellular lipopolysaccharide (LPS) and the CARD domains of caspase 4/5/11 (Shi *et al.*, 2014). This interaction triggers caspase 4/11 oligomerization and subsequent activation, culminating in cleavage of gasdermin D (GSDMD) at Asp276 (Kayagaki *et al.*, 2015). Murine caspase 11 and its human homologs, caspase 4 and 5, directly bind and cleave GSDMD upon encountering cytosolic LPS. Notably, the catalytic domains of these inflammatory caspases are responsible for GSDMD cleavage. Interestingly, caspase 11 activation within the non-canonical inflammasome can also activate NLRP3, leading to further maturation of IL-1β and IL-18 (Lee *et al.*, 2018).

Cytosolic lipopolysaccharide (LPS) or Gram-negative bacteria can trigger non-canonical inflammasome signalling, leading to GSDMD-dependent pyroptosis in neutrophils. This subsequently leads to the extrusion of neutrophil extracellular traps (Kuznetsov *et al.*), a distinct form of regulated neutrophil cell death in response to pathogen infection (Burgener *et al.*, 2020). This observation establishes a crucial link between the non-canonical inflammasome and NETosis.

1.6.4.3 Caspase 3 / Gasdermin E mediated pathway

Building upon existing knowledge, Wang *et al* proposed that specific chemotherapy drugs can trigger pyroptosis in epithelial cells via caspase 3-mediated cleavage of gasdermin E (GSDME) (Wang *et al.*, 2017). They found that the activation of caspase 3 by TNF-α leads to the specific cleavage of human and mouse GSDME at the aspartic acid residues 267 or 270. Importantly, the mutation of these residues abolished GSDME's ability to induce pyroptosis.

Historically, caspase activation, particularly caspase 3, was considered a defining hallmark of apoptosis. However, this paradigm has shifted with the recognition that caspase 3 activation can occur in processes outside apoptosis. Recent research, such as the aforementioned study by Wang *et al*, revealed that gasdermins, rather

than caspases, may be the key players in dictating the switch between apoptosis and pyroptosis in response to various death stimuli.

1.6.4.4 The granzymes mediated pathway

A recent study indicated that both natural killer cells and cytotoxic T lymphocytes trigger pyroptosis in cancer cells via granzyme-mediated cleavage of specific gasdermin family members (Zhou *et al.*, 2020). More specifically, lymphocyte-derived granzyme A (GZMA) cleaves gasdermin B (GSDMB) at its linker region, activating its pore-forming activity and culminating in pyroptotic cell death.

Interestingly, granzyme B (GZMB) from natural killer cells or chimeric antigen receptor (CAR) T cells directly targets GSDME at a site also recognised by caspase 3. This cleavage liberates the cytotoxic N-terminal of GSDME, enabling pore formation and pyroptosis in GSDME-expressing cancer cells. Furthermore, Zhou *et al* proposed that granzyme-mediated pyroptosis of cancer cells might amplify inflammatory signals within the tumour microenvironment (TME), potentially contributing to the recruitment of immune cells and further boosting antitumor immunity (Zhou *et al.*, 2020).

1.6.4.5 Gasdermins

The gasdermin family comprises pivotal pore-forming proteins that orchestrate the execution phase of pyroptosis. In humans, this family consists of six conserved members: gasdermin A, B, C, D, E, and DFNB59 (Kovacs *et al.*, 2017).

Gasdermin family members showcase a fascinating autoinhibited structure, harboring a cytotoxic N-terminal domain restrained by a C-terminal repressor via a flexible linker (Ding *et al.*, 2016). This intramolecular interaction serves as a safety switch, precluding the N-terminal's pore-forming activity and preventing pyroptosis. However, upon encountering inflammatory insults, specific caspases like caspase 1 and caspase 11 are activated, leading to a precise cleavage at the linker. This cleavage event releases the N-terminal domain, triggering its oligomerisation on the membrane and the formation of large pores (Ding *et al.*, 2016, Sborgi *et al.*, 2016). These pores serve as conduits for the efflux of pro-inflammatory cytokines like IL-1β and IL-18.

Notably, GSDMD stands unique as the only caspase 1 substrate known to induce pyroptosis. This critical role is further emphasised by the resistance of GSDMD-deficient cells to pyroptosis induced by inflammasome activation (Tsuchiya *et al.*, 2019). Despite lacking GSDMD, cells can still undergo caspase 1-mediated cell death, albeit through a distinct pathway. The absence of GSDMD redirects caspase 1 activity towards the apoptotic cascade, leading to downstream activation of caspase 3 and 7 (Tsuchiya *et al.*, 2019).

This finding highlights the multifaceted role of caspase 1, capable of orchestrating both pyroptosis and apoptosis depending on the presence of specific downstream effectors like GSDMD. Indeed, this view challenges the aforementioned perspective by Wang *et al* that propose gasdermins hold the key role to dictate the switch between apoptosis and pyroptosis (Wang *et al.*, 2017). The mixed findings highlight the need for further research to extend our knowledge on the role of gasdermins.

1.6.5 Role of pyroptosis in disease processes

Despite its recent emergence, the field of pyroptosis research is flourishing, with discoveries continuously expanding our understanding of pyroptosis and its contributions to various disease processes. This ongoing exploration has profoundly expanded our understanding of this programmed cell death pathway, holding immense potential for future research and the development of novel therapeutic strategies. The following subsections will briefly outline our current understanding of pyroptosis in different diseases.

1.6.5.1 Role of pyroptosis in infectious diseases

Since its early inception, pyroptosis emerges as a critical component of the host's anti-pathogen defence, serving as a mechanism for both eliminating intracellular pathogens and controlling their dissemination. Pyroptosis has been found to be activated in response to various infections caused by bacteria like Anthrax, Salmonella, Shigella, and Legionella, as well as viruses like influenza, herpes simplex virus, and even HIV (Friedlander, 1986, Zychlinsky *et al.*, 1992, Cookson *et al.*, 2001, Xia *et al.*, 2019, Hu *et al.*, 2022, He *et al.*, 2020).

1.6.5.2 Role of pyroptosis in inflammatory bowel diseases

Recent research highlights the contribution of pyroptosis to the pathophysiology of inflammatory bowel disease encompassing Crohn's disease and ulcerative colitis (Zhang *et al.*, 2022). Studies demonstrate that chronic inflammation and tissue damage in these conditions are directly exacerbated by inflammasome activation and subsequent pyroptosis (Chen *et al.*, 2019, Gao *et al.*, 2021). For instance, Gao *et al* found that colitis development correlated with commensal *Escherichia Coli* overgrowth and subsequent dysregulation, leading to GSDMD activation. Activated GSDMD, triggered IL-18 release and goblet cell loss, promoting colitis. This study highlights GSDMD as a key mediator of IL-18 release in colitis and emphasises the potential role of the microbiota in influencing colitis pathogenesis through GSDMD regulation.

1.6.5.3 Role of pyroptosis in autoimmune diseases

Emerging evidence suggests a potential role for pyroptosis, a distinct pro-inflammatory cell death pathway, in the pathogenesis of autoimmune diseases like rheumatoid arthritis and systemic lupus erythematosus (SLE) (Ren *et al.*, 2023, Gong *et al.*, 2023). These studies indicate that dysregulation of inflammasome activation and subsequent pyroptosis may contribute to the characteristic inflammation and tissue damage observed in these conditions, highlighting potential therapeutic targets for disease management.

1.6.5.4 Role of pyroptosis in neurodegenerative diseases

Recent research explores the potential role of pyroptosis in the development of neurodegenerative diseases like Alzheimer's and Parkinson's disease (Cai *et al.*, 2022, Wang *et al.*, 2019). Cai *et al* found that the administration of pharmacological dose of salidroside can inhibit NLRP3 inflammasome-mediated pyroptosis and alleviate neuroinflammation in Alzheimer’s disease (Cai *et al.*, 2022). This study, along with other emerging evidence, suggests that inflammasome activation and subsequent pyroptosis might exacerbate the neuroinflammation and neuronal injury observed in neurodegenerative conditions, opening avenues for further investigation as potential therapeutic targets.

1.6.5.5 Role of pyroptosis in cardiovascular diseases

Emerging evidence shows pyroptosis in the pathogenesis of cardiovascular diseases like atherosclerosis and myocardial infarction. Specifically, activation of the NLRP3 inflammasome and subsequent pyroptosis in vascular cells are evidently linked to both arterial inflammation and plaque development, underscoring a crucial role for this cell death pathway in cardiovascular disease progression (Liu *et al.*, 2018). Rauf *et al* provided a comprehensive review on the role of pyroptotic inflammasome in myocardial infarction, with evidence that inflammation induced by ischaemic reperfusion injury through the pyroptotic pathway contributes to cardiomyocyte death, excessive scar formation, and poor ventricular remodelling (Rauf *et al.*, 2019). In addition, the introduction of caspase 1 inhibitor was shown to reduce the infarct size in a Langendorff model of ischaemia reperfusion injury on an isolated rat hearts (Do Carmo *et al.*, 2018).

1.6.5.6 Role of pyroptosis in anthracycline induced cytotoxicity

As previously described, chemotherapeutic agents such as doxorubicin are essential in the treatment of cancer. However, its anti-tumour effect can be a double-edged sword that may inflict an irreversible damage to normal cells like the heart. Thus, understanding the molecular mechanisms of cytotoxicity induced chemotherapeutic agents in healthy cells will help to showcase potential therapeutic targets to alleviate the issue.

Meng *et al* proposed that doxorubicin triggers pyroptosis through Terminal Differentiation-Induced Non-Coding RNA (TINCR) (Meng *et al.*, 2019, Christidi *et al.*, 2021). Up-regulation of TINCR recruits IGF2BP, leading to a subsequent increase in NLRP3 expression. This enhanced NLRP3 inflammasome assembly activates caspase 1, culminating in cleavage GSDMD-NT and the release of pro-inflammatory cytokines, IL-1β and IL-18. Notably, pharmacological inhibition of NLRP3 with MCC950 effectively protected cells from doxorubicin-induced pyroptosis, supporting the central role of this inflammasome in the process (Meng *et al.*, 2019).

An alternative pathway for doxorubicin-induced pyroptosis involving mitochondrial Bnip3 activation has been suggested (Zheng *et al.*, 2020). Doxorubicin upregulates the BH3-only protein Bnip3, triggering a downstream cascade that

activates caspase 3 and culminates in GSDME-dependent pyroptosis. Disrupting GSDME or silencing Bnip3 expression effectively protects cardiomyocytes from doxorubicin-induced cell death in vitro.

1.7 Assessment of anthracycline-induced cardiotoxicity: the role of biomarkers

Prompt diagnosis of anthracycline-induced cardiotoxicity is paramount for mitigating detrimental side effects. Although commonly employed as a non-invasive diagnostic assessment, electrocardiogram, echocardiography and radionuclide angiography demonstrate limited diagnostic sensitivity and predictive power. Endomyocardial biopsy remains the most sensitive and specific test, yet its invasive nature restricts its applicability.

Serum protein biomarkers play an important role in the clinical assessment of myocardial injury. These macromolecules, primarily found within cardiac myocytes, serve as indicators of both cellular damage and the loss of sarcolemmal integrity. Notably, the diagnostic utility of many cardiac biomarkers hinges on their limited half-life, necessitating precise timing of sample collection for accurate diagnosis of cardiac dysfunction and myocardial injury. The following subchapters will outline briefly the common cardiac biomarkers used in the assessment of anthracycline-induced cardiotoxicity.

1.7.1 Cardiac troponins

Cardiac troponin release holds substantial prognostic value in myocardial infarction and other heart diseases.

When investigated as an early biomarker for cancer cardiotoxicity, consistent troponin elevations are observed in 21%-40% of patients following anthracycline chemotherapy, regardless of the specific assay employed (Cardinale *et al.*, 2004). Within the context of cancer chemotherapy-induced cardiotoxicity, rising troponin levels are likely to reflect both cardiomyocyte death and myofibril degradation, serving as a predictor of both cardiotoxicity itself and major adverse cardiovascular events.

However, McGowan *et al* contended that baseline troponin might be elevated due to the burden of malignant disease itself (McGowan *et al.*, 2017). They reviewed a study that evaluated 78 patients with mixed acute myeloid and non-Hodgkin

lymphoma (Auner *et al.*, 2003). Autner *et al* found that baseline troponin-T levels exceeding 70 ng/L were observed in 3.8% of the cohort, highlighting the potential influence of the underlying malignancy itself on this biomarker.

1.7.2 B-type natriuretic peptide

B-type natriuretic peptide (BNP), a cardiac neurohormone secreted by the ventricles in response to volume overload and pressure stress, serves as a marker of myocardial dysfunction (Luchner *et al.*, 1998). Its release directly correlates with ventricular wall tension, generally aligning with echocardiographic indices of systolic and diastolic dysfunction as well as clinical heart failure. While BNP is included in European guidelines for diagnosing chronic heart failure and cardio-oncology, numerous studies suggest its limited sensitivity for detecting drug-induced cardiotoxicity (Sandri *et al.*, 2005, Nousiainen *et al.*, 2002). Individual patient variability in BNP levels, influenced by physiological characteristics, further complicates the establishment of a universal cut-off value (Vogelsang *et al.*, 2008).

1.7.3 MicroRNA

MicroRNAs (miRNAs), small non-coding RNAs, play a crucial role in regulating gene expression by post-transcriptionally silencing messenger RNA (mRNA) or inhibiting its translation. In particular, miRNA expression profiles exhibit substantial heterogeneity within organs, as exemplified by distinct profiles observed in cardiac arteries compared to the myocardium itself. Such heterogeneity highlights cell-type-specific expression patterns.

Few studies have looked at the expression of mRNA during doxorubicin induced cardiotoxicity. For instance, the role of miRNAs as cardiotoxicity biomarkers was investigated using human-induced pluripotent stem cells-derived cardiomyocytes (hPSC-CM) that were exposed with doxorubicin (Chaudhari *et al.*, 2016). Following exposure of 156 nM doxorubicin over 6 days, quantitative reverse transcription-PCR (qRT-PCR) analysis revealed significant alterations in the expression levels of 14 miRNAs. Notably, this detection preceded the release of cytotoxicity marker lactate dehydrogenase .

Unfortunately, many established cardiac biomarkers lack the sensitivity and specificity required for early detection of myocardial damage or failure, particularly in

the context of drug-induced cardiotoxicity. For example, the translation of troponin I from pre-clinical to clinical settings for assessing cardiotoxicity has proven challenging. An in vivo rat study demonstrated no significant changes in troponin I levels following administration of a clinically relevant doxorubicin dose, underlining its limitations (Borders *et al.*, 2013).

Moreover, our understanding of these biomarkers' effectiveness in identifying subclinical myocardial injury induced by drugs remains limited. Therefore, the need for a randomised controlled trial in human, such as ERIC-ONC trial, will prove pivotal in determining the value biomarkers such as troponin T, BNP, and miRNA as well as echocardiography in the assessment of subclinical myocardial injury in anthracycline-treated cancer patients (Chung *et al.*, 2016).

1.8 Prevention, knowledge gap and research contribution

1.8.1 Prevention

To counteract the risk of anthracycline-induced cardiotoxicity, clinicians implement various preventive measures. Primary preventive strategies prioritise limiting cumulative anthracycline dose, using less cardiotoxic anthracycline analogues, and utilising liposomal formulations of anthracyclines. Additionally, serial electrocardiogram or echocardiogram are used to monitor arrhythmias (i.e. QT prolongation) and left ventricular dysfunction, respectively,

Lifestyle corrective measures is of paramount importance as a strong link exists between cancer and cardiovascular risk factor. Furthermore, new evidence emerge on the protective role of exercise on cardiotoxicity (Barish *et al.*, 2019).

Withholding chemotherapy treatment temporarily or adjusting the chemotherapy cycle interval are implemented following multi-disciplinary assessment between cardiology, oncology, and other relevant specialties when clinical concerns of cardiotoxicity are suspected.

The use of cardioprotective drugs emerges as a potential complementary approach to anthracycline treatment modifications, dosage limitations, or interruptions, aiming to mitigate the cardiotoxic effects and potentially improve treatment outcomes.

Meanwhile, dexrazoxane, an iron chelator, has been used in small clinical studies and proven to be an effective cardioprotector. Importantly, administration of dexrazoxane does not lead to a reduction in anti-tumour efficacy, overall survival, or a clinically significant increase in the risk of developing second primary malignancies. In a systematic review and meta-analysis study by Macedo *et al*, the cardioprotective efficacy of dexrazoxane was evaluated in anthracycline-treated breast cancer patients, including those receiving trastuzumab. While acknowledging the limitations of the included studies (seven randomized and two retrospective non-randomized), the analysis suggests that dexrazoxane may independently reduce the risk of heart failure and cardiac events, even in patients with prior anthracycline exposure (Macedo *et al.*, 2019).

In addition, several commonly used heart failure medications, including beta-blockers, angiotensin-converting enzyme inhibitors (ACEis), angiotensin receptor blockers (ARBs), aldosterone antagonists, and statins, have demonstrated potential cardioprotective effects against anthracycline-induced cardiotoxicity. Cardinale *et al* comprehensively reviewed the existing literature on each of these agents, highlighting relevant studies (Cardinale *et al.*, 2020). However, limitations to these studies include relatively small sample sizes, necessitating further investigation with larger, well-designed clinical trials to establish their efficacy and optimal use in preventing anthracycline cardiotoxicity.

A recent meta-analysis encompassing 17 randomised clinical trials and 1,984 adult patients, who underwent chemotherapy and received either cardiovascular therapies or placebo with follow-up (four weeks or longer), revealed moderately higher left ventricular ejection fraction (LVEF) values in the group receiving neurohormonal therapies at follow-up (Vaduganathan *et al.*, 2019). However, it is important to note that the observed changes in LVEF were relatively small and the benefit of having relatively small LVEF protection over the long course of chemotherapy remains unanswered.

This section has provided an overview of some established strategies for managing anthracycline-induced cardiotoxicity. However, it is vital to acknowledge other promising preventative and therapeutic approaches that are undergoing evaluation in pre-clinical and clinical studies (Chung *et al.*, 2016, Kuno *et al.*, 2022,

Boutagy *et al.*, 2020). These additional strategies, while not discussed here, remain equally significant in the ongoing pursuit of cardioprotection against anthracycline-induced cytotoxicity.

1.8.2 Knowledge gap and research contribution

Despite the exponential growth of our knowledge in anthracycline-induced cardiotoxicity, review of existing literature suggest that there remains a gap in our knowledge.

First, anthracycline cytotoxicity involves a multitude of proposed molecular mechanisms. However, emerging evidence points towards additional cell death pathways such as autophagy, necroptosis and pyroptosis, opening new avenues for understanding anthracycline-induced cytotoxicity. Without overlooking their significance, autophagy and necroptosis, along with other new potential death pathways, are not discussed in this chapter. Notably, anthracyclines might trigger distinct pathways in cancer cells compared to cardiomyocytes with potential interplay, but this remains uncertain due to the historical research focus on individual pathways in isolation.

Second, studies of anthracycline cytotoxicity historically put a great emphasis on cardiomyocytes (Michihiko *et al.*, 2006, Cappetta *et al.*, 2018). However, recent evidence shows other structures such as endothelial lining of coronary vessels are also disrupted leading to endothelial dysfunction (Wojcik *et al.*, 2015, Luu *et al.*, 2018, Galan-Arriola *et al.*, 2021).

Third, studies of anthracycline cytotoxicity predominantly investigate doxorubicin rather than its supposed active metabolites, doxorubicinol. It is not fully elucidated whether doxorubicinol triggers the same cytotoxicity pathway as doxorubicin.

Recognising the existing gap in knowledge regarding the diverse cell death pathways involved in anthracycline-induced cytotoxicity, particularly the potential role of pyroptosis, this thesis aims to contribute to the development of this field by investigating the potential involvement of pyroptosis in anthracycline-induced cytotoxicity. As detailed in the following chapters, my research will explore whether doxorubicin or doxorubicinol administration triggers dose-dependent cell death and

elucidates the predominant cell death pathway. This objective will be achieved by comparing GSDMD-mediated pyroptosis with caspase 3-mediated apoptosis across five distinct cell types: cardiomyocyte cell line, coronary artery endothelial cells, cardiac microvascular endothelial cells, breast cancer and acute myeloid leukaemia cell lines. This multi-cellular approach will enable a comprehensive assessment of potential differences in anthracycline-induced cytotoxicity among these diverse cell types.

1.9 Conclusion

Rising cancer survival rates elevate concerns about the future prevalence of anthracycline-induced cardiotoxicity. While recent discoveries shed light on promising new therapeutic targets, a significant gap remains in our understanding of the complex mechanisms underlying this condition.

Notably, pyroptosis emerges as one of the potential contributors to anthracycline cytotoxicity, but the precise role of pyroptosis in anthracycline cytotoxicity in the heart remains unclear. Therefore, elucidating the intricate interplay between pyroptosis and anthracycline cytotoxicity, particularly in both cardiomyocytes and their vascular supply, presents a valuable opportunity to deepen our understanding of this issue. By bridging this knowledge gap, this doctoral research can add to the growing knowledge of anthracycline cytotoxicity and pave the way for the identification and development of novel therapeutic targets capable of conferring cardioprotection during anthracycline treatment. To address this need, my research examines the hypothesis whether pyroptotic cell death contributes to anthracycline-induced cytotoxicity.

Chapter 2 Hypothesis and Research Aims

2.1 Hypothesis

The overall aim of this doctoral research is to investigate whether the pyroptotic cell death pathway contributes to anthracycline-induced cardiotoxicity.

The hypothesis is that the pyroptotic cell death pathway contributes to anthracycline-induced cardiotoxicity.

2.2 Research aims

There are five main research aims as outlined below, which will be further delineated in detail in the subsequent chapters.

In this research, doxorubicin and its active metabolite doxorubicinol will be used in the experiments. Doxorubicin is a widely used chemotherapy drug to treat a wide range of malignancies and it is well-documented to inflict cardiotoxicity. Using doxorubicin in the experiments will be clinically relevant as it contributes to the growing need to further evaluate its mechanism of action.

2.2.1 To establish and assess an *in vitro* model cell death following treatment with doxorubicin or its active metabolite doxorubicinol.

The following cells or cell lines will be used:

1. H9c2 cell line (an immortalised rat ventricular myoblast cell line).
2. Human Coronary Artery Endothelial Cells (HCAEC), a primary coronary artery endothelial cell from a healthy human donor.
3. Human Coronary Microvascular Endothelial Cells (HCMEC), a primary coronary microvascular capillary endothelial cell from a healthy human donor.

2.2.2 To characterise the morphological alterations observed in treated cells.

In addition to the cells mentioned in Section 2.2.1, the following cells will be used:

1. MCF-7 cell line, a breast cancer cell line harvested from the pleural fluids of a human donor.
2. THP-1 cell line, an acute myeloid leukaemia cell line from a human donor.

2.2.3 To evaluate the role of pyroptosis and apoptosis in treated cells.

Using the fluorescent staining methods, apoptosis was investigated following the treatment of doxorubicin or doxorubicinol, with the Annexin V staining which was known to be a specific staining for the apoptosis process . The propidium iodide staining was used as a marker to visualise cells with damaged cell membranes, which may be attributable to the pyroptosis process

2.2.4 To evaluate whether Gasdermin D processing occurs in treated cells.

Using the Western blot technique, the expression of the full-length Gasdermin D and its cleaved N-Terminal Gasdermin D were investigated on the following cells:

1. H9c2 cell line.
2. Primary human HCAEC.
3. Primary human HCMEC.
4. MCF-7 breast cancer cell line.
5. THP-1 acute myeloid leukaemia cell line.

2.2.5 To evaluate whether Caspase 3 processing occurs in treated cells.

Using the Western blot technique, the expression of caspase 3 and its cleaved form were investigated to evaluate whether the apoptotic process contributes to anthracycline-induced cardiotoxicity instead of pyroptosis. The cells of interest are similar to those outlined in Section 2.2.4 above.

Chapter 3 General research methods

The practical recommendation in preclinical studies outlined by Bøtker *et al* was adopted as standard where applicable (Bøtker *et al.*, 2018). When possible, positive or negative controls were used while respecting the principle of the 3Rs: Replacement, Reduction, and Refinement, throughout the setting of the experiment design and execution.

3.1 Cell Culture

3.1.1 Types of Cells

Table 3.1 summarises the types of cells being used in this thesis

Cell	Company (Catalogue number)	Origin	Desired confluency (%)
H9c2	n/a	Rat	70-80
Human Coronary Artery Endothelial Cells (HCAEC)	PromoCell (C-12221)	Human	90
Human Cardiac Microvascular Endothelial Cells (HCMEC)	PromoCell (C-12285)	Human	90
MCF-7 breast cancer cell line	ATCC (HTB-22)	Human	70-80
Undifferentiated THP-1 monocytic cell line from acute myeloid leukaemia	A gift from the Eastman Dental Institute, UCL	Human	100,000 cells / mL

Table 3.1 Types of cells used in this PhD project.

The rationale for different cell types used will be discussed further in the introduction subsection of the respective chapters.

3.1.2 General cell culture method

3.1.2.1 Materials

	Cells		
Materials	H9c2, MCF7 (adherent cells)	HCAEC, HCMEC (adherent cells)	THP-1 (suspension cells)
Cell media	Dulbecco's Modified Eagle solution (DMEM) 500 mL (Gibco, 41966-029) 50 mL Fetal Bovine Serum (FBS) (Sigma-Aldrich, F9665) 5 mL Penicillin / Streptomycin (Sigma-Aldrich, P4333)	Endothelial Cell Growth medium MV2 + Supplement Mix (Promo Cell, Cat No C-22022)	RPMI-1640 medium with L-glutamine and sodium bicarbonate 500 mL (Sigma-Aldrich, R0883) 0.05 mM Beta-Mercaptoethanol (BME) (Merck, M3148) 50 mL Fetal Bovine Serum (FBS) (Sigma-Aldrich, F9665) 5 mL Penicillin / Streptomycin (Sigma-Aldrich, P4333)
Cell washing	Dulbecco's Phosphate Buffer Saline (PBS) 500 mL bottle (Sigma-Aldrich, D8537)	Dulbecco's PBS 500 mL bottle (Sigma-Aldrich, D8537)	Dulbecco's PBS 500 mL bottle (Sigma-Aldrich, D8537)
Dissociating agent	TrypLE™ Express Enzyme (Gibco, 12604-013)	Accutase (Promo Cell, Cat No C-41310)	Accutase (Promo Cell, Cat No C-41310)
Cryopreservative agent	CellBanker™2 (Nippon Zenyaku Kogyo, Cat No 11914)	Cryo-SFM (PromoCell, Cat No C-29912)	CellBanker™2 (Nippon Zenyaku Kogyo, Cat No 11914)

Table 3.2 List of materials for cell culture.

Standard laboratory personal protective equipment will be adhered to throughout conducting all experiments. Table 3.2 outlines the materials required for general cell culture. All cells were cultured under sterile conditions in the tissue culture hood with regulated ventilation. All cells were incubated at 37ºC in a humidified atmosphere of 95% air and 5% CO_2 in an incubator.

3.1.2.2 General Cell Culture Subculture Protocol

The following method of cell subculture was adopted as the standard practice. The steps illustrated are in the context of cell subculture in a T75 flask.

Cells were cultured in the T75 flask (Greiner, reference number 65185) using their respective cell media and its growth supplement. The cells were regularly monitored every 48-72 h for growth and no bacterial contamination. Every cell culture cultivation method was conducted under a sterile hood. The hood was cleaned with a spray mixture of 80% ethanol and 20% sterilised water before and after. All cells were cultured in a humidified atmosphere of 95% air and 5% CO_2 at 37°C.

For subculturing or plating cells for experiments, cell media was removed, and the traces of serum were washed away with phosphate buffer saline (PBS). Cells were detached with the detaching agent (TrypLE™ Express Enzyme or Accutase) at 37°C in the incubator for 3 min and pelleted using the centrifugation machine for 5 min at 1.5 rpm for H9c2 and MCF7 cell, or 5 min at 1.1 rpm for HCAEC, HCMEC, and THP-1 cell.

The steps following cell subculture depended on the required task outlined in the subsequent sub-section below and thus would be explained accordingly.

3.1.2.3 Cell counting, splitting, freezing and storage

Following centrifugation, the supernatant was removed, and the pellet was resuspended with the supplemented media. Ten microliters were mixed with 10 µL of Trypan blue in a separate Eppendorf tube (1:1 dilution factor). From this mixture, 10 µL was laid onto the haemocytometer for cell counting under the microscope. The cells were plated according to the estimated number of cells counted and the desired seeding density.

For cell splitting, the cell was reinserted into the new flask following cell counting. The flask was left in the incubator for further culture. Alternatively, the cell was resuspended and mixed with cryopreserving agents such as CellBanker^{TM}2 for H9c2, MCF-7 and THP-1, or Cryo-SFM for HCAEC and HCMEC cells in a 1:1 volume ratio. The mixture was distributed into a cryopreservation vial and was subsequently stored in a -80^{o}C freezer until further use.

3.2 Drugs

The pharmacological agents used in this thesis are summarised in Table 3.3.

Drug	Company (catalogue number)	Concentration(s)
Doxorubicin Hydrochloride (DOX)	European Pharmacopeia (D2975000)	2.5 μM, 5 μM, 7.5 μM, 10 μM, 20 μM, 30 μM, 40 μM, 50 μM
Doxorubicinol Hydrochloride (DOXOL)	CaymanChem (22386)	2.5 μM, 5 μM, 7.5 μM, 10 μM, 20 μM, 30 μM, 40 μM, 50 μM
Lipopolysaccharides from Escherichia Coli O111:B4 (LPS)	Sigma-Aldrich (L2630)	50 ng/mL
Nigericin sodium salt	Sigma-Aldrich (N7143)	15 μM

Table 3.3 List of pharmacological agents used in this PhD.

The concentration of doxorubicin and doxorubicinol used in this research study is discussed in detail in Chapter 4 Subchapter 4.5.1. In brief, a plasma concentration of doxorubicin up to 2.5 μM is considered clinically relevant and covers the possible variation in the plasma concentration of doxorubicin of patients undergoing anthracycline-based chemotherapy. The doxorubicin dose between 5 μM and 10 μM may be appropriate in a subgroup of patients with impaired drug clearance, for instance, individuals with liver disease, or elderly patients. Concentrations of 10 μM and beyond are considered supraphysiological.

3.3 Measurement of LDH activity using a cytotoxicity assay

There is a range of commercially available cytotoxicity markers to estimate dead cells, but the LDH assay is the most common marker used to assess cytotoxicity (Riss *et al.*, 2019). LDH is a cytosolic enzyme present in many cell types. Damage to the plasma membrane releases LDH from the cytoplasm into the surrounding cell media *in vitro*. The presence of LDH in the cell media can be measured in which LDH catalyses the conversion of lactate to pyruvate via NAD+ reduction to NADH. NADH is then oxidised by diaphorase leading to the reduction of tetrazolium salt (INT) and, subsequently, formazan formation. Formazan can be measured using a spectrophotometer at 490 nm. Its level is directly proportional to the amount of LDH released and thus is indicative of cytotoxicity. Figure 3.1 gives a visual summary of the principle of LDH assay.

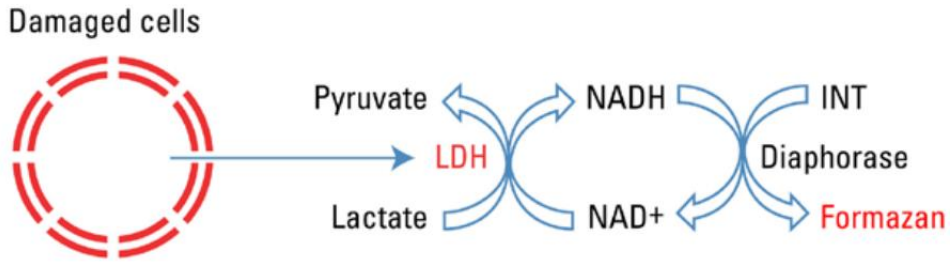

Figure 3.1 The principle of lactate dehydrogenase assay.

Following 18 h of treatment, the cytotoxic effect of doxorubicin and doxorubicinol on cell lines or primary cells was evaluated with an LDH Cytotoxicity Assay kit (CytoTox 96® Non-Radioactive Cytotoxicity Assay, Promega (G1781)) on a 96-well plate. LDH activity was assessed with a spectrophotometer to measure the absorbance value at two separate wavelengths. Using the Fluostar Omega plate reader (BMG Labtech), Omega MARS and Omega Data Analysis software, the absorbance was read at 490 nm and 680 nm.

To estimate the percentage of cell death, the absorbance of samples at 680 nm was subtracted from the respective absorbance at 490 nm. The absorbance of diluents was subtracted from the corresponding sample absorbance. The proportion of dead cells was then determined relative to the total absorbance value of cell media (control or varying concentration of doxorubicin or doxorubicinol) and live cells lysed using Triton X-100 (Sigma-Aldrich, CAS number 9036-19-5).

$$\%\ dead\ cells = \frac{dead\ cells}{dead\ cells + live\ cells}\ X\ 100$$

The mean percentage of dead cells was calculated from two technical replicates.

3.4 Microscopical analysis and fluorescent staining

Microscopical analysis using a brightfield or light microscope was performed to evaluate morphological alterations that occurred following the treatment of doxorubicin, doxorubicinol, or other variables such as LPS and Nigericin.

The fluorescent staining method was used to identify different types of cell death. An investigation was carried out to examine whether apoptosis occurs in cells following the treatment of doxorubicin or doxorubicinol with the Annexin V staining, a fluorescent staining dye known to be specific for apoptosis (Van Engeland *et al.*, 1998, Demchenko, 2013) (Figure 3.2). In brief, the Annexin V dye binds to apoptotic cells due to a structural change in its plasma membrane by surface exposure to phosphatidylserine (PS) while preserving its membrane integrity. PS is detected by its affinity to bind with Annexin V.

Propidium iodide (PI) staining was also used as a marker to visualise cells with damaged cell membranes. PI is a fluorescent dye that binds to DNA. PI is not permeant to cells with intact cell membranes. Thus, PI uptake can be used to distinguish dead cells with damaged plasma membranes regardless of the mechanism of death. Combining the Annexin V and PI staining helps distinguish between apoptotic cells (Annexin V-stained only), and cells that have damaged cell membranes such as pyroptotic cells allowing co-staining of Annexin V and PI, or PI-stained only.

Microscopical analysis was conducted using the GX-Capture-T light microscope and the GX-Capture-T software. The microscopical analysis and fluorescent staining were conducted after the cells were treated with doxorubicin or doxorubicinol at different concentrations for 18 h. Once the treatment was complete, the cell media in each group was replaced with a fresh cell media mixed with the fluorescein isothiocyanate (FITC)-Annexin V, Alexa Fluor™ 488 conjugate (Invitrogen, A13201) and Propidium Iodide (Invitrogen, P3566 at 1:500 ratio to the respective cell media volume. For instance, 1 µL of each Annexin V and propidium iodide (PI) into

cells in 500 µL of cell media. The cells were put back into the incubator for one hour to complete the incubation period as recommended by the supplier's manual.

Images of the cells were taken in a dark environment with the GX-Capture-T light microscope and its software program. Three images were obtained: one in a brightfield channel, one in a red channel to visualise the PI staining, and one in a green channel to visualise the Annexin V staining. The brightfield, red and green channel images were superimposed to generate one merged phase-contrast image with the aid of the software program. Similarly, the fluorescent-only pictures were generated by superimposing the red and green channels only. In this manner, the phase-contrast image with the fluorescent-only image can be visualised and compared side by side. Each image was taken under 10x and 20x power magnification. However, the 20x magnification was found to be the optimal power of magnification to appreciate the morphological alterations as well as fluorescent staining.

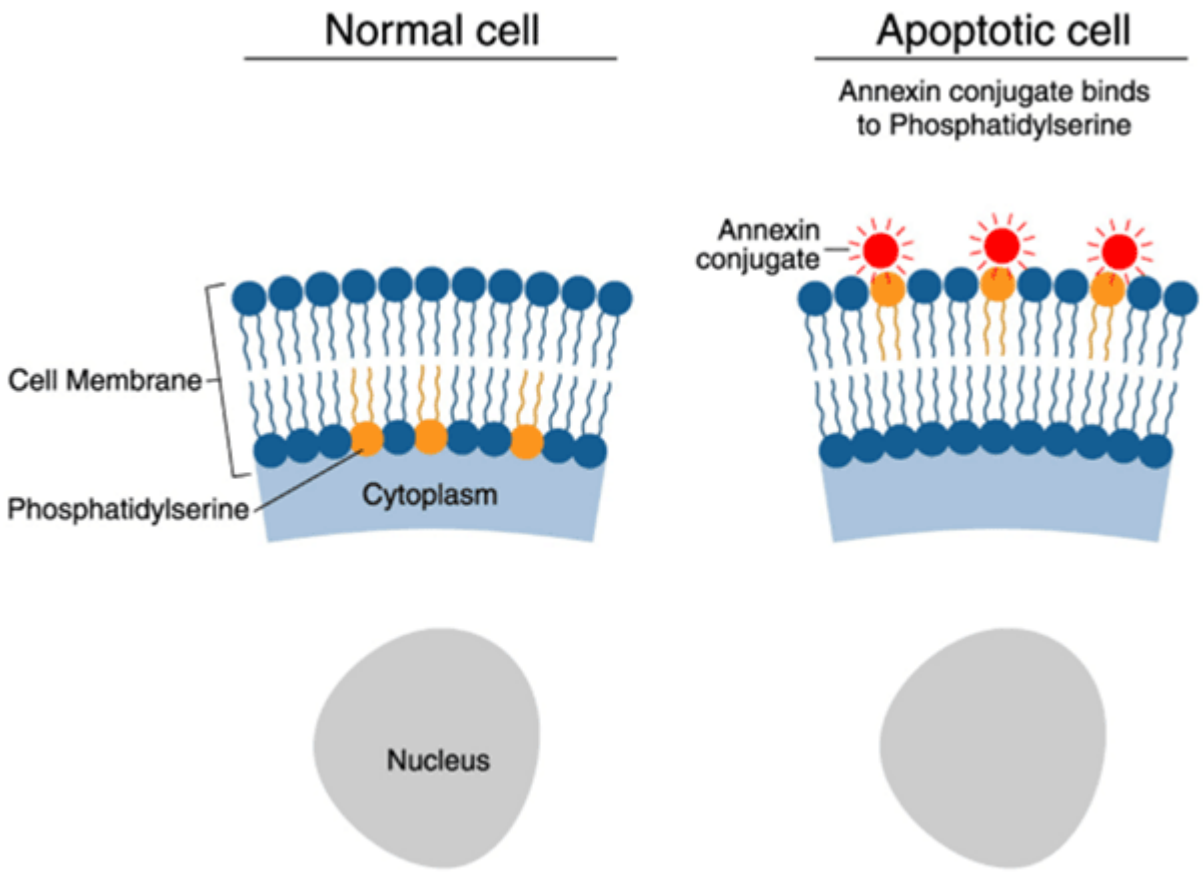

Figure 3.2 The principle of Annexin V binding to the exposed phosphatidylserine (PS). In normal healthy cells, PS is located on the cytoplasmic side of the cell membrane. In apoptotic

cells, PS is translocated to the extracellular side of the membrane, where Annexin V binds to PS. Adapted from ThermoFisher website (https://www.thermofisher.com/uk/en/home/life-science/cell-analysis/cell-viability-and-regulation/apoptosis/annexin-v-staining.html)

3.5 Cell lysis and Western blot

Western blot is a widely accepted semi-quantitative analytical method to detect specific proteins in a given sample. This method was first published in 1979 by two different groups proposing different methods of protein transfers (Renart *et al.*, 1979, Towbin *et al.*, 1979). Renart *et al* transferred proteins from the sodium dodecyl sulphate (SDS) gel into paper, whereas Towbin *et al* transferred proteins from nitrocellulose gel. Nowadays, nitrocellulose or Polyvinylidene Difluoride (PVDF) membranes are commonly used, including in the lab this research was carried out at the Hatter Cardiovascular Institute. Interestingly, the technique was not named Western blot until Neal W. Burnette published his paper in 1981 (Burnette, 1981). Despite the advancement in molecular biology techniques, Western blot remains one of the indispensable tools in the field of cell and molecular biology and one that led me to persevere through numerous and lengthy troubleshooting throughout PhD research.

The Western blot technique follows four main objectives: protein separation by size, transfer to a solid support (for example, PVDF membrane), marking target protein with primary and secondary antibodies, and visualisation. Figure 3.3 illustrates the visual summary of the Western blot workflow.

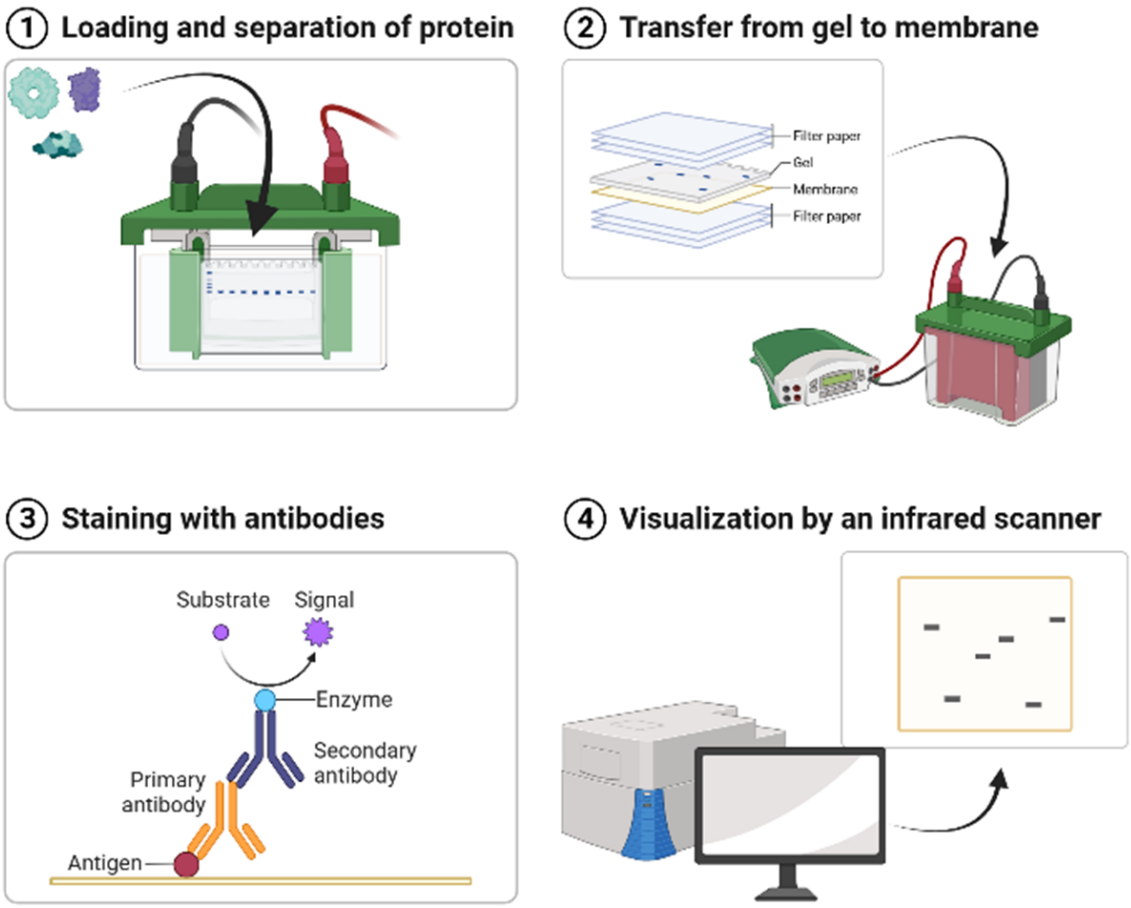

Figure 3.3 The visual summary of the Western blot workflow. The visual summary was created on www.BioRender.com

The primary antibodies used in the Western blot experiments are listed in Table 3.4 below.

Gasdermin D primary antibody				
Name	Source	Immunogen	Reactivity	Supplier (Reference)
Gasdermin D E9S1x	Rabbit monoclonal antibody	Recombinant synthetic peptide	Human, Rat, Mouse, Hamster	Cell Signal (#39754)
Anti-GSDMD 219800	Rabbit monoclonal antibody	Recombinant fragment	Mouse, Rat	Abcam (EPR20859)

Anti-GSDMD 209845	Rabbit monoclonal antibody	Recombinant synthetic peptide	Mouse	Abcam (EPR19828)
Caspase 3 antibody				
Name	Source	Immunogen	Reactivity	Supplier
Anti Caspase 3 Antibody (#9662)	Rabbit polyclonal antibody	Synthetic peptide	Human, rat, mouse, monkey	Cell Signal (#9662)
Housekeeping antibody				
Name	Source	Immunogen	Reactivity	Supplier
Beta-actin antibody (C4)	Mouse monoclonal antibody	n/a	Mouse, rat, human, rabbit	Santa Cruz (sc-4778)

Table 3.4 List of antibodies used in the Western blot experiments. The dilution factor of all primary antibodies is 1:1000, except the housekeeping antibody (1:2000).

Several different anti-GSDMD primary antibodies were tested in this research Western blot analysis. The respective suppliers of these antibodies suggested that their products should work against the cell lines or primary cells of human, rat, or mouse sources. However, having tested all three anti-GSDMD primary antibodies, it was found that E9S1X from Cell Signal appeared to be the only one that was able to detect both full-length Gasdemin D (~53 kDa) and the N-Terminal Gasdermin D (~32 kDa), particularly in the positive control sample (See Figure 3.4). Similarly, the caspase 3 antibody was able to detect both full-length caspase 3 (~30 kDa) and its cleaved form (~17 kDa) appropriately.

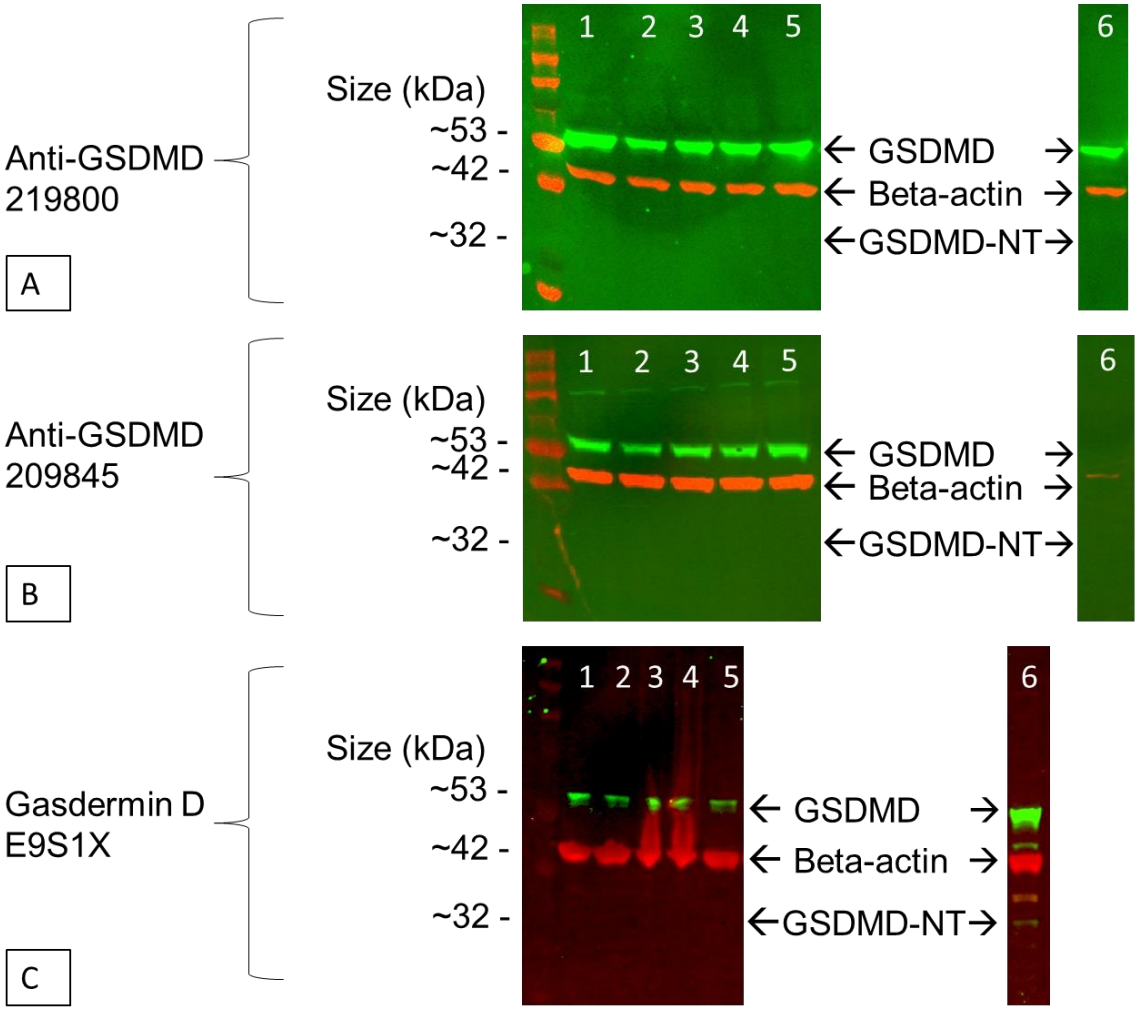

Figure 3.4 The Western blot sample of three different anti-GSDMD primary antibodies. H9c2 cell line treated with DOX at different doses (lanes 1-5) for 18 h. THP-1 cell (lane 6) was treated with LPS 50 ng/mL for 4 h and Nigericin 15 μM for 1 h, as a positive control of pyroptosis. GSDMD was detected in H9c2 lanes by all three anti-GSDMD primary antibodies, but not the GSDMD-NT. Anti-GSDMD 219800 detected GSDMD in THP-1, but not GSDMD-NT (A). Anti-GSDMD 209845 did not detect GSDMD and GSDMD-NT in THP-1 (B). Both GSDMD and GSDMD-NT were detected by Gasdermin D E9S1X (C).

Lane 1: H9c2 control, Lane 2: H9c2 + DOX 2.5 μM, Lane 3: H9c2 + DOX 5 μM, Lane 4: H9c2 + DOX 7.5 μM, Lane 5: H9c2 + DOX 10 μM, Lane 6: THP-1 + LPS 50 ng/mL & Nigericin 15 μM.

Gasdermin E9S1X is a recombinant monoclonal antibody. Traditional polyclonal and monoclonal antibodies are the product of normal B cell development and genetic recombination. While polyclonal antibodies are secreted by multiple B cell clones and they recognise multiple antigenic epitopes, monoclonal antibodies come

from a single B cell clone and are specific to one epitope The production of recombinant monoclonal antibodies involves *in vitro* genetic manipulation. After cloning the antibody genes into an expressive vector, it is then transfected into an appropriate host cell line for antibody expression. Mammalian cell lines are usually used for recombinant antibody production.

β-Actin Antibody (C4) is an IgG_1 κ mouse monoclonal beta-Actin antibody that detects the beta-Actin protein in mammalian and non-mammalian cells. At least six types of Actin are present in mammalian tissues and fall into three classes. α-Actin expression is limited to various types of muscle, whereas β-Actin and γ-Actin are the principal constituents of filaments in other tissues. Since β-Actin is expressed in all eukaryotic cells, it serves as a good target protein the Western blot experiments in this research as a single housekeeping antibody could be used across cell lines or primary cells from different origins.

3.5.1 Collecting protein sample for cell lysis and Western blot

The expression GSDMD, GSDMD-NT, and full-length caspase 3 and its cleaved caspase 3 in respective cells were evaluated using Western blot. Following the relevant cell culture protocol, the cells were plated at 1 x 10^6 cells per 100 mm dish. The cell media were changed every two or three days until the cells reached target confluency. Thereafter, the cell media were changed with the respective treatment, such as control (cell media only), doxorubicin or doxorubicinol, added accordingly. The cell dishes were left incubated for 18 h. Afterwards, the cells were washed with ice-cold PBS twice. Then, they were scrapped into ice-cold PBS and pelleted at 600 rpm at 4°C for 5 min. The pellet was lysed in 50 µL of radioimmunoprecipitation assay (RIPA) lysis buffer mixed with EDTA, protease inhibitor, and phosphatase inhibitor (Tris pH 6.8 [100 mM], NaCl [300 mM], NP40 0.5%, Halt protease inhibitor cocktail, Halt phosphatase inhibitor cocktail, 5 mM EDTA (all from Thermo Scientific, UK) adjusted to pH 7.4). The protease inhibitor, phosphatase inhibitor, and EDTA were each supplemented into the RIPA lysis buffer at a 1:100 ratio. This amount of lysis buffer was sufficient to dissolve cells and gentle vortex through an insulin syringe. Cell debris was pelleted at 10,000 rpm at 4°C for 10 min to remove debris and DNA.

Next, protein quantity in samples was quantified by bicinchoninic assay (BCA) Protein assay (Thermo Scientific, UK, 23208). Briefly, this 96-well plate colourimetric assay uses bicinchoninic acid and copper sulphate at a 50:1 ratio. A set of bovine serum albumin (BSA) at known concentrations was used as protein standard samples. Two µl of each sample was then added into 198 µL of BCA/copper sulphate mix per well and incubated for 30 min at 37°C. FLUOstar Omega microplate reader (BMG Labtech, UK) was used to measure the absorbance value of the samples. The protein concentrations of the samples were then interpolated by plotting the absorbance results against the protein standard curve.

From this, the samples were accordingly diluted to load the same amount of protein in each gel well. If not specified in subsequent sections, 25 µg was the standard protein load. Protein lysates were denatured by mixing lysates with 10% Beta-mercaptoethanol (BME) in NuPAGE LDS buffer (Protein lysate: BME&LDS ratio of 3:1). Samples were then heated at 80°C for 10 min. The samples can be used immediately for western blot analysis or cooled and stored at -80°C for use at a later date.

3.5.2 Western blot analysis

For Western blot, 25 µg of samples were loaded into a 10% or 4-12% NuPAGE Bis-Tris gel (Thermo Fisher, UK) depending on the size of the target protein. Additionally, 8 µL of the Precision Plus Protein™ Dual Xtra protein standard (BioRad, UK) was loaded on the gel to estimate the molecular weight of sample proteins. The gels were placed in the XCell SureLock™ Mini Cell chamber (Invitrogen, UK), filled with NuPAGE SDS MOPS Bis-Tris Running Buffer (Thermo Scientific, UK). Sample proteins were separated by electrophoresis at 90 V for 30 min and subsequently, at 120 V for 1 h and 30 min using a high current power supply.

The proteins were transferred from the gel to the PVDF membrane (Immobilon-FL or Immobilon-P hydrophobic PVDF transfer membrane, Merck Millipore, UK) which was activated in 100% methanol for 2 min. The gel and the transfer membrane were sandwiched between filter paper and a fibre pad/sponge in a cassette. The cassette was subsequently loaded into the Mini Protean II™ chamber system (BioRad, UK) filled with transfer buffer (containing 25 mM Tris base, 200 mM glycine and 20% methanol). An ice pack was slotted in the chamber tank and the external surrounding

was filled with ice. The transfer was run at 120 V for 1 h and 20 min with a magnetic stirrer rotating in the base of the chamber.

Thereafter, the membrane was briefly immersed with the ponceau stain solution to confirm the binding of protein on the PVDF membrane blot, before blocking the membrane with 5% Bovine Serum Albumin (BSA) in 0.1% Tween in Tris-buffered saline (TBST) to prevent unspecific binding for 1 h.

The membrane was incubated with monoclonal primary rabbit antibodies mixed in BSA/TBST, namely a recombinant GSDMD E9S1X monoclonal antibody (1:1000 ratio) (Cell Signal, #39754), or Caspase 3 rabbit antibody (1:1000 ratio) (Cell Signal, #9662). The housekeeping protein used in this research was an anti-Beta-actin (C4) mouse monoclonal antibody (1:2000 ratio) (Santa Cruz, sc-47778). The incubation was 18 h at 25 oscillations/min at 4°C. The GSDMD E9S1X, Caspase 3, and Beta-actin antibodies all have cross-reactivity with human and rat cells according to the respective supplier's product information.

The following day, the membrane was washed with 0.1% TBST three times for 10 min. The membrane was subsequently incubated with goat anti-rabbit IRDye® 800CW secondary antibody (1:15,000) and goat anti-rabbit IRDye® 680LT secondary antibody (1:20,000) in 5% BSA in 0.1% TBST. After 1 h of incubation at 25 oscillations/min at room temperature, the membrane was washed. The goat anti-rabbit IRDye® 800CW secondary antibody will give off green colour immunolabelled bands, whereas the goat anti-rabbit IRDye® 680LT secondary antibody will give off red colour immunolabelled bands. Immunolabelled bands were visualised with an Odyssey infrared scanner and its imaging software from Li-Cor Biosciences (Image Studio Lite Ver 5.2). Protein expression was quantified using Odyssey software. The background signal was subtracted from the data. Figure 3.5 illustrates the simplified schematic of the Western blot process conducted in this research.

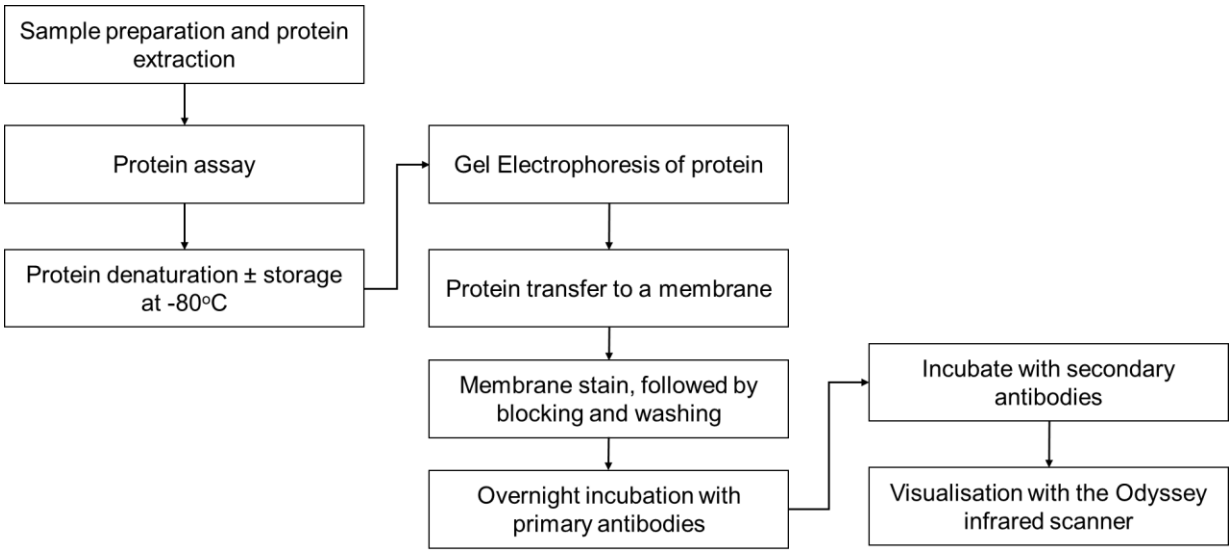

Figure 3.5 The visual summary of Western blot workflow.

3.6 Statistical analysis

GraphPad Prism 6.0 software was used to perform statistical analysis. Results were presented as mean ± standard error of the mean.

Mean is calculated as the sum of all the values obtained from individual experiments divided by the total number of experiments (N).

The standard error of the mean is the standard deviation of the distribution of sample means. SEM is calculated as standard deviation divided by the square root of the sample size.

Repeated measures of two-way analysis of variance (ANOVA) followed by Tukey's multiple comparison tests were used unless specified otherwise. Two-way ANOVA was conducted to compare data between the means of three or more samples that have been split into two variables or factors. This statistical analysis helps to interpret how the two factors (concentration and drugs) affect a variable response (i.e. cell death) and whether there is an interaction effect between the two factors on the response variable. A value of $p < 0.05$ was considered statistically significant and is labelled as * in the result graphs. In addition, **$p < 0.01$, ***$p < 0.001$, ****$p < 0.0001$, ns not significant.

Chapter 4 Anthracycline-induced cytotoxicity in a rat cardiomyocyte cell line

4.1 Introduction

The H9c2 cell line is an immortalised embryonic rat cardiomyocyte of ventricular origin. It is a sub-clone line of the original cell line derived from embryonic BD1X rat heart tissue by Kimes and Brandt (Kimes *et al.*, 1976). The H9c2 cell line is widely used as a substitute for primary cardiomyocytes *in vitro* models in cardiovascular research, particularly in cardiotoxicity studies (Hescheler *et al.*, 1991, Kuznetsov *et al.*, 2015, Dallons *et al.*, 2020).

Apart from the H9c2 cell line, there are alternative cardiac myocytes-like rodent cell lines such as the HL-1 cell line. The HL-1 cell line is an immortalised, adult mouse cardiomyocyte of atrial origin (Kuznetsov *et al.*, 2015). Although both cell lines have been widely used to investigate the mechanism of cardiotoxicity, the H9c2 cell line is more appropriate for my experiment as it would allow assessment of the role of anthracycline-induced cytotoxicity in a cell line of ventricular origin.

4.2 Research hypothesis, aims and objectives

The main hypothesis investigated in this chapter was that the pyroptotic cell-death pathway contributes to anthracycline-induced cardiac myocyte injury.

To investigate this hypothesis, the extent of lytic cell death observed in H9c2 cells treated with doxorubicin (DOX) or doxorubicinol (DOXOL), was measured using the lactate dehydrogenase cytotoxicity assay. The assessment of whether the morphological alterations in treated cells resembled the pyroptotic process and whether Gasdermin-D (GSDMD) with its N-Terminal Gasdermin-D (GSDMD-NT) were detected in treated cells using Western blot analysis was also carried out.

The specific experimental objectives addressed in this chapter are:

1. To establish and assess an *in vitro* model of cardiac cell death following treatment with doxorubicin or its metabolite doxorubicinol.
2. To characterise the morphological alterations observed in treated cells.
3. To determine the extent of pyroptosis and apoptosis in treated cells.

4. To evaluate whether Gasdermin D processing and caspase 3 processing occur in treated cells.

4.3 Methods

4.3.1 H9c2 cell cultivation

The H9c2 cell line was cultured in DMEM containing high glucose supplemented with 10% FBS, and 1% penicillin/streptomycin in T75 tissue culture flasks (surface area 75 cm^2). All cells were incubated at 37^oC in a humidified atmosphere of 5% CO_2. H9c2 cells growth medium was replaced every 2-3 days and the cells were serially passaged to achieve 70-80% confluency for the experiment. The detailed cell cultivation technique and its material are described in Chapter 3 Section 3.1.2 and Table 3.2, respectively.

4.3.2 Doxorubicin or doxorubicinol treatment

Once the cells reached the target confluency, the medium was subsequently replaced with a fresh media (control) or with medium containing either doxorubicin (DOX) or doxorubicinol (DOXOL).

The concentrations of doxorubicin and doxorubicinol used were described in Chapter 3 (See Table 3.3). Doxorubicin and doxorubicinol concentrations between 10 µM and 50 µM were initially used to set up an experimental model using the H9c2 cell line. This model was used to assess whether measuring the dose–cell death response using LDH assay works consistently. The concentration range was subsequently reduced from 0 µM (control) to 10 µM.

4.3.3 Lactate dehydrogenase assay

The lactate dehydrogenase assay experiment was conducted to estimate cell death based on LDH release from lethally injured cells and was measured by the mass spectrophotometer.

The H9c2 cells were seeded at 20,000 cells per well in a 24-well tissue culture plate. Each group was conducted in two technical replicates. Once seeded in a 24-well plate, the cells were left to grow for another 24 h before the medium was changed

to either a control or exposure to different concentrations of doxorubicin or doxorubicinol.

Following 18 h of treatment, the cytotoxic effect of doxorubicin and doxorubicinol on cell lines was evaluated with an LDH Cytotoxicity Assay kit (CytoTox 96® Non-Radioactive Cytotoxicity Assay, Promega (G1781)) on a 96-well plate. LDH release in cell supernatants was assessed with a spectrophotometer by measuring absorbance value at two separate wavelengths. Using the Fluostar Omega plate reader (BMG Labtech), Omega MARS and Omega Data Analysis software, the absorbance was read at 490 nm and 680 nm (background absorbance value). To estimate the percentage of cell death, the absorbance of samples at 680 nm was subtracted from the respective absorbance at 490 nm. The results were expressed as a percentage of LDH release normalised to total lysis using Triton X-100 (Sigma-Aldrich, CAS number 9036-19-5). The mean percentage of dead cells was calculated based on the two technical replicates.

Each treatment with doxorubicin and doxorubicinol was repeated with at least five biological replicates (N=5). Figure 4.1 presents a visual framework for the LDH assay method.

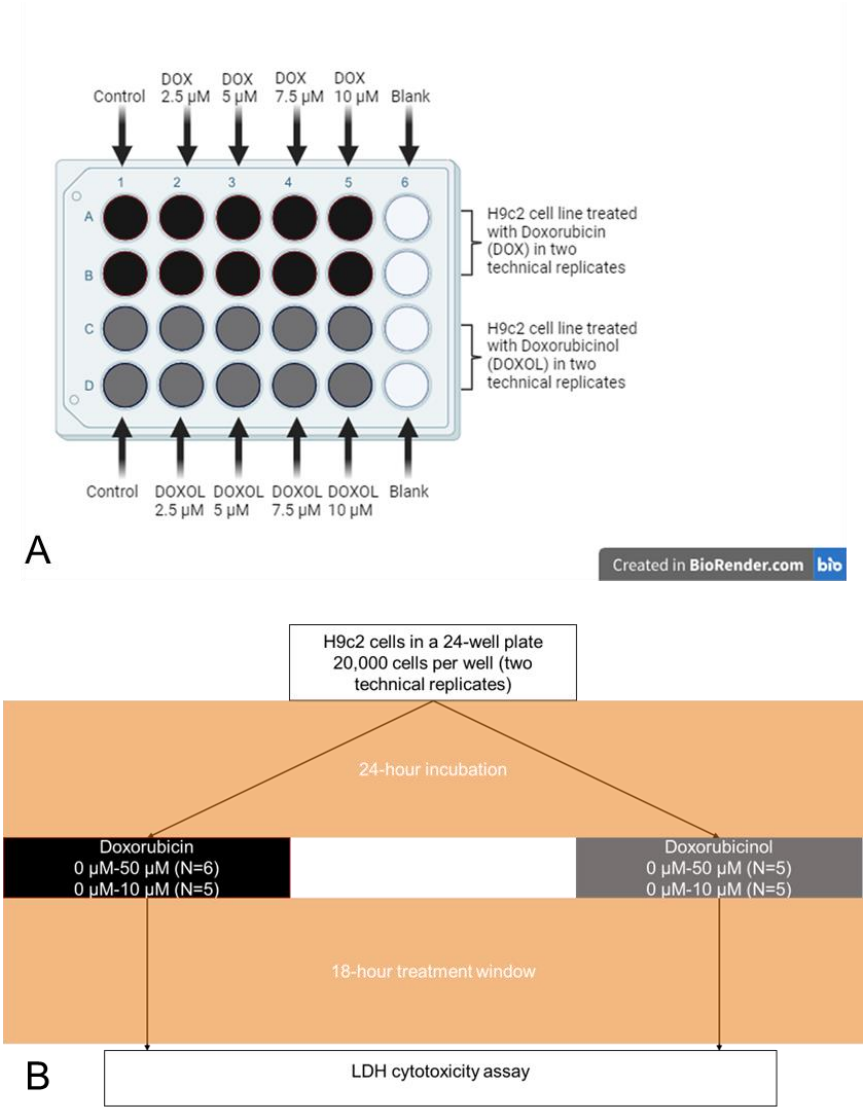

Figure 4.1 Visual summary of the LDH cytotoxic assay method on the H9c2 cell line. The H9c2 cell line was seeded at 20,000 cells per well in a 24-well plate and was incubated for 24 h before the respective treatment was given **(A)**. The general workflow of the LDH assay is illustrated in **(B)**.

4.3.4 Microscopical analysis and fluorescent staining

In a separate experiment, the H9c2 cells were cultured in a 24-well plate (20,000 cells per well) and treated with doxorubicin or doxorubicinol for 18 h. The concentration range of doxorubicin and doxorubicinol used was between 0 µM (control) and 10 µM. In addition, a separate well with H9c2 cells was treated with 50 ng/mL LPS for 4 h followed by 5 µM Nigericin for 1 h, a treatment known to induce pyroptosis. This was to evaluate the possible different cellular alterations between doxorubicin, doxorubicinol, and LPS & Nigericin on the H9c2 cell line.

One hour before the 18-hour treatment completion, the fluorescent staining propidium iodide (PI) and FITC-Annexin V were administered into the respective cell media (each with dilution factor 1:500) in a sterile hood. The cells were returned to the incubator to complete the remaining treatment. The cells were then visualised in the dark under a brightfield and fluorescence microscope (GX-Capture-T microscope, 20x power of magnification), respectively. The images were captured and processed using GX-Capture-T software to produce a phase contrast plus fluorescence and fluorescence-only image.

4.3.5 Western Blot

4.3.5.1 Types of cells and treatment used in Western blot experiment

The H9c2 cells were seeded at 1 x 10^6 cells per 100 mm cell dish with the cell media changed every two or three days until the cells reached target confluency. Thereafter, the cell media were changed with the respective treatment, such as control (cell media only), doxorubicin or doxorubicinol, added accordingly. The concentration range of doxorubicin and doxorubicinol used was between 0 μM (control) and 10 μM.

Hypoxia has been shown to induce apoptotic cell death in doxorubicin-treated H9c2 cell lines (Reeve *et al.*, 2007). Therefore, three additional treatment groups were added to test an experimental model in addition to the above treatment group. These additional groups were the H9c2 cell line treated with 18 h hypoxic buffer, the H9c2 cell line treated with 18 h hypoxic buffer mixed with 2.5 μM doxorubicin, and the H9c2 cell line treated with 18 h hypoxic buffer followed by 15 μM Nigericin for 1 h before the end of hypoxia. Table 4.1 shows the hypoxic buffer composition.

Hypoxic buffer in 125 mL deionised H_2O (pH adjusted to 6.2)			
Material	Concentration (mM)	Material	Concentration (mM)
KH_2PO_4	1	NaCl	74
$NaHCO_3$	10	KCL	16
$MgCL_2.6H_2O$	1.2	Na-Lactate	20
NA Hepes	25	CaCl2	1.26

Table 4.1 Composition of the hypoxic buffer.

Three additional wells of H9c2 cells were cultured and cultivated following the same cell culture protocol in 100 mm cell dishes. Once the hypoxic buffer was prepared and filtered using a 2 µm membrane filter in a sterile condition, a gas mixture of 95% Nitrogen and 5% CO_2 was administered into the hypoxic buffer for 10 min. Thereafter, the cell media of the H9c2 cell line in cell dishes was replaced with a hypoxic buffer. An additional 2.5 µM doxorubicin was added in one of the cell dishes along with the hypoxic buffer. The cell dishes were placed into a secure gas chamber, where the gas mixture of 95% nitrogen and 5% CO_2 was administered again into the chamber for 10 minutes. The chamber with the cell dishes inside was subsequently put into the incubator at 37^{o}C for 18 h according to the treatment protocol. 15 µM nigericin was added to one of the cell dishes 1 h before the end of hypoxia. Following the completion of hypoxia and respective treatment, the H9c2 cell line was prepared for protein collection and lysis as outlined in Section 4.3.5.2.

THP-1 cell, a human monocyte cell of acute myeloid leukaemia, was used as a positive control. THP-1 cell was seeded at 1 x 10^6 cells per 100 mm cell dish. Two groups of THP-1 cells were used, control and treatment with 50 ng/mL LPS for 4 h and 15 µM Nigericin for 1 h. This LPS & Nigericin regime was used as an inducer of pyroptosis as per the supplier's recommendation.

4.3.5.2 Protein collection, quantification, and Western blot methods

The methodology used for protein collection, quantification, and Western blot was described in detail in Chapter 3 Section 3.5.

Following the relevant cell culture protocol, the cells were plated at 1 x 10^6 cells per 100 mm dish with the cell media changed every two or three days until the cells reached target confluency. Thereafter, the cell media were changed with the respective treatment, such as control (cell media only), doxorubicin or doxorubicinol added accordingly. The cell dishes were left incubated for 18 h before protein lysis and quantification.

25 µg of sample proteins were loaded into a 10% or 4-12% NuPAGE Bis-Tris gel (Thermo Fisher, UK) and were separated by electrophoresis at 90 V for 30 min and subsequently, at 120 V for 1 h and 30 min.

Following gel electrophoresis, the sample proteins underwent immunoblot transfer from the gel to the PVDF membrane. The gel and the PVDF membrane were sandwiched between filter paper and a fibre pad/sponge in a cassette. The cassette was subsequently loaded into a chamber system, where the transfer was run at 120 V for 1 h and 20 min.

Thereafter, the membrane was blocked with 5% Bovine Serum Albumin (BSA) in 0.1% Tween in Tris-buffered saline (TBST) for 1 h and was subsequently incubated for 18 h with primary antibodies, such as GSDMD E9S1X or Caspase 3 antibody. The anti-Beta-actin antibody was used as the housekeeping protein.

Once the incubation was complete, the membrane was washed with 0.1% TBST three times. The membrane was subsequently incubated for 1 h with two secondary antibodies in 5% BSA in 0.1% TBST. The immunolabelled bands were visualised with an Odyssey infrared scanner and its imaging software from Li-Cor Biosciences (Image Studio Lite Ver 5.2). Protein expression was quantified using Odyssey software.

4.4 Results

This section will outline the results of the LDH cytotoxicity experiments, microscopical and fluorescent staining imaging, and Western blot experiments in the H9c2 cell line.

4.4.1 LDH cytotoxic assay assessment

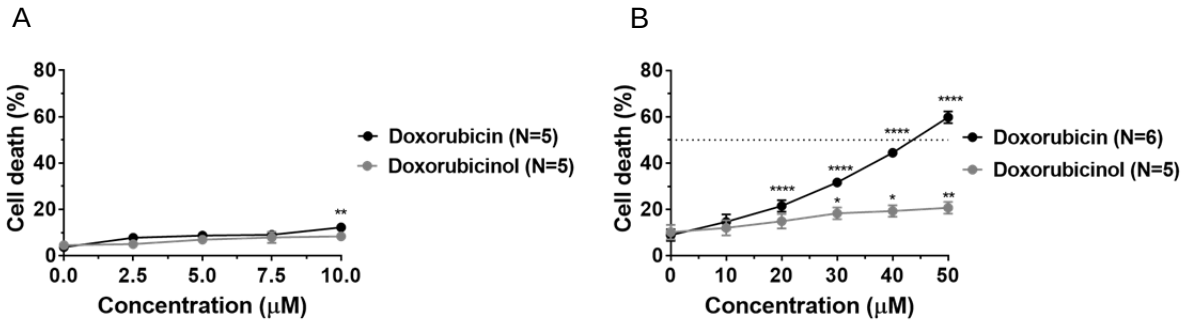

Figure 4.2 LDH cytotoxicity experiments of the H9c2 cell line. Figures 4.2 **A and B** show the average percentage of cell death in H9c2 cells treated with the indicated concentration of doxorubicin (black line) or doxorubicinol (grey line). The statistical analysis was performed with two-way ANOVA and Tukey's multiple comparison test. The * on the graphs represents the P value of the cell death caused by the drug concentration relative to control. *P value < 0.05, **P < 0.01, ****P < 0.0001.

Concentration	Doxorubicin (%)	Doxorubicinol (%)
Control (0 μM)	3.8 ± 1.0	4.6 ± 1.2
2.5 μM	7.8 ± 1.9	5.1 ± 1.1
5 μM	8.8 ± 1.9	7 ± 1.6
7.5 μM	9 ± 1.0	7.9 ± 2.4
10 μM	12.3 ± 1.5	8.4 ± 1.4

Table 4.2 The mean percentage of cell death in H9c2 cell line with doxorubicin or doxorubicinol treatment. The values correspond to the graph in Figure 4.2A (N=5). The values are mean ± standard errors of the mean.

Concentration	Doxorubicin (%)	Doxorubicinol (%)
Control (0 μM)	9 ± 2.5	10.2 ± 3.1
10 μM	14.7 ± 3.2	12.1 ± 3.3
20 μM	21.6 ± 2.5	15 ± 3.2
30 μM	31.7 ± 1.9	18.3 ± 2.6
40 μM	44.5 ± 0.4	19.4 ± 2.5
50 μM	59.9 ± 2.6	20.8 ± 2.5

Table 4.3 The mean percentage of cell death in H9c2 cell line with doxorubicin or doxorubicinol treatment. The values correspond to the graph in Figure 4.2B (N=5). The values are mean ± standard errors of the mean.

The LDH cytotoxic assay experiment on the H9c2 cell line was conducted with at least five biological replicates (Figure 4.1). Figure 4.2 A and B show the LDH cytotoxicity graph of the H9c2 cell line treated with doxorubicin or doxorubicinol. The LDH released is reflected as a marker of cell death percentage.

Figure 4.2A shows the LDH cytotoxicity assay result in the H9c2 cell line following 18 h treatment between control (0 μM) and 10 μM doxorubicin or doxorubicinol. There was a dose-dependent cell death response with increasing concentration of doxorubicin or doxorubicinol, but only the effect of doxorubicin at 10 μM (12.3% ± 1.5%) was significantly different from control. Tukey's post-hoc test suggested that there was a significant effect of concentration on cell death on both arms relative to control ($P = 0.007$), but there was no difference between the overall effects of the two drugs on H9c2 cell death ($P = 0.241$) by two-way ANOVA.

When tested at higher concentrations up to 50 μM, the LDH cytotoxicity assay showed noticeable dose-dependent cell death (Figure 4.2B). Significant cell death was observed in H9c2 cells treated with doxorubicin 20 μM (21.6% ± 2.5%), whereas H9c2 cell death started to be significant when treated with doxorubicinol at 30 μM (18.3% ± 2.6%). Tukey's post-hoc test suggested that there was a significant difference between the H9c2 cell death with increasing concentration of doxorubicin to the response change with increasing concentration of doxorubicinol ($P < 0.0001$). Furthermore, there was a significant difference between the overall effect of the two drugs on H9c2 cell death in these supraphysiological doses ($P = 0.0008$) by two-way ANOVA.

4.4.2 Phase-contrast and fluorescent imaging of treated H9c2 cells

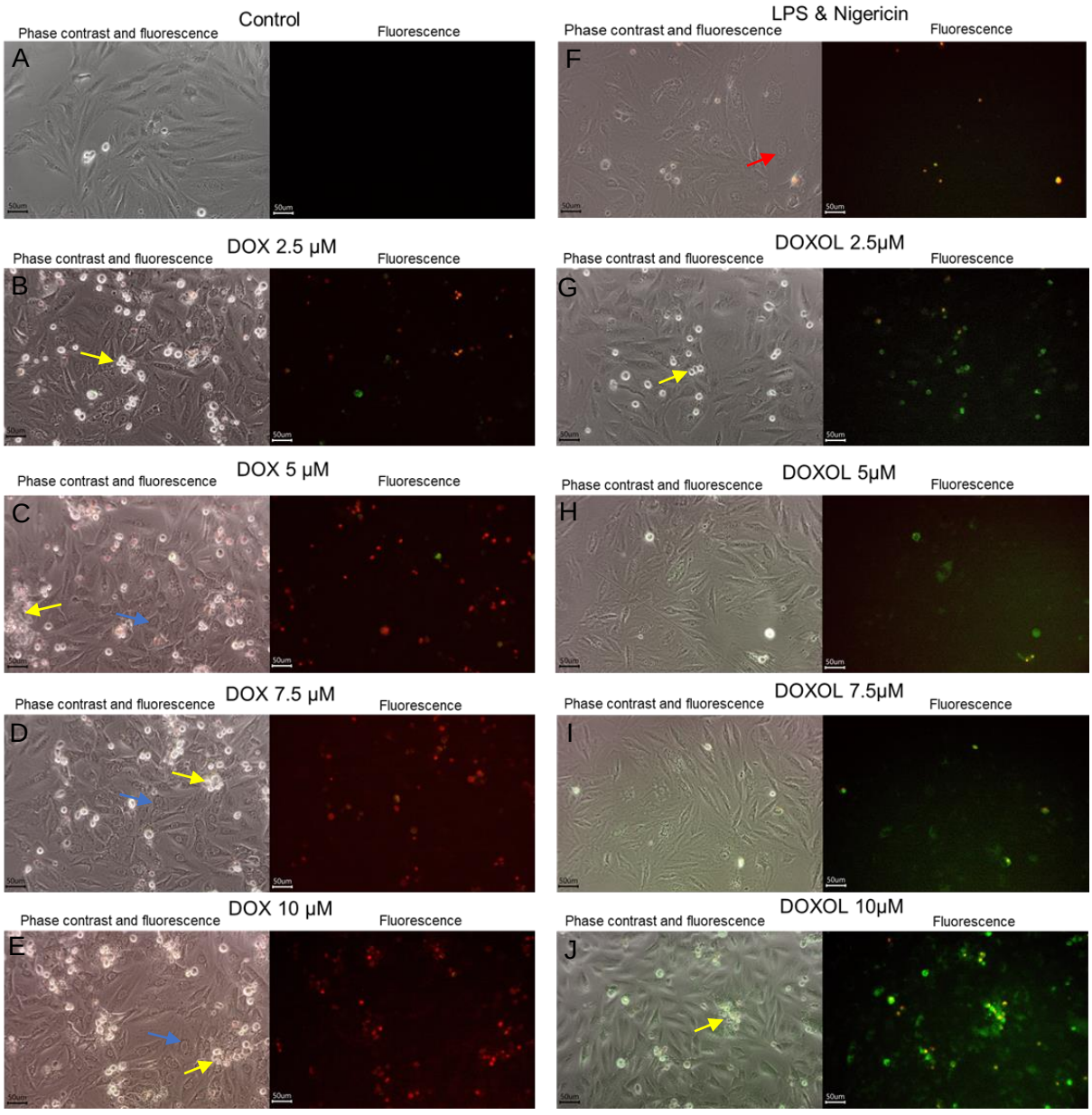

Figure 4.3 Phase-contrast and fluorescent staining images of the H9c2 cell line treated with the indicated concentration of doxorubicin (DOX), doxorubicinol (DOXOL), or LPS & Nigericin. In images **A-J**, phase-contrast images are shown side-by-side with matching fluorescent images indicating lethally injured (propidium iodide staining, red) and apoptotic (FITC-Annexin V, green) cells. Each scale bar represents 50 µm. Doxorubicin or doxorubicinol caused H9c2 cells to alter appearance (blue arrows) or condense in a round shape and cluster together (yellow arrows). H9c2 cells treated with LPS & Nigericin exhibited protrusions or 'blebs' in the plasma membrane (red arrow).

Figure 4.3 A-J show the phase contrast and/or fluorescent images of the H9c2 cells with their respective treatment. The fluorescent dye propidium iodide (PI) appears red stain and FITC-Annexin V appears green stain. Some cells could be stained by both PI and Annexin V, resulting in an orange appearance

Figure 4.3A shows the image of the H9c2 cell without any treatment (control). Healthy H9c2 cells looked spindle-shaped with a tapered periphery and can be mono- or multi-nucleated cells. There was no fluorescent staining was detected in the control group.

Figure 4.3 B-E show images of H9c2 cells following 18 h treatment with doxorubicin 2.5 μM to 10 μM. Morphological alterations were observed following doxorubicin treatment (blue arrow). Furthermore, some cells appeared to condense, round, and cluster together (yellow arrow). In the doxorubicin-treated cells, the fluorescent stain was predominantly red. The PI was observed to stain cells that were condensed and clustered together.

Figure 4.2F shows images of H9c2 cells treated with 50 ng/mL LPS for 4 h and 15 μM Nigericin for 1 h. The phase contrast image showed protrusions in the plasma membrane in some of the cells or blebbing (red arrow). Few scattered round cells were observed. The fluorescent image showed that these round cells were stained with both PI and Annexin V, resulting in an orange appearance.

Figure 4.2 G-J show images of H9c2 cells following 18 h treatment with doxorubicinol 2.5 μM to 10 μM. Doxorubicinol also induced morphological changes. Rounded and clustered cells were observed, particularly at 10 μM doxorubicinol (yellow arrow). The fluorescent staining images in doxorubicinol-treated groups appeared to be predominantly green, suggestive of Annexin V binding, a specific marker of the apoptotic process. Annexin V appeared to bind more to the round and clustered cells and it was more visible in cells treated with 10 μM doxorubicinol.

4.4.3 Western blot analysis on Gasdermin D processing in H9c2 cell line treated with doxorubicin and doxorubicinol

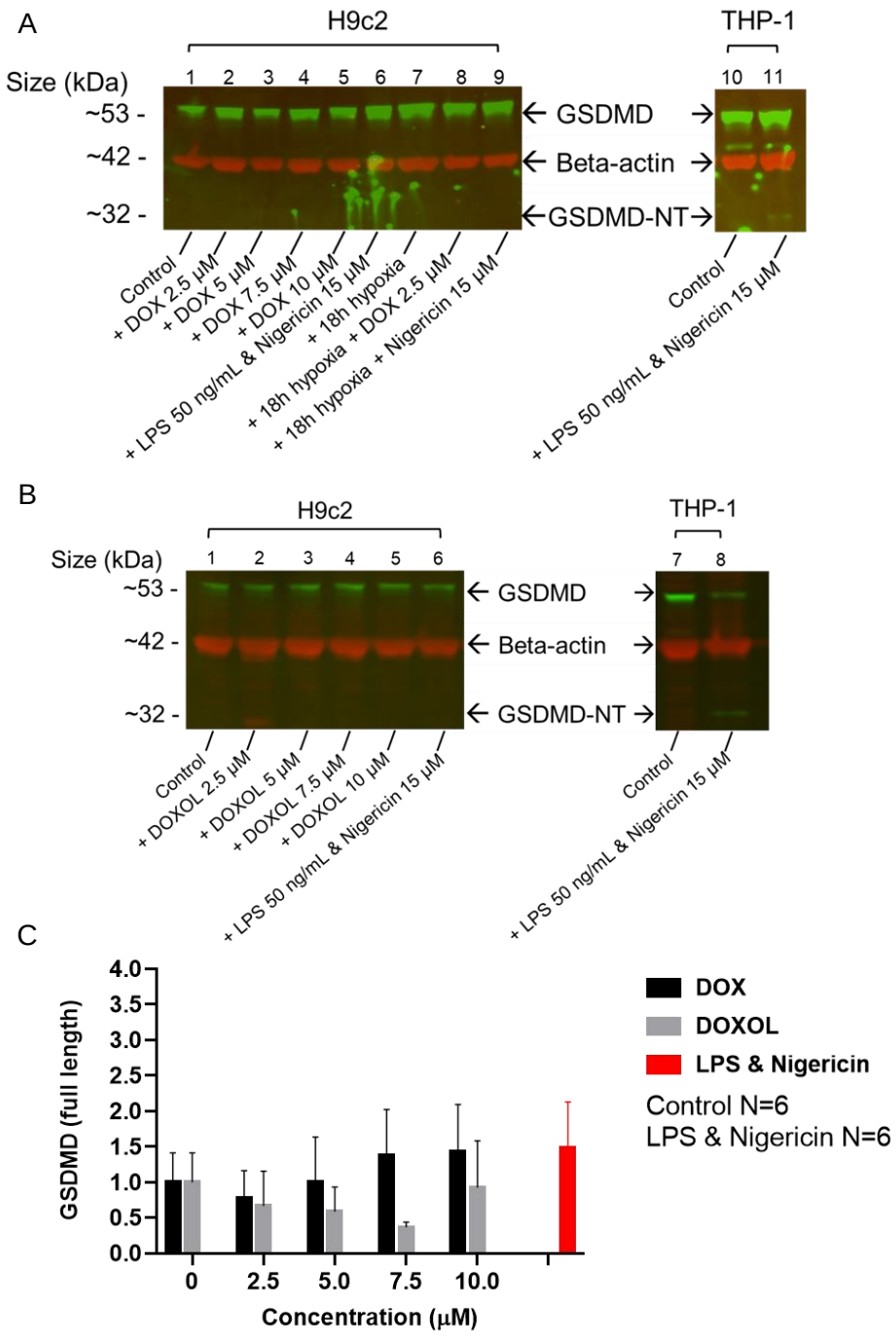

Figure 4.4 Western blot analysis of GSDMD in H9c2 cell line. **(A, B)** Representative immunoblots of H9c2 that had been treated with DOX (A) or DOXOL (B), probed for GSDMD and beta-actin following treatments (N=3). Quantification of GSDMD in H9c2 is shown in **(C)** (N=3, unless stated otherwise). The Y-axis showed the arbitrary unit quantification of the detected GSDMD protein band density, normalised to beta-actin, relative to the control group. THP-1 cells treated with LPS & Nigericin were used as a positive control for pyroptosis and

GSDMD-NT cleavage. Statistical analysis was performed using two-way ANOVA and Tukey's multiple comparison test.

Concentration	Doxorubicin (arbitrary units)	Doxorubicinol (arbitrary units)
Control (0 μM)	1 ± 0.41	1 ± 0.41
2.5 μM	0.78 ± 0.40	0.67 ± 0.49
5 μM	1 ± 0.63	0.59 ± 0.35
7.5 μM	1.37 ± 0.65	0.38 ± 0.07
10 μM	1.43 ± 0.67	0.93 ± 0.66
LPS & Nigericin	1.49 ± 0.64	

Table 4.4 Quantification of GSDMD band density in H9c2 cell line following treatment with doxorubicin or doxorubicinol. The values are normalised to beta-actin and relative to the control group (N=3, except control and LPS & Nigericin N=6). The values correspond to the graph in Figure 4.4C. The values are mean ± standard errors of the mean.

Figure 4.4 A-B show a representative Western blot membrane of H9c2 cells treated with doxorubicin or doxorubicinol. Each membrane shown in the figure was representative of three biological replicates (N=3). The housekeeping protein, beta-actin (B-actin), was similar in all lanes, indicating equivalent loading.

In both Figure 4.4 A-B, the full-length Gasdermin D (GSDMD) band was detected in the untreated H9c2 cells (lane 1) as well as H9c2 following all treatments. However, the N-Terminal of Gasdermin D (GSDMD-NT) was not detected in any samples, including the LPS & Nigericin-treated sample.

THP-1 cell was used as a positive control for the detection of cleaved GSDMD, as it is known to undergo GSDMD-mediated pyroptosis. In Figure 4.4 A and B, full-length GSDMD was detected in the untreated THP-1 cells as well as the LPS & Nigericin-treated THP-1 cells, as expected. Importantly, the cleaved GSDMD-NT band was detected only in the LPS & Nigericin-treated THP-1 cells, indicating that the positive control for pyroptosis had worked. THP-1 cells, when treated with LPS and Nigericin, have been shown to induce pyroptotic pathway and a good positive control for pyroptosis (Taabazuing *et al.*, 2017).

Figure 4.4C shows the quantification of the full-length of Gasdermin D protein expression, normalised to beta-actin, relative to the control group. In brief, there was

no statistical difference observed in the expression of full-length GSDMD in all treatments.

4.4.4 Western blot analysis on Caspase 3 processing in H9c2 cell line treated with doxorubicin and doxorubicinol

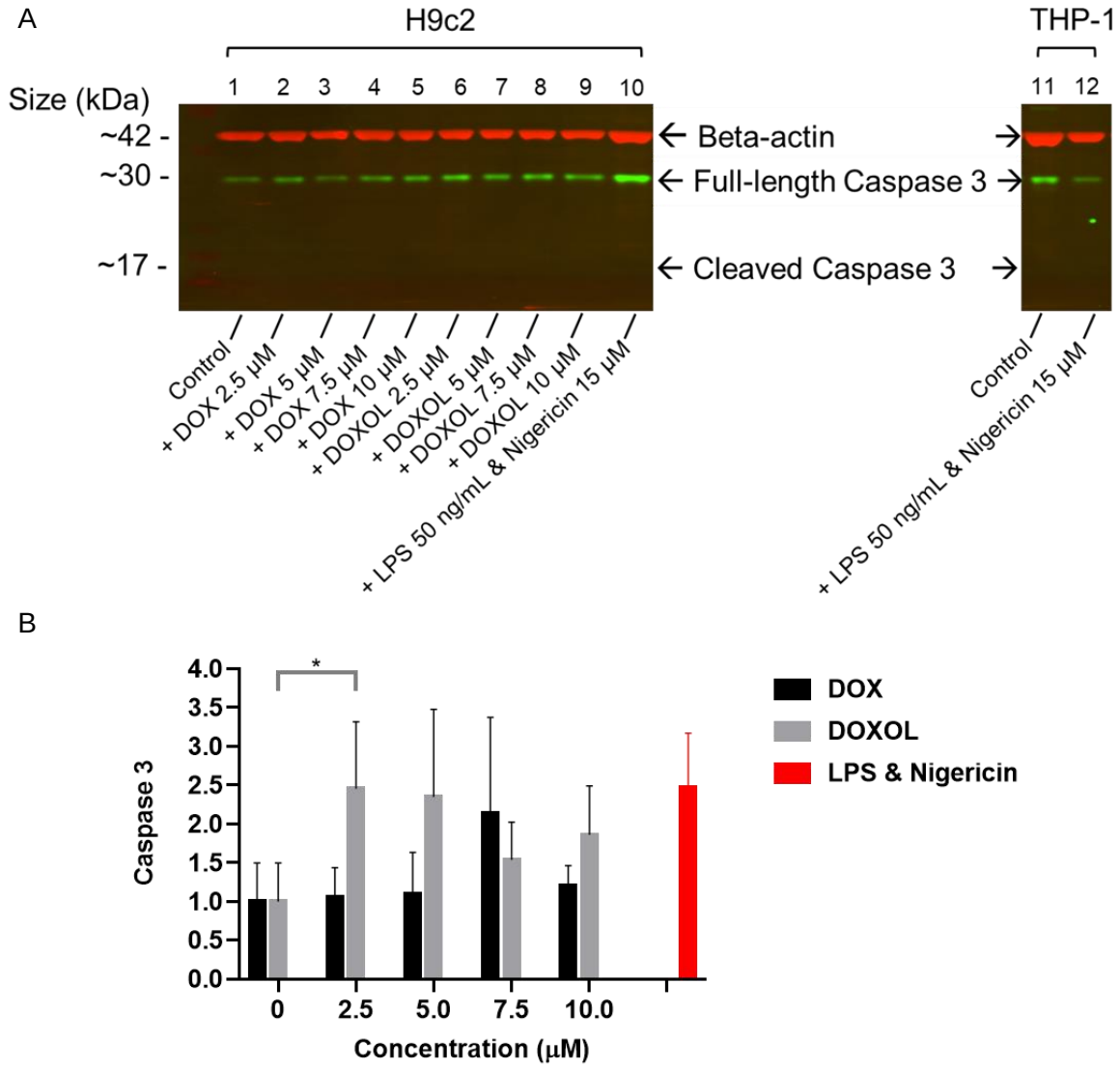

Figure 4.5 Western blot analysis of full-length Caspase 3 in H9c2 cell line. **(A)** Representative immunoblots of H9c2 that had been treated with DOX or DOXOL, probed for Caspase 3 and beta-actin (N=3). Quantification of full-length Caspase 3 in H9c2 is shown in **(B)** (N=3). The Y-axis showed the arbitrary unit quantification of the detected full-length Caspase 3 protein band density, normalised to beta-actin, relative to the control group. THP-1 cell treated with LPS & Nigericin was used as a negative control of apoptosis. Statistical analysis was performed using two-way ANOVA and Tukey's multiple comparison test. *P value < 0.05.

Concentration	Doxorubicin (arbitrary units)	Doxorubicinol (arbitrary units)
Control (0 μM)	1 ± 0.5	1 ± 0.5
2.5 μM	1.05 ± 0.39	2.46 ± 0.86
5 μM	1.09 ± 0.54	2.35 ± 1.13
7.5 μM	2.14 ± 1.24	1.54 ± 0.49
10 μM	1.21 ± 0.26	1.86 ± 0.63
LPS & Nigericin	2.47 ± 0.70	

Table 4.5 Quantification of full-length Caspase 3 band density in H9c2 cell line following treatment with doxorubicin or doxorubicinol. The values are normalised to beta-actin and relative to the control group (N=3, except control and LPS & Nigericin N=6). The values correspond to the graph in Figure 4.5C. The values are mean ± standard errors of the mean.

Figure 4.5A shows a representative Western blot membrane of the H9c2 cells treated with doxorubicin, doxorubicinol, and LPS & Nigericin (N=3). The housekeeping protein, beta-actin (B-actin), was similar in all lanes, indicating equivalent loading.

The full-length caspase 3 (~42 kDa size) was detected in untreated H9c2 cells (lane 1) and all treated groups. However, the expression of activated or cleaved caspase 3 (~ 17 kDa size) was not detected in any H9c2 lanes. Similarly, the full-length caspase 3 was detected in the untreated as well as the LPS & Nigericin-treated THP-1 cell samples, but the cleaved caspase 3 was not detected.

Figure 4.5B shows the quantification of the caspase 3 protein expression, normalised to beta-actin, relative to the control group. There was no statistical difference observed in the expression of full-length caspase 3 in all treatments. Overall, the graph suggested that the caspase 3 expression in the doxorubicin group was lower than in the doxorubicinol group.

4.5 Discussion

In summary, there was a higher LDH release or cell death in the H9c2 cells treated with doxorubicin than doxorubicinol. Dose-dependent cytotoxicity was observed in each group, particularly at higher concentrations. Both doxorubicin and doxorubicinol induced morphological changes more suggestive of apoptosis instead of pyroptosis. These were supported further by the fluorescent staining showing late apoptosis/necrosis and early apoptosis in the doxorubicin and doxorubicinol groups,

respectively. In addition, despite the detection of GSDMD and caspase 3 protein bands in the Western blot experiment with doxorubicin or doxorubicinol, neither GSDMD-NT or cleaved caspase 3 protein was detected. Positive control for caspase 3, such as Jurkat cell treated with cytochrome c, was not used in this research due to time constraint.

4.5.1 Doxorubicin and doxorubicinol concentration

In clinical practice, doxorubicin is administered intravenously and its plasma concentration can be measured. A plasma concentration of doxorubicin up to 2.5 μM is considered clinically relevant and covers the possible variation in the plasma concentration of doxorubicin of patients undergoing anthracycline-based chemotherapy. The doxorubicin dose between 5 μM and 10 μM may be relevant in a subgroup of patients with low drug clearance, for instance, individuals with liver disease, or immediately after doxorubicin administration (Frost *et al.*, 2002, Palle *et al.*, 2006). The peak plasma concentration (Cmax) of doxorubicin is considered to be 5 μM (Greene *et al.*, 1983). Concentrations of 10 μM and beyond are considered supraphysiological. Thus, setting up a concentration range between control and 10 μM should give a good representation of cardiotoxicity in a variety of clinical profiles. Furthermore, a similar concentration range of doxorubicin has been used previously at the Hatter Cardiovascular Institute, where *ex vivo* experiments with Sprague-Dawley rats were conducted to study whether the ischaemic preconditioning conferred cardioprotection from anthracycline-induced toxicity via the PI3K pathway (Maulik *et al.*, 2018).

Doxorubicinol, as illustrated in Chapter 1, is an active metabolite of doxorubicin. Although a wide range of doxorubicin concentrations have been tested in the literature, doxorubicinol has not been as extensively investigated. Further challenge pertains to the fact that doxorubicin cardiotoxicity can be chronic due to the accumulation of doxorubicin and its eventual conversion to doxorubicinol within the cells. In addition, different cell types may respond differently to doxorubicin or doxorubicinol. One cell type may be more vulnerable to the cytotoxicity induced by anthracyclines. Thus, it can be challenging to ascertain the dose of doxorubicinol that is appropriate to simulate the chronic nature of anthracycline-induced cardiotoxicity.

Nonetheless, this thesis intended to assess the anthracycline-induced cytotoxicity in its acute or subacute phase. Salvatorelli *et al* exposed human myocardial strips to 10 μM of doxorubicin (Salvatorelli *et al.*, 2006). Following 4 h of exposure, they found that the concentration of doxorubicin in the myocardial strips was 6 ± 1 μM, whereas the concentration of doxorubicinol was 0.06 ± 0.02 μM. From this data, it appears that the concentration of doxorubicinol was ~100 times lower than the doxorubicin concentration in the myocardial strip.

However, the aforementioned study did not specifically look at cell death or LDH release in the myocardial strips. Therefore, although it is useful to learn the possible conversion ratio of doxorubicin to doxorubicinol in the myocardial strips, it may not be applicable to the model used in this thesis which assesses cell death and, potentially, introduces an agent to attenuate cytotoxicity. Notably, the conversion ratio of doxorubicin to doxorubicinol may differ in different cells. Therefore, the decision was made to use the same concentration range both in doxorubicin and doxorubicinol where the concentration range is set to be uniform across the experiments with different cells.

The concentration of doxorubicin or doxorubicinol between 10 μM and 50 μM was used to set up an experimental model using the H9c2 cell line. This model was used to assess whether measuring the dose–cell death response using LDH assay works consistently. The concentration range was subsequently reduced from 0 μM (control) to 10 μM. This concentration range was used for the subsequent experiment models on microscopical analysis, fluorescent staining, and Western blot.

4.5.2 LDH cytotoxicity assay

In the LDH cytotoxicity assay experiment, the dose-dependent LDH release as a marker of cell death was observed in the H9c2 cell line treated with doxorubicin or doxorubicinol. There was a significant difference between the H9c2 cell death with increasing concentration of doxorubicin to the cell death response inflicted by increasing concentration of doxorubicinol ($P < 0.0001$). Doxorubicin caused higher cytotoxicity than doxorubicinol.

With regards to doxorubicin and H9c2, findings in this thesis on LDH cytotoxicity share some similarities to those reported in the literature (Sardão *et al.*, 2009). In their

study, the H9c2 cell line was treated with doxorubicin up to 10 μM and measured the percentage of LDH release over 6, 12, and 24 h. Their experiment suggested statistically significant cell death at 24 h in H9c2 cells treated with doxorubicin 1 μM, 5 μM, and 10 μM. The LDH released appeared to plateau at 24 h among the three doxorubicin concentrations. They also showed higher LDH release with longer incubation time at 12 h and 24 h, irrespective of the dose. Their findings suggested the cytotoxicity effect induced by doxorubicin in the H9c2 cell line was likely attributable to a higher dose and longer treatment time.

The LDH experiment with the H9c2 and doxorubicin treatment in this thesis appeared to share similar observations to Sardão *et al* despite different duration of treatment. The LDH release of up to 20% was observed at 10 μM doxorubicin in my two LDH cytotoxicity assay experiments, whereas Sardão *et al* found statistically significant death around 20-25% at the same concentration at 24 h.

The difference in cell death between doxorubicin and doxorubicinol was unexpected, given the fact that doxorubicinol is believed to be the major active metabolite of doxorubicin (Olson *et al.*, 1988).

Is the difference observed because doxorubicinol is less cytotoxic? One of the early studies of doxorubicinol by Olson *et al* found that doxorubicinol profoundly depressed both systolic and diastolic function of the isolated right ventricular papillary muscles of rabbits *ex vivo*. Reduction in the ventricular systolic function is one of the criteria that define clinical cardiotoxicity by international guidelines such as one from the European Society of Cardiology (ESC) (Lyon *et al.*, 2020). Doxorubicinol inhibited calcium loading and ATPase activities of the sarcoplasmic reticulum, mitochondria, and sarcolemma. Olson *et al* further showed that doxorubicin, on the contrary, had little effect on systolic and diastolic function, calcium loading, or ATPase activities. Olson *et al* also demonstrated that the heart could metabolise doxorubicin to doxorubicinol in a dose- and time-dependent manner, which might explain the chronic cumulative impact of doxorubicin cardiotoxicity. Although doxorubicinol was shown to exert more effect on the functional aspect of the ventricular muscle, its cytotoxic effect was less than doxorubicin. In their *in vitro* experiments investigating the cytotoxic nature between doxorubicin and doxorubicinol on tumour cell lines, Olson *et al*

demonstrated that doxorubicin was more potent at inducing cytotoxicity at a much lower concentration.

Another study by Reis-Mendes *et al* found that, using the MTT cytotoxicity assay, 1 μM doxorubicin was more toxic than 1 μM doxorubicinol in differentiated H9c2 cells over 48 h, despite both drugs showing statistically significant cell death with their respective control (Reis-Mendes *et al.*, 2019). In addition, a study by Bains *et al* exposed eight human cell lines derived from different tissues and one rat embryonic cardiac cell line (undifferentiated H9c2 cells) to doxorubicin at different concentrations up to 150 μM and to doxorubicinol at several concentrations up to 3000 μM, for 48 h (Bains *et al.*, 2013). In that study, Bains *et al* showed that doxorubicin was significantly more toxic to all tested cell lines than its metabolite, doxorubicinol, using the MTT reduction assay. Putting the pharmacodynamic variability on each of those tested cell lines aside, these findings suggest that both doxorubicin induced cytotoxicity more rapidly than doxorubicinol.

Another possible explanation is that the alcohol-based doxorubicinol is not as permeable as sugar-based doxorubicin. Doxorubicin, as previously described, was able to be metabolised intracellularly in the heart into doxorubicinol. Doxorubicinol is formed after a side chain of the C-13 carbonyl group undergoes two-electron reduction, a reaction mediated by aldo-keto reductase (AKR) and short-chain dehydrogenase/reductase. This event took place in the cytosolic environment. A study found that, when the permeability of both doxorubicin and doxorubicinol in the rat's heart and H9c2 cells was assessed, doxorubicinol was not as permeable as doxorubicin to enter the cell (Zeng *et al.*, 2019). Doxorubicinol slowly diffused from plasma or medium into the cell and hence was subsequently less cytotoxic.

Experimental design limitations may also contribute to the observed difference in cytotoxicity between doxorubicin and doxorubicinol, such as the LDH cytotoxicity assay. As described in Section 3.3, the LDH cytotoxicity assay works in the principle that the LDH is released when the cell membrane is damaged. The level of LDH in cell media can be measured in the form of formazan by the spectrophotometer machine. The level of formazan is directly proportional to the amount of the LDH release and, therefore, an indication of cytotoxicity.

Following the principle of LDH cytotoxicity, the cell membrane needs to be damaged by doxorubicin or doxorubicinol to release the LDH. Cell death pathways that may inflict damage to the plasma membrane include necrosis, pyroptosis, and can also appear in late apoptosis. However, cells undergoing an early apoptotic process may not release the LDH yet as the integrity of the plasma membrane is relatively intact. Another point to be considered is that the LDH cytotoxicity assay is unable to differentiate between LDH release from damaged cells originating from a particular cell death pathway.

Therefore, to complement the findings of the LDH cytotoxicity assay, microscopical and fluorescent staining experiments were valuable in assessing the possible cell death pathway induced by doxorubicin and doxorubicinol.

4.5.3 Microscopical and fluorescent staining analysis

The role of microscopical and fluorescent staining is to elucidate possible morphological alterations that occurred in the H9c2 cell line. Phase-contrast and fluorescent staining images may help direct our observation whether the morphological cell alterations represent a certain cell death pathway, such as apoptosis or pyroptosis. In conjunction with the light microscopy images, the use of fluorescent staining such as Annexin V or propidium iodide (PI) is valuable as it may help ascertain early apoptotic (Annexin V positive, PI negative), or late apoptotic/necrotic injury (Annexin V negative, PI positive).

Häcker wrote about how cells undergoing the apoptotic process might exhibit different cellular alterations at the different stages of apoptosis (Häcker, 2000). It is also important to note that different cells may have different variations in response to apoptotic changes. At the early stage of apoptosis, the dying cells' organelles usually start to swell before the nucleus condenses. The dying cells subsequently separate from the adjacent cells and the extracellular matrix attachment and start to round up. Protrusions of the plasma membrane, commonly referred to as ‘blebs’ start to form. The whole cell eventually disintegrates into apoptotic bodies. Apoptotic bodies are membrane-bound vesicles which contain any part of cellular components. These apoptotic bodies are taken up by neighbouring cells and digested via a lysosomal pathway.

Chen *et al* looked at the morphological difference between necrosis and pyroptosis in RAW-asc cells (Chen *et al.*, 2016). They described cells undergoing pyroptotic process feature cellular swelling, with protrusions and pore formation in the plasma membrane before the membrane integrity was lost with membrane rupture. In comparison, the cells undergoing the necrotic process began with the cell body being rounded up and swollen before it “exploded” like an over-inflated balloon. Thus, although both necrosis and pyroptosis may share some similarities that lead to plasma membrane disruption, they possess distinct morphological features.

In doxorubicin-treated H9c2 cells (Figure 4.3 B-E), some cells began to condense and appeared clustered with a notably bright round plasma membrane. These visible changes seen under the light microscopy appeared to resemble apoptotic changes. The fluorescent staining images were taken at the same time as the phase-contrast images, and these showed predominantly PI-positive, Annexin V-negative fluorescent in doxorubicin-treated cells. These fluorescent staining pattern might suggest that the cells may have undergone necrotic or late apoptotic injury.

In doxorubicinol-treated H9c2 cells (Figure 4.3 G-J), the morphological changes were not as clear as those in the doxorubicin group. Some cells appeared to condense and cluster together, particularly with doxorubicinol 10 μM. The fluorescent staining images in doxorubicinol groups showed predominantly Annexin V positive, and PI negative. These fluorescent staining images might suggest that doxorubicinol-treated cells were undergoing an early apoptotic process.

Annexin V binding and PI uptake is one of the most commonly used assays to measure apoptosis and necrosis (Crowley *et al.*, 2016). Co-staining with both Annexin V and PI is valuable because apoptosis is a rapid process that is complete in a few hours followed by secondary necrosis (Elmore, 2007).

In healthy cells, the lipids on the cell surface are distributed asymmetrically on the extra- and intracellular side of the plasma membrane. The phosphatidylserine (PS) lipid is usually restricted in the intracellular side of the plasma membrane. Lipid asymmetry is lost during apoptosis and PS is transferred to the extracellular side of the plasma membrane. Annexin V binds to PS exposed to the extracellular side of the plasma membrane. Furthermore, PS exposure may occur and precede morphological

changes such as nuclear or cell condensation. This may explain why Annexin V is bound to cells despite normal cell appearance.

The findings on the H9c2 microscopical analysis and fluorescent staining in this thesis suggest that the morphological changes caused by doxorubicin and doxorubicinol resemble apoptotic changes. The morphological changes observed in the H9c2 cells treated with doxorubicinol lead to early apoptotic changes which is in line with the predominant Annexin V fluorescent staining. Doxorubicin appeared to accelerate the apoptotic process over the same treatment duration, as shown in the fluorescent staining that was PI-predominant.

Similar findings were described by Hu *et al* in their experiment where the H9c2 cells were treated with 1 μM doxorubicin over 12 h (Hu *et al.*, 2020). The Annexin V and PI fluorescent stains were used to assess the extent of apoptosis. The stained cells were analysed with flow cytometry and they found doxorubicin caused late apoptosis.

4.5.4 Western blot analysis

Western blot analysis was conducted to assess whether Gasdermin D (GSDMD) processing or caspase 3 processing took place in doxorubicin or doxorubicinol-treated H9c2 cells. This analysis aims to further evaluate whether pyroptosis or apoptosis took place in the context of GSDMD or caspase 3 detection along with their respective cleaved or activated proteins.

The Western blot experiments carried out in this research did not detect the GSDMD-NT. A potential explanation for the absence of GSDMD-NT might be because the cytotoxicity in treated H9c2 cells was not driven by GSDMD-mediated pyroptosis. There have been conflicting findings in the literature on whether pyroptosis is involved in the cytotoxic process of doxorubicin-treated H9c2 cells. Cai *et al*, for instance, were able to detect GSDMD-NT bands in their H9c2 cell treated with 1 μM doxorubicin over 24 h (Cai *et al.*, 2023). The variation in the type of GSDMD antibody, the concentration of doxorubicin and the treatment duration may factor in the different findings observed in this doctoral research. Another study by a different group claimed to demonstrate pyroptosis in doxorubicin-treated H9c2 cells by detecting inflammasome cascade from

NLRP3 to GSDMD in their Western blot models, but did not assess GSDMD-NT, which is a hallmark of a complete pyroptosis cascade (Tavakoli Dargani *et al.*, 2019).

It has been suggested that doxorubicin induced apoptosis through increased caspase 3 activation via mitochondrial pathway (Michihiko *et al.*, 2006). The release of mitochondrial cytochrome c from damaged mitochondria into the cytosol activates caspase 3-mediated apoptosis cascade (Green *et al.*, 1998). Therefore, this thesis assessed the detection of caspase 3 and its cleaved end-product as the central executioner of apoptosis. The experiments in this study were not able to detect the cleaved caspase 3 in treated H9c2 cells. These findings differ from those who were able to show cleaved caspase 3, such as Liu *et al*, in which they were able to detect cleaved caspase 3 protein in their H9c2 cell treated with 1 μM doxorubicin (Liu *et al.*, 2008). They demonstrated that the cleaved caspase 3 protein was upregulated over time, with statistically significant upregulation observed beginning at 6 h.

The difference between the Western blot results in this doctoral research with the findings from previous research could be due to the difference in dose and incubation window. All the findings in previous research generally used 1 μM doxorubicin over 24 h, whereas higher doses and shorter incubation were used in this thesis. Furthermore, different GSDMD and caspase 3 primary antibodies were used, which might explain the difference seen in this study's results. In this regard, it was therefore important to demonstrate that the antibodies were effective in a positive control, i.e. THP-1 cells. As deliberated in the Western blot experiments in this research, GSDMD-NT protein was detected in LPS and Nigericin-treated THP-1 cells (see Section 4.4, Figure 4.4). This means the GSDMD antibody worked appropriately with THP-1 as a positive control. The caspase 3 antibody with THP-1 cell treated with LPS and Nigericin was also tested, resulting in no cleaved caspase 3 observed in a treatment that is known to induce pyroptosis instead of apoptosis (see Section 4.4, Figure 4.5). Further experiments with THP-1 cells will be elaborated in detail in Chapter 6.

4.6 Limitations

The main limitation of the H9c2 cell line experiment is its uncertainty as to the extent to which the findings are translatable to human cardiac myocyte cells. The challenge in obtaining healthy human heart cells as well as maintaining and replicating

in vitro are the main factors contributing to the limitation, calling for the use of an alternative cell line use. As previously mentioned in the introduction of this chapter, the immortalised rat ventricular myoblast cell line such as H9c2 has been widely used in anthracycline cardiotoxicity studies, so this has the advantage of permitting comparison to previous results.

A recent model of using human pluripotent stem cell-derived cardiomyocyte (hPSC-CM) may offer a new avenue into more physiologically relevant human cardiac cells. An interesting study conducted by Maillet *et al* explored an experiment model to study doxorubicin-induced cardiotoxicity using hPSC-CM (Maillet *et al.*, 2016). They found the cell viability of hPSC-CM started to reduce with a doxorubicin dose of 5 μM over 24 h. They also observed a dose-dependent decrease in cell viability over 24 h of doxorubicin exposure with IC_{50} 30 μM doxorubicin. Furthermore, they found that hPSC-CM treated with 3 μM doxorubicin exhibited increased staining intensity of both Annexin V and propidium iodide.

However, several limitations in using hPSC-CM should be considered. hPSC-CM usually resembles foetal cardiomyocytes instead of adult cardiomyocytes. Furthermore, current common protocols of hPSC-CM yield a variety of atrial- and ventricular-like cells. This will generate many unused cells if only one particular phenotype is of interest, such as ventricular cells in this research. This hopefully may be overcome with better and more innovative protocol in the future.

4.7 Conclusion

This chapter examined whether pyroptosis contributes to the H9c2 cell line treated with doxorubicin or doxorubicinol. When treated with doxorubicin, data from the experiments suggested that H9c2 cells undergo late apoptosis/necrosis. On the contrary, H9c2 cells underwent early apoptosis injury when treated with doxorubicinol. A summary of the results from the experiments in the H9c2 cells is presented in Table 4.2. This chapter concludes that doxorubicin and doxorubicinol are likely to induce cytotoxicity through apoptosis at a different potency.

Assays	H9c2 cell line	
	Doxorubicin	Doxorubicinol
LDH cytotoxicity assay	Significant cytotoxicity was detected at 10 μM after 18 h (12.3% ± 1.5%)	Significant cytotoxicity was detected at 30 μM after 18 h (18.3% ± 2.6%)
Morphological changes	Apoptotic (condensed and clustered cells, membrane blebbing)	Apoptotic
Fluorescent staining	Propidium Iodide positive, indicating permeability due to damaged plasma membrane in late apoptosis/necrosis	Annexin-V green positive indicating apoptosis
Western blot	Full-length GSDMD and caspase 3 bands were detected GSDMD-NT and cleaved caspase 3 bands were not detected	Full-length GSDMD and caspase 3 bands were detected GSDMD-NT and cleaved caspase 3 bands were not detected

Table 4.6 Table summary of H9c2 experiments with doxorubicin and doxorubicinol.

The next chapter will evaluate the effect of anthracycline-induced cytotoxicity in the human coronary artery endothelial and cardiac microvascular endothelial cells. This evaluation is valuable to assess whether the different element of the heart cells responds to the anthracycline-induced cytotoxicity differently and, thus, triggers different cell death pathway mechanism.

Chapter 5 Anthracycline-induced cytotoxicity in human vascular endothelial cells

5.1 Introduction

Historically, the study of anthracycline-induced cardiotoxicity has put much emphasis on cardiac myocytes. With the advance in studies of anthracycline-induced cytotoxicity, a growing number of studies have shown that other components of the heart, such as coronary artery endothelial cells, are affected by toxicity induced by chemotherapy (Wojcik *et al.*, 2015).

A recent *in vivo* study performed on pigs suggested that the administration of anthracycline induced irreversible structural changes in the coronary arteries following three, fortnightly, injections of doxorubicin (Galan-Arriola *et al.*, 2021). Furthermore, the continuation of doxorubicin therapy ultimately led to severe deterioration of the left ventricular (LV) function. Interestingly, these changes persisted even after the cessation of doxorubicin therapy (Galan-Arriola *et al.*, 2021).

The salient takeaway point from this insightful study is that the heart's vascular endothelial cell may be susceptible to anthracycline-induced cytotoxicity at the early subclinical stage before the development of cardiomyopathy. It is therefore important to evaluate further the effect of anthracycline cytotoxicity on human coronary artery and cardiac microvascular cells. Conducting experiments on macrovascular and microvascular endothelial cell would give an insight whether the heterogeneity in these cells pose different effects induced by anthracycline-induced cardiocytotoxicity.

5.2 Research hypothesis, aims and objectives

The main hypothesis investigated in this chapter was that the pyroptotic cell-death pathway contributes to anthracycline-induced cytotoxicity in human vascular endothelial cells.

To investigate this hypothesis, the extent of lytic cell death observed in HCAEC and HCMEC cells treated with doxorubicin (DOX) or doxorubicinol (DOXOL) was first measured using the lactate dehydrogenase cytotoxicity assay. This thesis also assessed whether the morphological alterations in treated cells resembled the

pyroptotic process and whether Gasdermin D (GSDMD) with its N-Terminal Gasdermin D (GSDMD-NT) were detected in treated cells using Western blot analysis.

The specific experimental objectives addressed in this chapter were:

1. To assess cell death *in vitro* using LDH cytotoxicity assay following treatment with doxorubicin or its metabolite doxorubicinol.
2. To characterise the morphological alterations observed in treated cells.
3. To determine the extent of pyroptosis and apoptosis in treated cells.
4. To evaluate whether Gasdermin D processing and caspase 3 processing occur in treated cells.

5.3 Methods

5.3.1 Cell cultivation

Human Coronary Artery Endothelial Cells (HCAEC) and Human Cardiac Microvascular Endothelial Cells (HCMEC) were obtained commercially. The supplier and the catalogue number are provided in Table 3.1 in Chapter 3. The HCAEC used here are primary cells isolated from a 55-year-old male Caucasian adult human donor with a known history of dilated cardiomyopathy. The donor never smoked and had no hypertension, coronary artery disease, or diabetes. The cells were isolated from the right and left coronary arteries, including the left anterior descending and circumflex arteries. The Human Cardiac Microvascular Endothelial Cells (HCMEC) used here are primary cells isolated from heart ventricles from a 15-year-old Caucasian male donor who had dilated cardiomyopathy. The donor never smoked and had no history of coronary artery disease, hypertension, or diabetes.

The HCAEC and HCMEC cells were cultured in endothelial cell culture medium MV2 mixed with a growth supplement (PromoCell, Cat No C-22022) in T75 tissue culture flasks (Greiner, reference number 65185). The maximum number of passages used in these primary cells was fifteen, as per the supplier's recommendation. The detailed cell cultivation technique and its material are described in Chapter 3 Subchapter 3.1.2 and Table 3.2, respectively.

5.3.2 Doxorubicin or doxorubicinol treatment

Once the cells achieved the target confluency, the medium was replaced with a fresh medium (control) or with a medium containing either doxorubicin (DOX) or doxorubicinol (DOXOL). The concentrations of doxorubicin and doxorubicinol used were between 0 µM (control) to 10 µM. The rationale of using these concentration was discussed in Section 4.5.1. The supraphysiological concentration beyond 10 µM was not used in this experiment, as it was to confirm a proof of concept on H9c2 cell line that the experiment design was able to demonstrate dose-dependent cell death response.

5.3.3 Lactate dehydrogenase assay

The lactate dehydrogenase assay experiment was conducted to estimate cell death based on LDH release from lethally injured cells.

The HCAEC or HCMEC cells were seeded at 20,000 cells per well in a 24-well tissue culture plate. The LDH cytotoxicity assay experiment with these human endothelial cells followed the same methods used in the LDH cytotoxicity assay on the H9c2 cell line described in Section 4.3.3. Each experiment was conducted with two technical replicates, and the experiment was repeated with five times using a different stock biological replicates (N=5). The supplier of HCAEC and HCMEC cells recommends the cell subculturing passage to be 15 or below to avoid cell senescence. The passage of HCAEC cells used were between 10 to 13, whereas the passage of HCMEC used were between 6 to 8.

5.3.4 Microscopical analysis and fluorescent staining

In a separate experiment, HCAEC and HCMEC cells were cultured in a 24-well plate (20,000 cells per well) and treated with doxorubicin or doxorubicinol for 18 h. The concentration range of doxorubicin and doxorubicinol used was between 0 µM (control) and 10 µM. In addition, a separate well with HCAEC or HCMEC cell was treated with 50 ng/mL LPS for 4 h followed by 5 µM Nigericin for 1 h, a treatment known to induce pyroptosis in various cell types. This was to evaluate the possible different cellular alterations between doxorubicin, doxorubicinol, and LPS & Nigericin on human vascular endothelial cells. The method of introducing fluorescent dyes has been described in Section 3.4 and Section 4.3.4.

5.3.5 Western Blot

5.3.5.1 Types of cells and treatment used in Western blot experiment

The HCAEC or HCMEC cells were seeded at 1 x 10^6 cells per 100 mm cell dish with the cell media changed every two or three days until the cells reached target confluency. Thereafter, the cell media were changed with the respective treatment, such as control (cell media only), doxorubicin or doxorubicinol, added accordingly. The concentration range of doxorubicin and doxorubicinol used was between 0 μM (control) and 10 μM.

THP-1 cell, a human monocyte cell of acute myeloid leukaemia, was used as a positive control as it is known to undergo pyroptosis. THP-1 cells were seeded at 1 x 10^6 cells per 100 mm cell dish. Two groups of THP-1 cells were used: control and treatment with 50 ng/mL LPS for 4 h followed by 15 μM Nigericin for 1 h. This LPS & Nigericin regime was used as an inducer of pyroptosis as per the supplier's recommendation.

5.3.5.2 Protein collection, quantification, and Western blot methods

The method used for protein collection, quantification, and Western blot was the same as what has been described in Section 4.3.5.2.

5.4 Results

This section will outline the results of the LDH cytotoxicity experiments, microscopical and fluorescent staining imaging, and Western blot experiments in the HCAEC and HMCEC cells.

5.4.1 LDH cytotoxicity assay of drug toxicity on HCAEC and HCMEC cells

Figure 5.1 shows the cytotoxicity of doxorubicin or doxorubicinol in the HCAEC (A) and HCMEC (B) treated with doxorubicin or doxorubicinol as measured by LDH release.

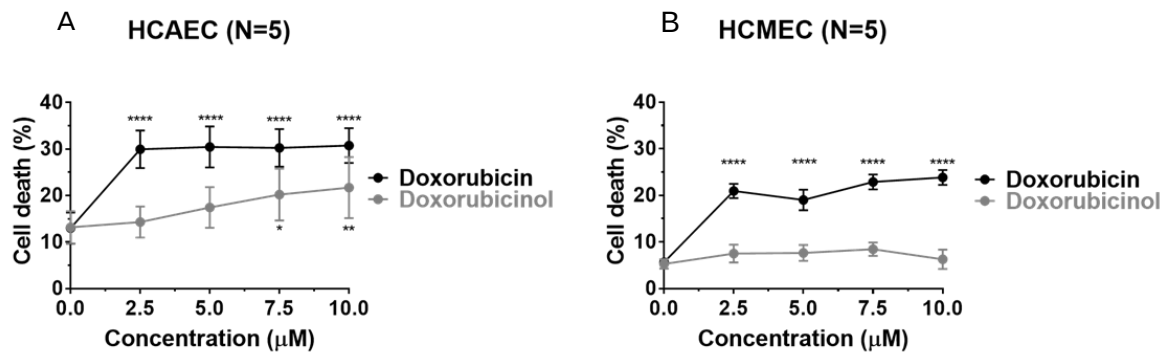

Figure 5.1 LDH cytotoxicity experiments of HCAEC and HCMEC cells. The average percentage of cell death in (**A**) HCAEC cells and (**B**) HCMEC cells treated with doxorubicin (black line) or doxorubicinol (grey line) 0 μM to 10 μM. The statistical analysis was performed with two-way ANOVA and Tukey's multiple comparison test. *P value < 0.05, **P < 0.01, ****P < 0.0001 represents the P value of the cell death caused by the drug concentration relative to control.

Concentration	Doxorubicin (%)	Doxorubicinol (%)
Control (0 μM)	13.0 ± 3.3	13.2 ± 3.5
2.5 μM	29.9 ± 4.0	14.3 ± 3.4
5 μM	30.5 ± 4.4	17.5 ± 4.4
7.5 μM	30.2 ± 4.0	20.2 ± 5.6
10 μM	30.7 ± 3.7	21.7 ± 6.6

Table 5.1 The mean percentage of cell death in HCAEC cells with doxorubicin or doxorubicinol treatment. The values correspond to the graph in Figure 5.1A (N=5). The values are mean ± standard errors of the mean.

Concentration	Doxorubicin (%)	Doxorubicinol (%)
Control (0 μM)	5.7 ± 0.9	5.3 ± 1.0
2.5 μM	20.9 ± 1.6	7.5 ± 1.9
5 μM	19.0 ± 2.2	7.7 ± 1.7
7.5 μM	22.0 ± 1.6	8.4 ± 1.4
10 μM	23.8 ± 1.6	6.3 ± 2.1

Table 5.2 The mean percentage of cell death in HCMEC cells with doxorubicin or doxorubicinol treatment. The values correspond to the graph in Figure 5.1B (N=5). The values are mean ± standard errors of the mean.

There was a significant increase in cell death in treated HCAEC cells (Figure 5.1A). In doxorubicin-treated groups, significant cell death was noted at doxorubicin 2.5 μM (29.9% ± 4%) and this plateaued at higher concentrations. In doxorubicinol-treated groups, there was a dose-dependent increase in cell death with increasing concentration of doxorubicinol, but started to be statistically significant relative to the control group in the doxorubicinol 7.5 μM group (20.2% ± 5.6%) and doxorubicinol 10 μM group (21.7% ± 6.6%). Tukey's post-hoc test was used to interpret whether there is an interaction effect between concentration and drug on cell death. There was a significant effect of concentration on cell death on both arms relative to control (P value = 0.0003), but there was no difference between the overall effects of the two drugs on HCAEC cell death (P value = 0.146) by two-way ANOVA.

In HCMEC cells, there was significant cell death in doxorubicin-treated groups (Figure 5.1B). A significant cell death was noted at 2.5 μM doxorubicin (20.9% ± 1.6%) and the cell death plateaued at higher concentrations. Interestingly, in doxorubicinol-treated groups, there was no significant increase in cell death at any concentration of doxorubicinol. Tukey's post-hoc test suggested that there was a significant difference between the HCMEC cell death with increasing concentration of doxorubicin to the response change with increasing concentration of doxorubicinol (P value < 0.0001). Furthermore, there was a significant difference in the overall effects of both drugs on HCMEC cells with the two curves being significantly different (P value = 0.0003) by two-way ANOVA.

5.4.2 Phase-contrast and fluorescent imaging of treated HCAEC and HCMEC cells

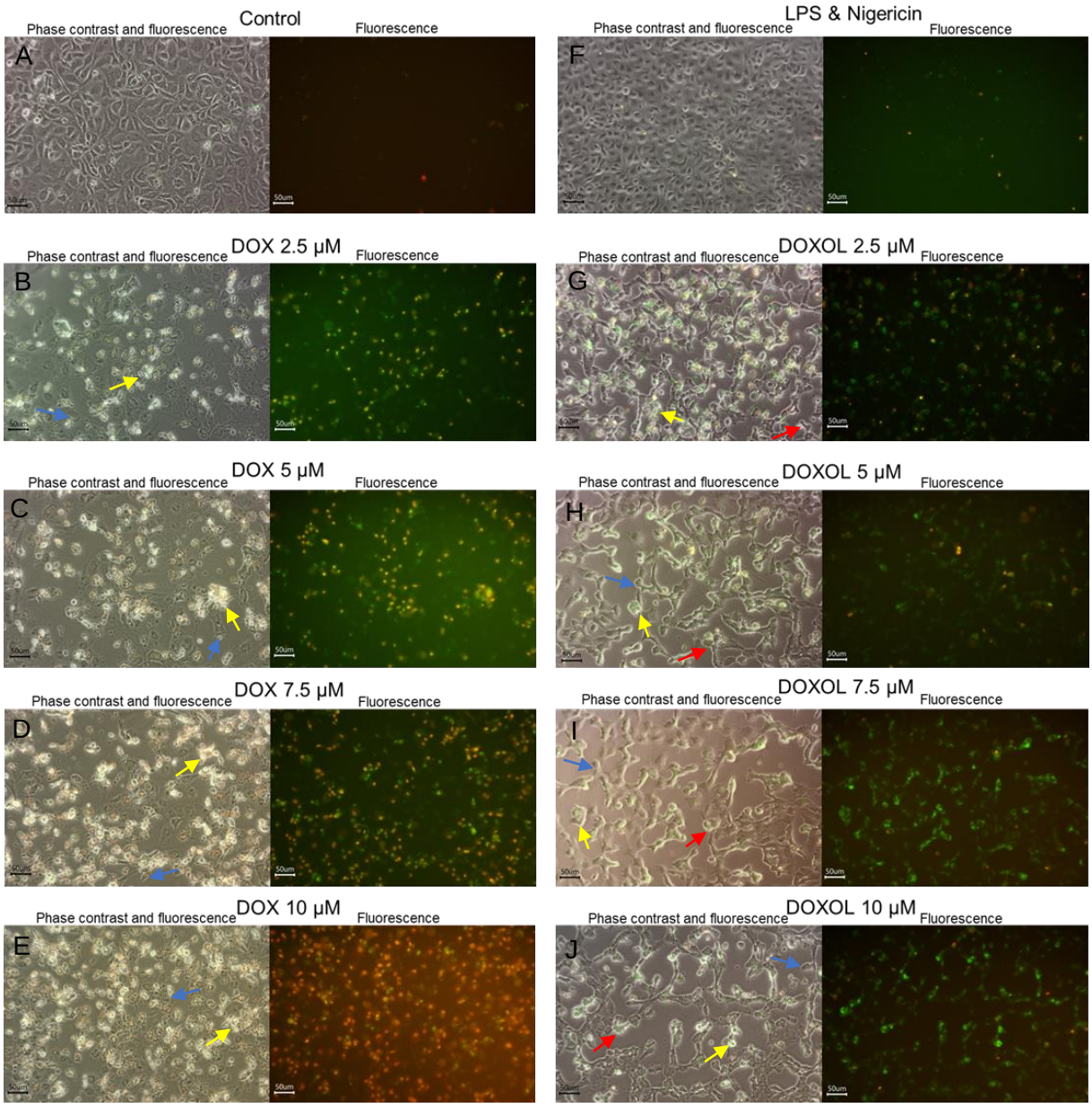

Figure 5.2 Phase-contrast and fluorescent staining images of HCAEC cells treated with the indicated concentration of doxorubicin (DOX), doxorubicinol (DOXOL), or LPS & Nigericin. Phase-contrast images are shown side-by-side with matching fluorescent images indicating lethally injured (propidium iodide staining, red) and apoptotic (FITC-Annexin V, green) cells. Each scale bar represents 50 µm. Doxorubicin or doxorubicinol caused HCAEC cells to alter appearance (e.g. blue arrows), condense in a round shape and cluster together (e.g. yellow arrows), or exhibit protrusions or 'blebs' in the plasma membrane (e.g. red arrows).

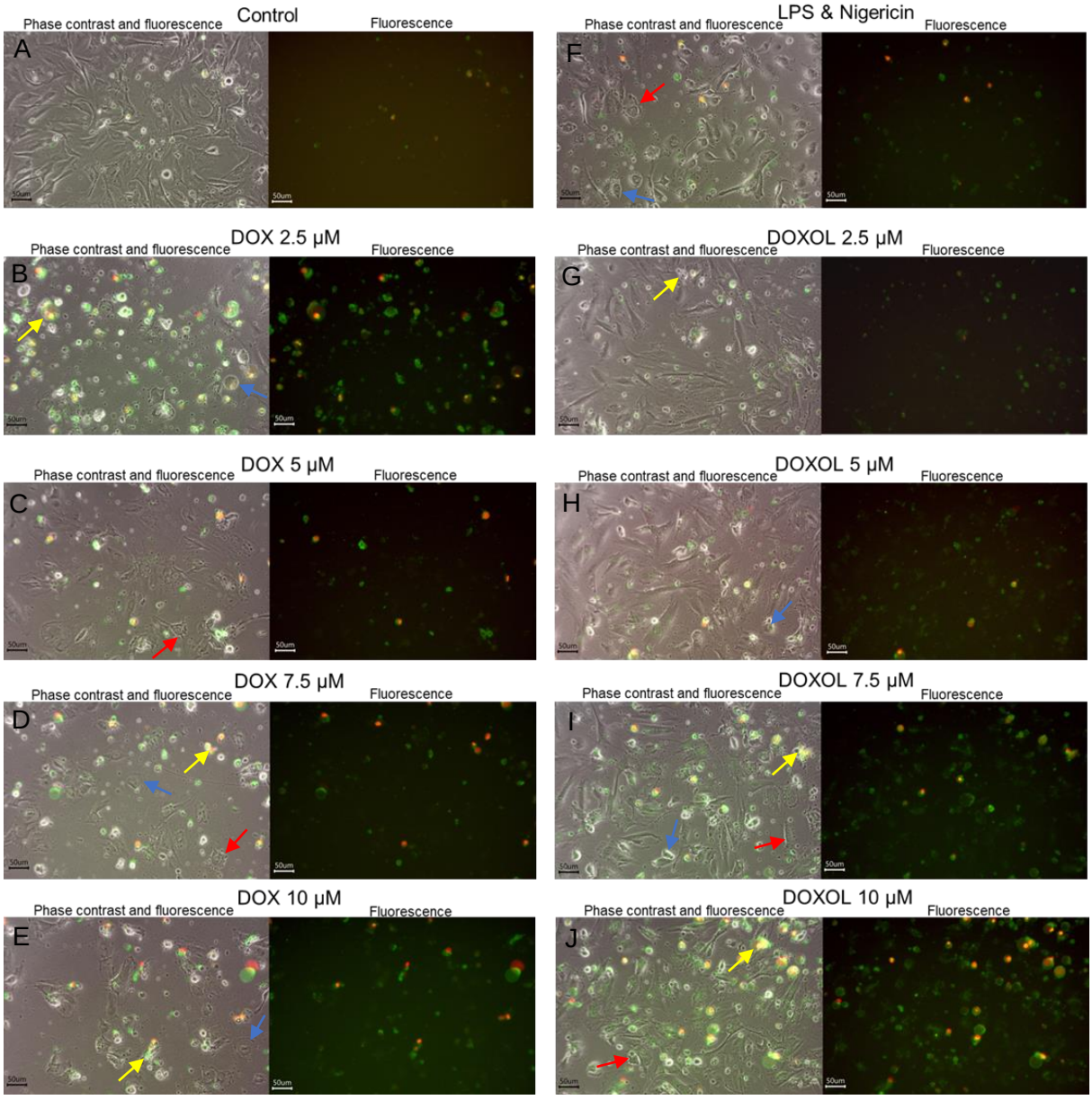

Figure 5.3 Phase-contrast and fluorescent staining images of HCMEC cells treated with the indicated concentration of doxorubicin (DOX), doxorubicinol (DOXOL), or LPS & Nigericin. Phase-contrast images are shown side-by-side with matching fluorescent images indicating lethally injured (propidium iodide staining, red) and apoptotic (FITC-Annexin V, green) cells. Each scale bar represents 50 µm. Doxorubicin or doxorubicinol caused HCMEC cells to alter appearance (e.g. blue arrows), condense in a round shape and cluster together (e.g. yellow arrows), or exhibit protrusions or 'blebs' in the plasma membrane (e.g. red arrows). HCMEC cells treated with LPS & Nigericin also exhibited cellular alterations and 'blebs' in the plasma membrane.

Figure 5.2 A-J depict the phase contrast and/or fluorescent images of the HCAEC cells with their respective treatment. The fluorescent dye propidium iodide (PI)

fluoresces red in cells in which the plasma membrane is permeabilised and FITC-Annexin V fluoresces green in cells undergoing apoptosis. Some cells (e.g. post apoptotic, lysed cells) may be stained by both PI and Annexin V, resulting in an orange appearance.

Cultured HCAEC cells generally appear small with dark, large nuclei and have a cobblestone-like appearance (Figure 5.2A). Figure 5.2 B-E show images of HCAEC cells following 18 h treatment with doxorubicin 2.5 μM to 10 μM. Morphological alterations were observed following doxorubicin treatment as the cells lost their cobblestone-like appearance and detached from the adjacent cells (blue arrow). Furthermore, some cells appeared condensed, round, and clustered together (yellow arrow). In the doxorubicin-treated cells, the fluorescent stain was predominantly green at 2.5 μM dose, suggestive of Annexin V binding, a specific marker of the apoptotic process, particularly early apoptosis injury (Figure 5.2B). However, the fluorescent stain was notably orange and red with increasing concentration, as seen at 10 μM concentration, suggesting more lethally injured cells were stained by propidium iodide (Figure 5.2E).

Figure 5.2F shows images of HCAEC cells treated with 50 ng/mL LPS for 4 h and 15 μM Nigericin for 1 h. The phase contrast image showed that the cobblestone-like appearance was still preserved. There was notably minimal fluorescent staining compared to doxorubicin- or doxorubicinol-treated groups.

Figure 5.2 G-J show images of HCAEC cells following 18 h treatment with doxorubicinol 2.5 μM to 10 μM. Doxorubicinol also induced similar morphological changes to those seen in doxorubicin-treated groups. The fluorescent staining images in doxorubicinol-treated groups appeared to be predominantly green irrespective of increasing concentration.

Figure 5.3 A-J show the phase contrast and/or fluorescent images of the HCMEC cells with their respective treatment. HCMEC cells share a relatively similar appearance to HCAEC cells, in which HCMEC cells have a cobblestone-like shape (Figure 5.3A). Both doxorubicin-treated and doxorubicinol-treated HCMEC cells exhibited cellular alterations in the forms of disruption of their normal cobblestone-like shapes, rounding and clustering with membrane ‘blebs’. The fluorescent staining in both groups was predominantly green staining, suggestive of FITC-Annexin V binding.

Treatment with 50 ng/mL LPS for 4 h and 15 μM nigericin for 1 h also caused cellular alterations and membrane ‘blebs’ in HCMEC cells, with Annexin V dyes staining the treated HCMEC cells (Figure 5.3F).

5.4.3 Western blot analysis on Gasdermin D processing in HCAEC and HCMEC cells treated with doxorubicin and doxorubicinol

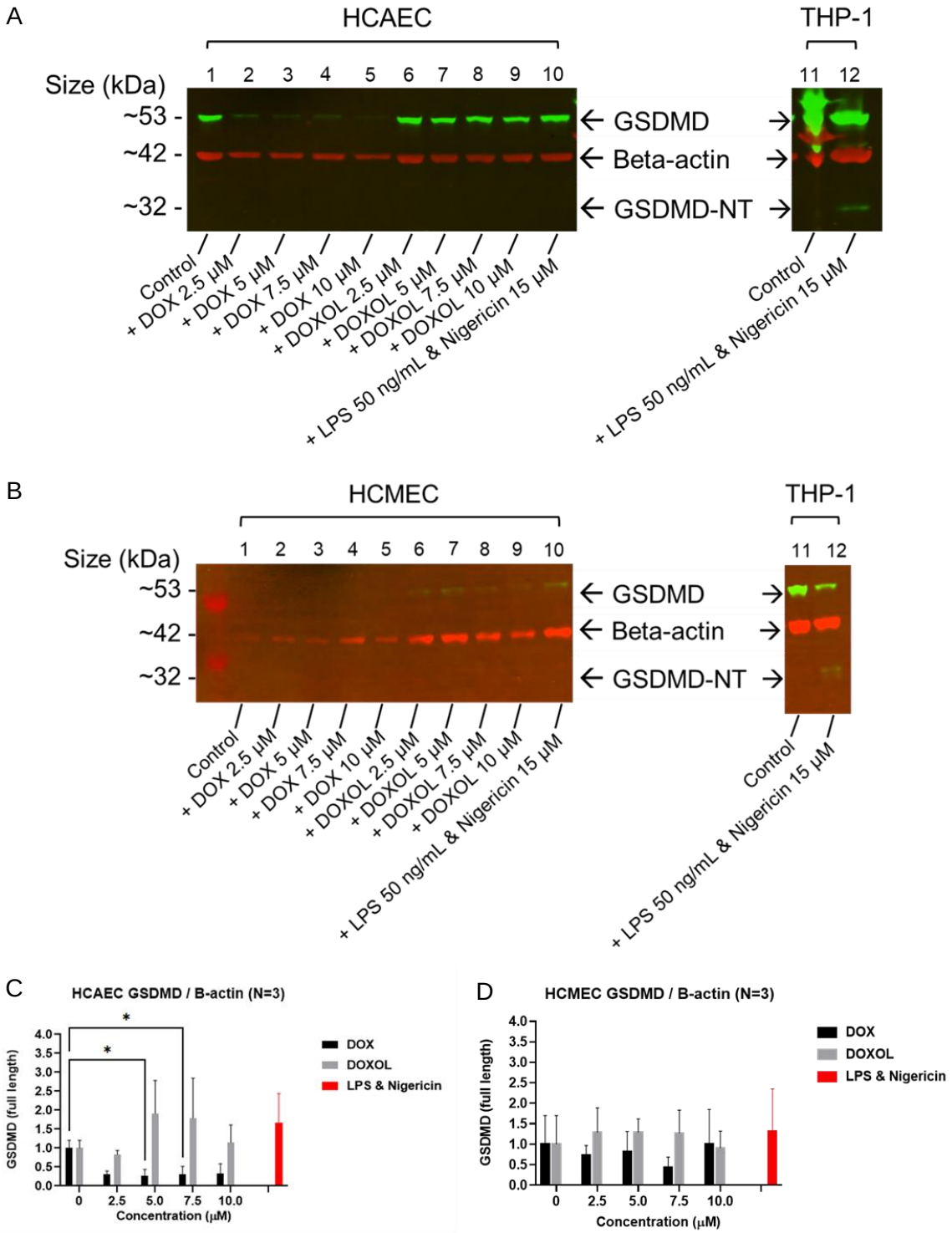

Figure 5.4 Western blot analysis of GSDMD in human vascular endothelial primary cells. **(A**,**B)** Representative immunoblots of HCAEC **(A)** and HCMEC **(B)** cells that were treated with doxorubicin (DOX) or doxorubicinol (DOXOL), probed for the indicated proteins following treatments with quantification of three replicates Western blots (**C-D**). The Y-axis showed the arbitrary unit quantification of the detected GSDMD protein band density, normalised to beta-actin, relative to the control group. THP-1 cell treated with LPS & Nigericin was used as a positive control for pyroptosis. Statistical analysis was performed using two-way ANOVA and Tukey's multiple comparison test.

Concentration	Doxorubicin (arbitrary units)	Doxorubicinol (arbitrary units)
Control (0 μM)	1 ± 0.21	1 ± 0.21
2.5 μM	0.31 ± 0.09	0.83 ± 0.10
5 μM	0.26 ± 0.16	1.91 ± 0.87
7.5 μM	0.30 ± 0.20	1.79 ± 1.06
10 μM	0.33 ± 0.25	1.15 ± 0.46
LPS & Nigericin	1.67 ± 0.76	

Table 5.3 Quantification of GSDMD band density in HCAEC cells following treatment with doxorubicin or doxorubicinol. The values are normalised to beta-actin and relative to the control group (N=3). The values correspond to the graph in Figure 5.4C. The values are mean ± standard errors of the mean.

Concentration	Doxorubicin (arbitrary units)	Doxorubicinol (arbitrary units)
Control (0 μM)	1 ± 0.7	1 ± 0.7
2.5 μM	0.73 ± 0.24	1.28 ± 0.60
5 μM	0.81 ± 0.50	1.29 ± 0.33
7.5 μM	0.43 ± 0.26	1.27 ± 0.57
10 μM	1.00 ± 0.84	0.90 ± 0.42
LPS & Nigericin	1.31 ± 1.04	

Table 5.4 Quantification of GSDMD band density in HCMEC cells following treatment with doxorubicin or doxorubicinol. The values are normalised to beta-actin and relative to the control group (N=3). The values correspond to the graph in Figure 5.4D. The values are mean ± standard errors of the mean.

Figure 5.4 shows the results of Western blot analysis of HCAEC (A) and HCMEC cells (B) treated with doxorubicin or doxorubicinol. The housekeeping protein, beta-actin (B-actin), was similar in all samples, indicating equivalent loading.

In Figure 5.4A, a full-length Gasdermin D (GSDMD) band was detected in the untreated HCAEC cells (lane 1). The intensity of the GSDMD band was notably less with the increasing doxorubicin concentration (lane 2-5). On the contrary, the GSDMD band was visible across doxorubicinol-treated and LPS & Nigericin-treated samples. The N-Terminal of Gasdermin D (GSDMD-NT) was not detected in any samples.

In Figure 5.4B, full-length GSDMD bands were not readily seen or detected in the untreated HCMEC cells (lane 1), as well as in doxorubicin-treated samples. The GSDMD bands were faintly detected in doxorubicinol-treated and LPS & Nigericin-treated samples. The GSDMD-NT was not detected in any samples.

As before, THP-1 cell was used as a positive control for the detection of cleaved GSDMD. In both Figure 5.3 A and B, full-length GSDMD was detected in the untreated as well as the LPS & Nigericin-treated THP-1 cells, as expected. The cleaved GSDMD-NT band was detected only in the LPS & Nigericin-treated THP-1 cells, indicating that the positive control for pyroptosis had worked.

Figures 5.4 C and D show the quantification of the full-length of Gasdermin D protein expression, normalised to beta-actin, relative to the control group in HCAEC and HCMEC cells (N=3 each). In doxorubicin-treated HCAEC cells (Figure 5.4C), there was statistically significant reduction in the full-length GSDMD band density observed in the 5 μM and 7.5 μM doxorubicin groups. There was no statistically significant difference observed in doxorubicinol-treated HCAEC cells. Post-hoc analysis suggested that the overall effect of doxorubicin and doxorubicinol treatment was statistically different on HCAEC cells ($P = 0.0009$).

There was no statistical difference observed in the expression of full-length GSDMD in all treatments on HCMEC cells (Figure 5.4D). Overall, both graphs illustrated that the GSDMD expression in the doxorubicin group was lower than in the doxorubicinol group for both HCAEC and HCMEC primary cells.

5.4.4 Western blot analysis on Caspase 3 processing in HCAEC and HCMEC cells treated with doxorubicin and doxorubicinol

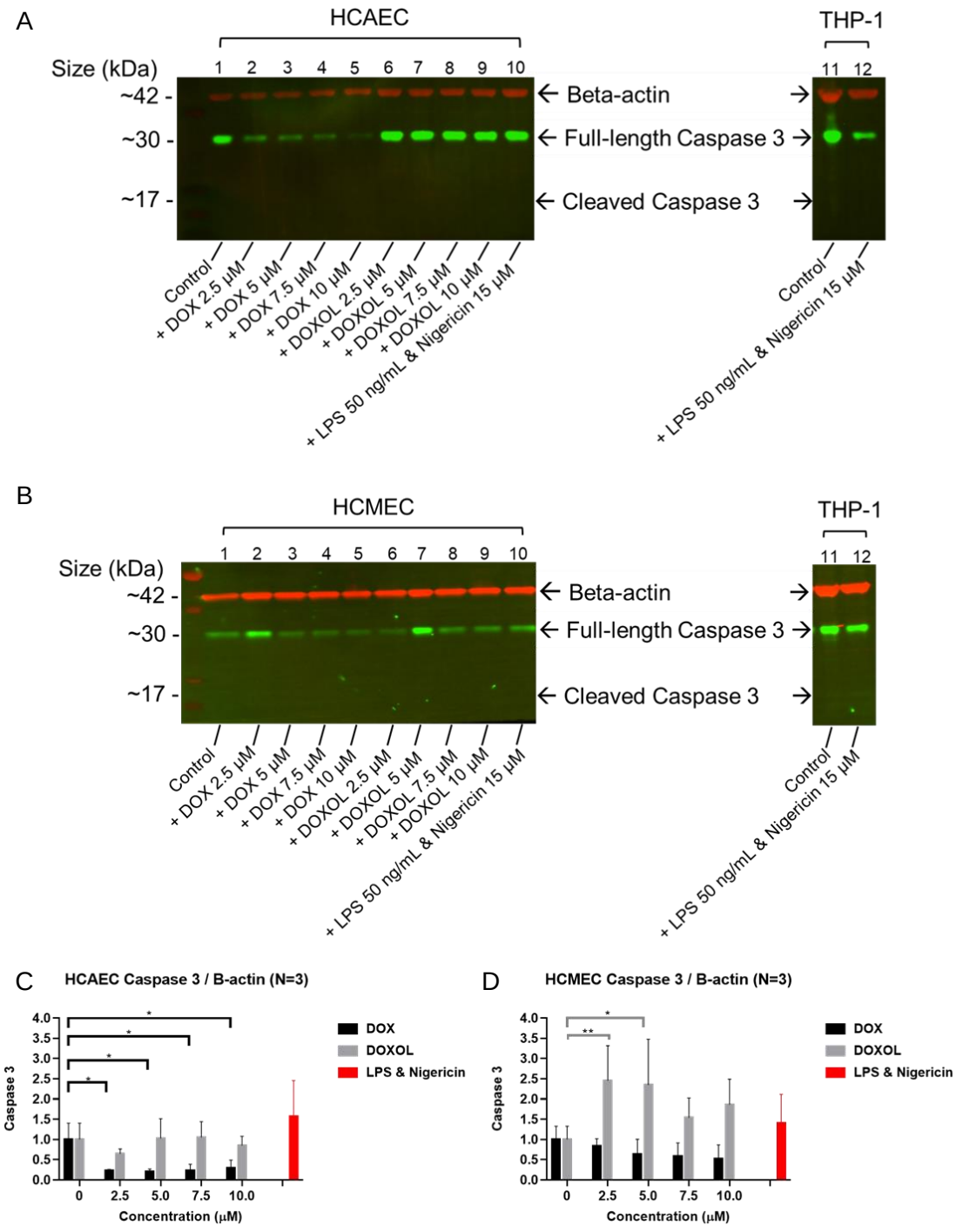

Figure 5.5 Western blot analysis of Caspase 3 in human vascular endothelial primary cells. **(A**,**B)** Representative immunoblots of HCAEC **(A)** and HCMEC **(B)** cells that were treated with doxorubicin (DOX) or doxorubicinol (DOXOL), probed for the indicated proteins following treatments with quantification of three replicates Western blots (**C-D**). The Y-axis showed the arbitrary unit quantification of the detected full-length Caspase 3 protein band density,

normalised to beta-actin, relative to the control group. THP-1 cell treated with LPS & Nigericin was used as a negative control for apoptosis. Statistical analysis was performed using two-way ANOVA and Tukey's multiple comparison test. *P value < 0.05, **P < 0.01 represents the P value of caspase 3 expression caused by the drug concentration relative to control and beta-actin.

Concentration	Doxorubicin (arbitrary units)	Doxorubicinol (arbitrary units)
Control (0 μM)	1 ± 0.40	1 ± 0.40
2.5 μM	0.23 ± 0.03	0.64 ± 0.12
5 μM	0.20 ± 0.07	1.03 ± 0.43
7.5 μM	0.24 ± 0.15	1.05 ± 0.39
10 μM	0.29 ± 0.20	0.85 ± 0.23
LPS & Nigericin	1.57 ± 0.89	

Table 5.5 Quantification of full-length Caspase 3 band density in HCAEC cells following treatment with doxorubicin or doxorubicinol. The values are normalised to beta-actin and relative to the control group (N=3). The values correspond to the graph in Figure 5.5C. The values are mean ± standard errors of the mean.

Concentration	Doxorubicin (arbitrary units)	Doxorubicinol (arbitrary units)
Control (0 μM)	1 ± 0.33	1 ± 0.33
2.5 μM	0.83 ± 0.18	2.46 ± 0.86
5 μM	0.64 ± 0.37	2.35 ± 1.13
7.5 μM	0.58 ± 0.33	1.54 ± 0.49
10 μM	0.52 ± 0.35	1.86 ± 0.63
LPS & Nigericin	1.40 ± 0.70	

Table 5.6 Quantification of full-length Caspase 3 band density in HCMEC cells following treatment with doxorubicin or doxorubicinol. The values are normalised to beta-actin and relative to the control group (N=3). The values correspond to the graph in Figure 5.5D. The values are mean ± standard errors of the mean

Figure 5.5 shows the results of Western blot analysis of HCAEC (A) and HCMEC cells (B) treated with doxorubicin or doxorubicinol. Each immunoblot shown in (A) and (B) is a representative immunoblots from three separate experiment (N=3). The housekeeping protein, beta-actin (B-actin), was similar in all samples, indicating equivalent loading.

In both HCAEC and HCMEC samples, the full-length caspase 3 was detected in the untreated sample (lane 1) and all treated groups. However, cleaved caspase 3 was not detected in any HCAEC or HCMEC samples. Similarly, full-length caspase 3 was detected in the untreated as well as the LPS & Nigericin-treated THP-1 cell samples. As expected, cleaved caspase 3 was not detected in THP-1 cells.

Figure 5.5 C-D show the quantification of the caspase 3 protein expression, normalised to beta-actin, relative to the control group in HCAEC and HCMEC cells. There was a statistically significant reduction observed in the expression of full-length caspase 3 in doxorubicin-treated HCAEC cells with increasing concentrations. In the doxorubicinol-treated HCAEC samples, the expression of full-length caspase 3 was generally higher than in doxorubicin-treated samples, but there was no significant increase or reduction observed.

The immunoblot in Figure 5.5B may suggest that there was an increase density band observed in certain groups relative to control, such as in doxorubicin 2.5 μM, but not reflected in the graph Figure 5.5D. The immunoblot was selected as the clearer representative immunoblot out of three separate experiments (N=3), whereas the graph in Figure 5.5D was a combined result of all three experiments.

In doxorubicin-treated HCMEC cells, there was a non-significant reduction in the detection of full-length caspase 3 bands. In the doxorubicinol-treated HCMEC cells, there was a significant reduction in the detection of full-length caspase 3 band in the doxorubicinol 2.5 μM and 5 μM groups. Overall, the graphs suggested that the caspase 3 expression in the doxorubicin group was lower than in the doxorubicinol group for both HCAEC and HCMEC primary cells.

5.5 Discussion

Doxorubicin, more so than doxorubicinol, caused a dose-dependent increase in cell death in HCAEC cells. However, in HCMEC cells, significant cell death was only observed in doxorubicin-treated cells.

Both doxorubicin and doxorubicinol induced morphological changes in HCAEC and HCMEC cells which were more suggestive of apoptosis instead of pyroptosis. The fluorescent staining in doxorubicin-treated HCAEC cells showed a mixture of Annexin V and Propidium Iodide, suggestive of cells that had undergone lethal injury with

damaged cell membranes, allowing PI nuclear staining and Annexin V staining of the inner and/or outer leaflet of the plasma membrane. The fluorescence in doxorubicin-treated HCMEC cells, as well as in doxorubicinol-treated HCAEC and HCMEC cells, with Annexin V staining being predominant, was suggestive of early apoptosis.

In addition, despite the detection of GSDMD and caspase 3 protein bands in the Western blot experiment with doxorubicin or doxorubicinol, the respective cleaved end-products, GSDMD-NT or cleaved caspase 3 protein, were not detected. Overall, the data analysis indicates that there was higher cytotoxicity with treated HCAEC and HCMEC cells, with apoptotic morphological alterations in the absence of the cleaved GSDMD-NT or cleaved caspase 3.

5.5.1 Doxorubicin and doxorubicinol concentration

The use of the doxorubicin and doxorubicinol concentration in this chapter has already been discussed previously in Section 4.5.1.

5.5.2 LDH cytotoxicity assay

In the LDH cytotoxicity assay experiment, a dose-dependent LDH release as a marker of cell death was observed in treated HCAEC or HCMEC cells. Overall, doxorubicin caused higher cytotoxicity than doxorubicinol.

Studies investigating the impact of anthracycline-induced cytotoxicity in human endothelial cells with a range of doxorubicin are limited. Furthermore, no studies have investigated the effect of doxorubicinol on endothelial cells. Several studies investigated the equally important functional aspects of endothelial cell such as their contractility and relaxation (Hader *et al.*, 2019, Galán-Arriola *et al.*, 2020).

Kaushal *et al* investigated doxorubicin-induced apoptosis on HCAEC cells as part of their study. They assessed the HCAEC cell viability treated with doxorubicin 1 µM from 2 h to 96 h using MTT cell viability assay in a 96-well plate (Kaushal *et al.*, 2004b). They found doxorubicin caused a progressive reduction in cell viability from 2 h to 96 h (100% to 19% cell viability over time). In particular, there was a 40 to 60% cell viability reduction between 8 h to 24 h. In a separate research study, Kaushal *et al* found 20 to 30% cell viability reduction in HCAEC cells in a 96-well plate treated with doxorubicin 0.5 µM for 12 and 24 h (Kaushal *et al.*, 2004a). Their studies found

that doxorubicin-treated HCAEC cell showed a reduction in cell viability in a time-dependent fashion. The difference found in my experiment could be attributable to the concentration of doxorubicin used, where doxorubicin 2.5 μM was the lowest dose used in this research. Using smaller concentration window for future studies may help to assess whether similar pattern to what was found by Kaushal *et al* was observed.

With regards to the HCMEC cell, Sun *et al* investigated the effect of doxorubicin on cell proliferation and vascular network formation in HCMEC as part of their study (Sun *et al.*, 2016). They plated 1,500 HCMEC cells per well in a 96-well plate. On day 0, the cells' nuclei were stained with Hoechst 33342 and imaged. On days 0, 2, and 4 plates were treated according to their protocol. The concentrations of doxorubicin used in their experiment were 4 nM, 8 nM, and 16 nM. It is worth noting that doses of doxorubicin used were considerably less and the duration was longer than my experiment protocol. On days 2, 4, and 6 plates were fixed and nuclei were stained with Hoechst 33342 and imaged. The change in cell number was expressed as a change concerning the cell counts made on day 0. Sun *et al* found doxorubicin-treated HCMEC showed a reduction in the number of endothelial cells counted in 8 nM and 16 nM doxorubicin groups after 6 days (Sun *et al.*, 2016). Surprisingly, the cell number was increased in the 4 nM doxorubicin group, suggesting that the cells could still grow with no significant cytotoxic impact at this doxorubicin concentration.

The results from data analysis in this research aligned with the findings from the aforementioned studies, in the context of higher cytotoxicity in doxorubicin-treated HCMEC cells. However, their doxorubicin dose and duration were considerably smaller and longer, respectively. The smaller dose and longer duration may be appropriate for their respective experiment protocol, given that their research used less number of plated cells and a 96-well plate; this research used a 24-well plate for cell culture and treatment. Similarly, using considerably less concentration in my experiment protocol might represent the physiological concentration of doxorubicin or doxorubicinol, but this lower concentration might influence the impact of cytotoxicity observed.

A different study investigated the anthracycline effect on cardiac microvascular cells using primary cardiac microvascular cells from adult male Wistar rats (Chiusa *et al.*, 2012). Cardiac microvascular cells were enzymatically released from the left

ventricular tissue of adult male Wistar rats (250 - 350 g). The cardiac microvascular cells were subsequently treated with doxorubicin 0.5 - 20 μM in 18 h and LDH release was measured. Chiusa *et al* found that there was no significant increase in LDH release at 1 μM doxorubicin, but a significant increase in LDH release was observed at the next subsequent dose of 5 μM and plateaued thereafter up to 20 μM. The *in vitro* data with HCMEC in the current research study echoed the *ex vivo* findings reported by Chiusa *et al* suggesting similarities in LDH release between HCMEC and isolated rat cardiac microvascular cells. This may offer a translational research study in the future, such as investigating a prospective treatment using *in vivo* and *ex vivo* in isolated human and rodent cells respectively.

In the current study, LDH cytotoxicity assay was used instead of MTT assay. Both LDH cytotoxicity assay and MTT cell viability assay are common laboratory methods employed in cell death experiments. However, both have their limitations. As discussed previously, LDH cytotoxicity assay measures LDH release, which may naturally decrease over time as a result of natural degradation. Furthermore, LDH release alone cannot be used to distinguish different cell death modalities, as it reflects LDH release when the cell membrane is damaged. Thus, it may not be relevant in early apoptosis injury. MTT cell viability assay measures mitochondrial activity in the conversion of MTT salt. The conversion of MTT by the mitochondria may reflect metabolic alteration but it does not necessarily correlate to cell viability. For instance, overconfluent cells can lead to a shutdown of mitochondrial function. In this condition, the use of MTT assay may lead to the underestimation of living cells. Ideally, the use of both methods will provide data on both cytotoxicity and cell proliferation.

Taking these observations together, results from this research suggest that the cytotoxicity was higher in HCAEC and HCMEC treated with doxorubicin compared to doxorubicinol. In addition, HCAEC was more vulnerable than HCMEC to doxorubicin and doxorubicinol-induced cytotoxicity. The *in vitro* findings from this current study corroborates the *in vivo* findings that suggest endothelial damage occurred early and preceded the classic manifestation of anthracycline induced cytotoxicity (Galan-Arriola *et al.*, 2021). Given the intravenous administration of anthracyclines in the clinical setting, macrovascular endothelial cell was likely to be exposed from higher plasma concentration of circulating anthracyclines before the remaining plasma concentration arrives in the microvascular environment.

5.5.3 Microscopical and fluorescent staining analysis

The findings of the microscopical analysis and fluorescent staining on treated HCAEC suggest that the morphological changes caused by doxorubicin and doxorubicinol resembled apoptotic changes. The fluorescent staining images were taken at the same time as the phase contrast images, and these showed predominantly Annexin V-positive fluorescent in doxorubicin-treated cells, with PI-positive fluorescence present at higher concentrations. The visible presence of PI fluorescence at higher doxorubicin concentrations might suggest that the cells had a lethal injury with damaged cell membranes. The fluorescent staining images of doxorubicinol-treated cells showed predominantly Annexin V-positive fluorescent, suggestive of early apoptosis injury where the integrity of the cell membrane was still preserved.

Similarly, the findings of the microscopical analysis and fluorescent staining on treated HCMEC suggest that the morphological changes caused by doxorubicin and doxorubicinol resembled apoptotic changes. Overall, the fluorescent staining images of treated HCMEC cells showed predominantly Annexin V-positive fluorescent.

As previously described in Section 4.5.3, cells undergoing the apoptotic process may exhibit different cellular alterations at the different stages of apoptosis. The changes that were observed in the HCAEC and HCMEC cells aligned with the description of apoptotic changes (Häcker, 2000). Morphological changes such as cellular condensation and disintegration, the formation of apoptotic bodies, and plasma membrane protrusions were observed. Similar descriptions were reported by Kaushal *et al*, in which they found that treatment with 1 μM doxorubicin over 24 h caused HCAEC cells to disintegrate and form apoptotic bodies (Kaushal *et al.*, 2004b).

In light of these observations, results from this research suggest that the cytotoxicity process induced by doxorubicin and doxorubicinol in HCAEC and HCMEC was predominantly driven by the apoptotic process. Further experiment using fluorescent staining-tracked flow cytometry may help strengthen the findings further.

5.5.4 Western blot analysis

Western blot analysis was conducted to assess whether Gasdermin D (GSDMD) or caspase 3 processing took place in treated HCAEC and HCMEC cells.

This analysis aims to further evaluate whether pyroptosis or apoptosis took place in the context of GSDMD or caspase 3 detections along with their respective cleaved or activated proteins.

There have been a limited number of studies exploring the role of pyroptosis in anthracycline-induced cytotoxicity on cardiac endothelial cells, particularly in coronary artery or cardiac microvascular cells. However, the majority of studies have looked at the role of pyroptosis outside the scope of anthracycline-induced cytotoxicity, such as cardiovascular disease (Ridker *et al.*, 2011), acute vasculitis syndromes such as Kawasaki disease (Jia *et al.*, 2019), or severe infection i.e. sepsis (Gao *et al.*, 2018). Therefore, there is evidence that vascular endothelial cells can be driven to pyroptotic-mediated cell death.

Much research has focused on studying the role of apoptosis-mediated cell death in cardiac endothelial cells (Wu *et al.*, 2002, Kotamraju *et al.*, 2000, Kaushal *et al.*, 2004b, Zhou *et al.*, 2022b). In all of the referenced studies, the investigators demonstrated cleaved caspase 3 in their immunoblot experiments using *in vivo* or *in vitro* models.

In the experiments conducted in this research, neither GSDMD-NT nor cleaved caspase 3 were detected. As the lack of GSDMD-NT and caspase 3 cleavage was also observed in the H9c2 experiments discussed in Chapter 4, the supplier confirmed that the primary antibodies, E9S1X and anti-Caspase 3, have cross-reactivity with rats and humans. Unequal protein loading or lower concentration could be a factor despite fastidious attempts to minimise it. In the literature, different primary antibodies could be used for assessing GSDMD or caspase 3 and their cleaved end products, and these different primary antibodies may be more sensitive. Nevertheless, the antibodies used in this research were confirmed to be capable of detecting GSDMD or caspase 3 and their cleaved end-products using a positive control of THP-1 cells.

5.6 Limitations

First, one inherent limitation of my study is the endothelial cell donor. As previously mentioned in Section 5.3.1, the donors of HCAEC and HCMEC were 55 and 15 years of age with a relevant cardiac history of dilated cardiomyopathy. Dilated cardiomyopathy is the most common phenotype of heart failure and it has been

associated with anthracycline-induced cardiomyopathy (Cardinale *et al.*, 2020, Chatterjee *et al.*, 2010). Both donors had not been treated with anthracyclines or diagnosed with coronary artery disease. Whether dilated cardiomyopathy affects microvascular endothelial cells warrants further studies (Crea *et al.*, 2014). This limitation could have been mitigated by adding the source of HCAEC cells from different suppliers, but it was not possible to achieve this within the timeframe of this PhD research.

Furthermore, endothelial cell cultures are recommended in a limited series of passages before senescence is reached. Efforts were made in this research to ensure that HCAEC and HCMEC cells were subcultured according to the supplier's recommendations. However, it is important to take into account that serial subculturing even before reaching the recommended passage limit may inevitably still result in senescent cells that can affect the experiment results.

Second, there are a range of experiment methods that could be used to complement my findings. For example, the use of flow cytometry may help objectively evaluate the proportion of cells undergoing early apoptosis and late apoptosis injury. This could be particularly useful to complement the fluorescent staining experiments, to provide a more quantitative assessment. Equally important, the findings of LDH cytotoxicity assay in HCAEC and HCMEC cells highlighted the need to repeat the experiments in a smaller drug concentration, i.e. 0.5 μM and 1 μM, to assess whether different dose-dependent cell death response and cell death pathway were observed.

Third, the scarcity of similar published studies limits comparison to previous results in the literature. As previously described, the role of pyroptosis in anthracycline-induced cytotoxicity on human vascular endothelial cells has not been extensively investigated. Although studies have examined microvascular endothelial cells and the impact of anthracycline cytotoxicity, the common microvascular endothelial cell used *in vitro* was of human umbilical vein endothelial cell (HUVEC).

HUVEC is a foetal tissue which is commercially available or can be isolated with a high success rate. HUVEC has widely been used to investigate a broad range of biological processes or diseases affecting endothelial cells, such as cancer, cardiovascular disease, and preeclampsia (Medina-Leyte *et al.*, 2020).

HUVEC may be the appropriate model to answer specific research questions. However, vascular endothelium is characterised by heterogeneity in its morphology and function. This heterogeneity may differentiate the biological characteristics of macro- and microvascular endothelial cells as well as endothelial cells isolated between different organs (Bachetti *et al.*, 2000). Therefore, the use of human coronary artery and cardiac microvascular endothelial cells in the current research study is aptly more relevant. Furthermore, there is no previous reference looking at doxorubicinol and its impact on vascular endothelial cells. These limitations underline the potential opportunity to contribute further to the scientific community on this growing subject.

5.7 Conclusion

Table 5.1 and 5.2 summarise the experiments in the human vascular endothelial cells, HCAEC and HCMEC, respectively. This chapter examined whether pyroptosis contributes to the anthracycline-induced cytotoxicity on HCAEC and HCMEC treated with doxorubicin or doxorubicinol.

Data from the current research study suggested that, when treated with doxorubicin, both primary cells underwent apoptosis with the fluorescent staining indicating more lethally injured cells or late apoptosis at higher concentrations. On the contrary, both primary cells underwent early apoptosis when treated with doxorubicinol. The take-home message from this chapter is doxorubicin and doxorubicinol are likely to induce cytotoxicity through apoptosis at different potency, with coronary artery endothelial cells appearing to be more sensitive to the anthracycline-induced cytotoxicity than cardiac microvascular endothelial cells. In the clinical setting, these findings could be translated that coronary artery endothelial dysfunction may accelerate coronary artery disease in cancer patients and precede anthracycline-induced cardiomyopathy or heart failure, particularly those who already have pre-existing cardiac risk factors such as obesity, diabetes, or hypertension.

The next chapter will evaluate the effect of anthracycline-induced cytotoxicity in two human cancer cell lines, MCF7 (breast cancer cell line) and THP-1 (acute myeloid leukaemia cell line). This will be valuable to assess whether these cancer cell lines trigger similar cell death pathway response to what has been observed in this and previous chapter. Furthermore, given the THP-1 cell line has been used as a positive

control of pyroptosis, the next chapter will provide valuable insight into whether treatment with doxorubicin or doxorubicinol triggers the same cell death pathway.

Assays	HCAEC	
	Doxorubicin	Doxorubicinol
LDH cytotoxicity assay	Significant cytotoxicity was detected at 2.5 μM after 18 h (29.9% ± 4%)	Significant cytotoxicity was detected at 7.5 μM after 18 h (20.2% ± 5.6%)
Morphological changes	Apoptotic (condensed and clustered cells, membrane blebbing)	Apoptotic
Fluorescent staining	Annexin V green positive indicating apoptosis At higher concentrations, a mixture with propidium iodide (PI) positive stain, indicating permeability due to damaged plasma membrane in late apoptosis/necrosis	Annexin V green positive indicating apoptosis
Western blot	Full-length GSDMD was faintly detected GSDMD-NT was not detected Full-length caspase 3 was detected Cleaved caspase 3 was not detected	Full-length GSDMD was detected GSDMD-NT was not detected Full-length caspase 3 was detected Cleaved caspase 3 was not detected

Table 5.7 Table summary of HCAEC experiments with doxorubicin and doxorubicinol.

Assays	HCMEC	
	Doxorubicin	Doxorubicinol
LDH cytotoxicity assay	Significant cytotoxicity was detected at 2.5 μM after 18 h (20.9% ± 1.6%)	No significant cytotoxicity was detected after 18 h
Morphological changes	Apoptotic (condensed and clustered cells, membrane blebbing)	Apoptotic
Fluorescent staining	Annexin V green positive indicating apoptosis	Annexin V green positive indicating apoptosis
Western blot	Full-length GSDMD and GSDMD-NT were not detected Full-length caspase 3 was detected Cleaved caspase 3 was not detected	Full-length GSDMD was detected. GSDMD-NT was not detected Full-length caspase 3 was detected Cleaved caspase 3 was not detected

Table 5.8 Table summary of HCMEC experiments with doxorubicin and doxorubicinol.

Chapter 6 Anthracycline-induced cytotoxicity in human cancer cell lines

6.1 Introduction

Since its discovery, anthracycline has been used to treat a range of malignancies. Anthracycline is a potent family of chemotherapy agents, but its cytotoxicity effect is not selective to malignant cells. Previous chapters have elaborated on the effect of anthracycline-induced cytotoxicity in both rat cardiac myocyte and human vascular endothelial cells.

This chapter presents the results from evaluating the effect of anthracycline-induced cytotoxicity on two types of cancer cells, which are human cancer breast cancer cell line (MCF-7) and human monocytic acute myeloid leukaemia cell line (THP-1). Specifically, it discusses the results from assessing whether the cell death pathway triggered by doxorubicin and its major metabolite is different between the cancer cell and cardiac myocyte and endothelial cells.

6.2 Research hypothesis, aims and objectives

The main hypothesis investigated in this chapter was that the pyroptotic cell-death pathway contributes to anthracycline-induced cytotoxicity in human cancer breast cancer cell line (MCF-7) and human monocytic acute myeloid leukaemia cell line (THP-1).

To investigate this hypothesis, this research assessed whether the morphological alterations in treated cells resembled the pyroptotic process and whether Gasdermin-D (GSDMD) with its N-Terminal Gasdermin-D (GSDMD-NT) were detected in treated cells using Western blot analysis. Due to time constraints, this research was not able to measure the extent of lytic cell death observed in treated MCF-7 and THP-1 cells using the lactate dehydrogenase cytotoxicity assay.

The specific experimental objectives addressed in this chapter were:

1. To characterise the morphological alterations observed in treated cells.
2. To determine the extent of pyroptosis and apoptosis in treated cells.

3. To evaluate whether Gasdermin D processing and caspase 3 processing occur in treated cells.

6.3 Methods

6.3.1 Cell cultivation

The MCF-7 cell line was originally harvested from the pleural fluids of a 69-year-old Caucasian female donor who suffered from metastatic breast adenocarcinoma and it is now the most extensively studied human breast cancer cell line in the world (Soule *et al.*, 1973, Lee *et al.*, 2015).

THP-1 cell line is a monocytic cell of acute myeloid leukaemia from a 1-year-old male donor (Tsuchiya *et al.*, 1980). For these studies, a frozen stock of MCF-7 cells that was stored in the lab was used, while the THP-1 cell line was generously donated by the Eastman Dental Institute, UCL.

The detailed cell cultivation technique and its material are described in Section 3.1.2 and Table 3.2, respectively.

6.3.2 Doxorubicin or doxorubicinol treatment

Once the cells achieved the target confluency, the medium was replaced with a fresh medium (control) or with a medium containing either doxorubicin (DOX) or doxorubicinol (DOXOL). For the THP-1 cell line, as it is a suspension cell, the treatment was administered directly to the medium. The concentrations of doxorubicin and doxorubicinol used were between 0 µM (control) to 10 µM.

6.3.3 Microscopical analysis and fluorescent staining

In a separate experiment, MCF7 and THP-1 cells were cultured in a 24-well plate (20,000 cells per well) and treated with doxorubicin or doxorubicinol for 18 h. The concentration range of doxorubicin and doxorubicinol used was between 0 µM (control) and 10 µM. In addition, a separate well with MCF-7 or THP-1 cells was treated with 50 ng/mL LPS for 4 h followed by 5 µM Nigericin for 1 h, a treatment known to induce pyroptosis in various cell types. This was to evaluate the possible different cellular alterations between doxorubicin, doxorubicinol, and LPS & Nigericin on human

vascular endothelial cells. The method of introducing fluorescent dyes has been described in Chapter 3 Subchapter 3.4 and Chapter 4 Subchapter 4.3.4.

6.3.4 Western Blot

6.3.4.1 Types of cells and treatment used in Western blot experiment

The MCF-7 and THP-1 cells were seeded at 1 x 10^6 cells per 100 mm cell dish with the cell media changed every two or three days until the cells reached target confluency. Thereafter, the cell media were changed with the respective treatment, such as control (cell media only), doxorubicin or doxorubicinol, added accordingly. The concentration range of doxorubicin and doxorubicinol used was between 0 μM (control) and 10 μM.

The THP-1 cell line was used as a positive control as it is known to undergo pyroptosis. THP-1 cells were seeded at 1 x 10^6 cells per 100 mm cell dish. Two groups of THP-1 cells were used: control and treatment with 50 ng/mL LPS for 4 h followed by 15 μM Nigericin for 1 h. This LPS & Nigericin regime was used as an inducer of pyroptosis as per the supplier's recommendation.

6.3.4.2 Protein collection, quantification, and Western blot methods

The method used for protein collection, quantification, and Western blot was the same as deliberated in Section 4.3.5.2.

6.4 Results

This section will outline the results of the LDH cytotoxicity experiments, microscopical and fluorescent staining imaging, and Western blot experiments in the HCAEC and HMCEC cells.

6.4.1 Phase-contrast and fluorescent imaging of treated MCF-7 and THP-1 cells

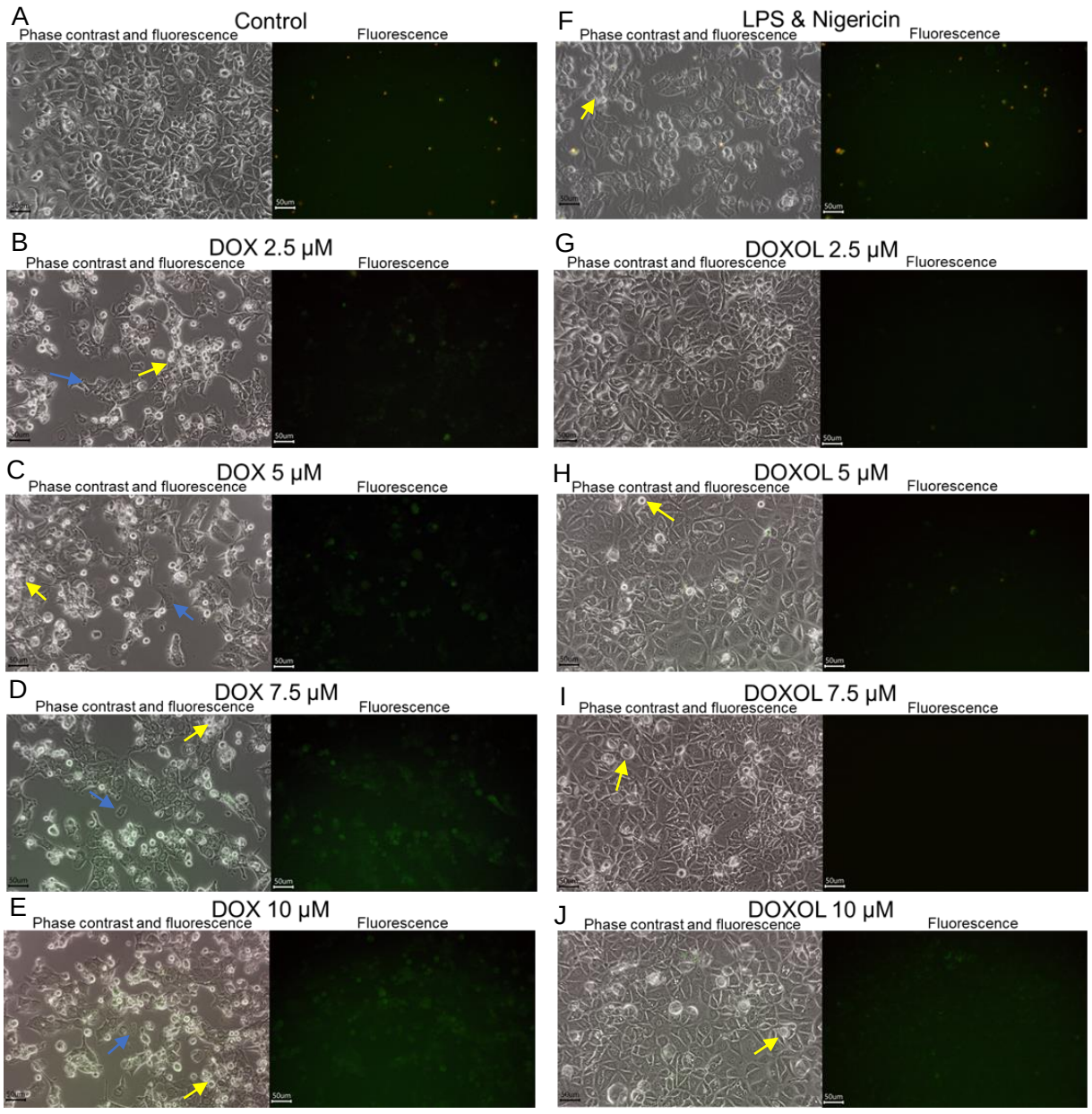

Figure 6.1 Phase-contrast and fluorescent staining images of MCF-7 cells treated with the indicated concentration of doxorubicin (DOX), doxorubicinol (DOXOL), or LPS & Nigericin. Phase-contrast images are shown side-by-side with matching fluorescent images indicating lethally injured (propidium iodide staining, red) and apoptotic (FITC-Annexin V, green) cells.

Each scale bar represents 50 µm. Doxorubicin more so than doxorubicinol caused MCF-7 cells to alter their appearance (blue arrows), condense in a round shape and cluster together (yellow arrows).

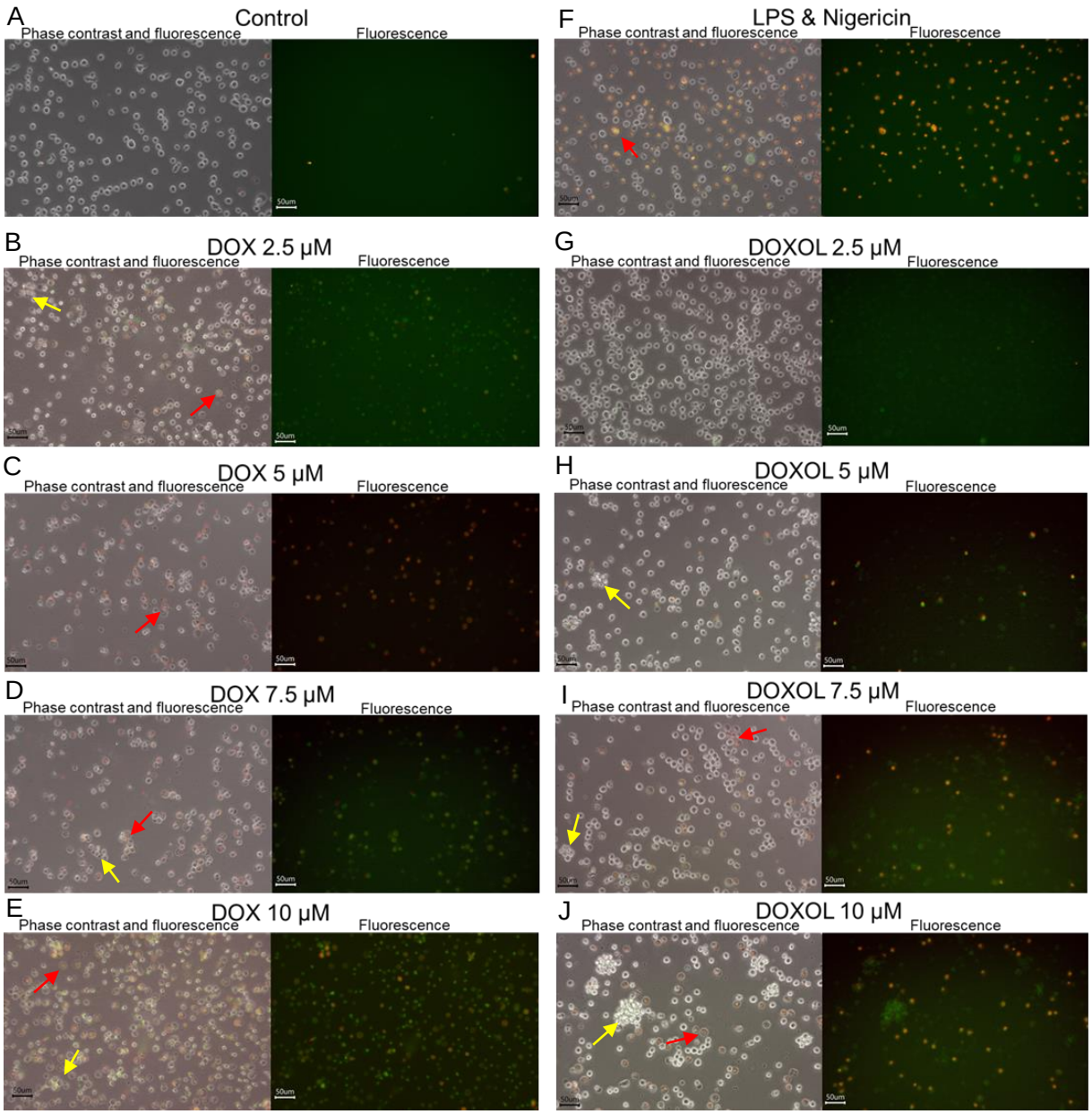

Figure 6.2 Phase-contrast and fluorescent staining images of THP-1 cells treated with the indicated concentration of doxorubicin (DOX), doxorubicinol (DOXOL), or LPS & Nigericin. Phase-contrast images are shown side-by-side with matching fluorescent images indicating lethally injured (propidium iodide staining, red) and apoptotic (FITC-Annexin V, green) cells. Each scale bar represents 50 µm. Doxorubicin or doxorubicinol caused THP-1 cells to condense in a round shape and cluster together (yellow arrows), and exhibit swelling in the nucleus and the plasma membrane (red arrows). THP-1 cells treated with LPS & Nigericin also exhibited nuclear and plasma membrane swelling.

Figure 6.1 A-J show the phase contrast and/or fluorescent images of the MCF-7 cells with their respective treatment. The fluorescent dye propidium iodide (PI) fluoresces red in cells in which the plasma membrane is permeabilised and FITC-Annexin V fluoresces green in cells undergoing apoptosis. Some cells (e.g. post apoptotic, lysed cells) may be stained by both PI and Annexin V, resulting in an orange appearance.

Healthy, cultured MCF-7 cells generally appear polygonal, clustered together, and display a cobblestone-like appearance (Figure 6.1A). Figure 6.1 B-E show images of MCF-7 cells following 18 h treatment with doxorubicin 2.5 μM to 10 μM. Morphological alterations were observed following doxorubicin treatment as the cells lost their cobblestone-like appearance and detached from the adjacent cells (blue arrow). Furthermore, some cells appeared condensed, round, and clustered together (yellow arrow). In the doxorubicin-treated cells, the fluorescent stain was predominantly green, suggestive of Annexin V binding, a specific marker of the apoptotic process, particularly early apoptosis injury. Interestingly, there was no propidium iodide fluorescent stain observed with increasing doxorubicin concentration.

Figure 6.1F shows images of MCF-7 cells treated with 50 ng/mL LPS for 4 h and 15 μM Nigericin for 1 h. The phase contrast image showed that the cobblestone-like appearance which was disrupted with some cells were co-stained with Annexin V and propidium iodide. However, there was notably minimal fluorescent staining compared to doxorubicin- or doxorubicinol-treated groups.

Figure 6.1 G-J show images of MCF-7 cells following 18 h treatment with doxorubicinol 2.5 μM to 10 μM. Doxorubicinol did not induce significant morphological changes in MCF-7 cells. Doxorubicinol-treated cells maintained cellular appearances as seen in the untreated cells.

Figure 6.2 A-J show the phase contrast and/or fluorescent images of the THP-1 cells with their respective treatment. THP-1 cells are generally small and round cells that suspend in the growth medium (Figure 6.2A). Both doxorubicin-treated and doxorubicinol-treated THP-1 cells exhibited cellular alterations in the forms of clustering as well as nuclear and plasma membrane swelling. The fluorescent staining in both groups was co-stained with FITC-Annexin V binding and propidium iodide, particularly with increasing concentration. THP-1 cells treated with 50 ng/mL LPS for

4 h and 15 μM Nigericin for 1 h, a known inducer of pyroptosis, notably caused nuclear and plasma membrane swelling with co-staining of Annexin V and propidium iodide (Figure 6.2F).

6.4.2 Western blot analysis on Gasdermin D processing in MCF-7 and THP-1 cells treated with doxorubicin and doxorubicinol

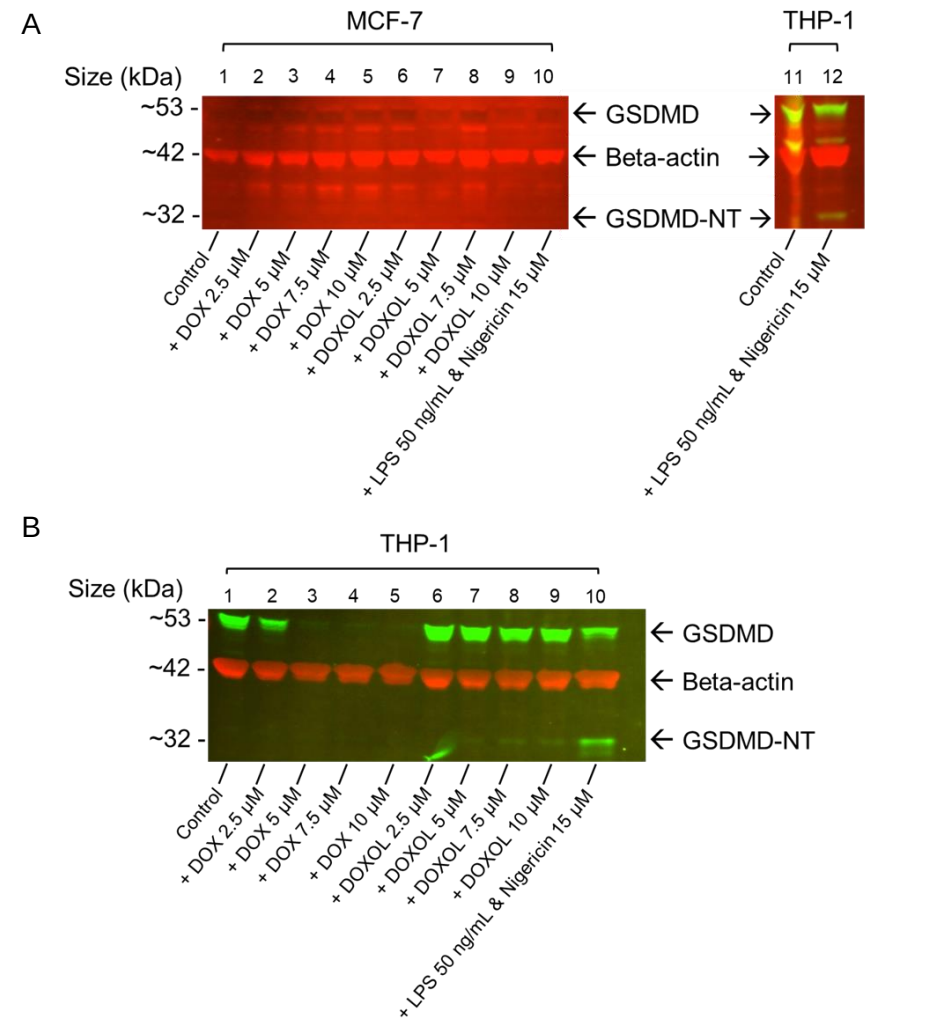

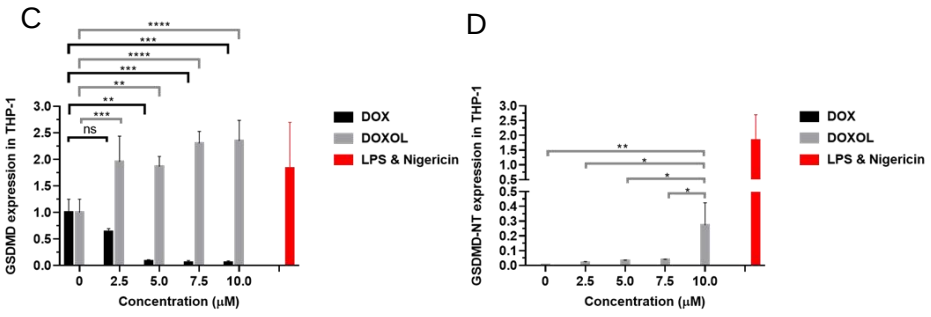

Figure 6.3 Western blot analysis of GSDMD in MCF-7 and THP-1 cell lines. **(A**, **B)** Representative immunoblots of MCF-7 (N=3) **(A)** and THP-1 (N=3) **(B)** cells that had been treated with doxorubicin (DOX) or doxorubicinol (DOXOL), probed for GSDMD and beta-actin following treatments. Quantification of GSDMD and GSDMD-NT levels in THP-1 cell **(B)** is shown in **C-D** (N=3). The Y-axis in **(C)** showed the arbitrary unit quantification of the detected GSDMD protein band density, normalised to beta-actin, relative to the control group. The Y-axis in **(D)** showed the arbitrary unit quantification of the detected GSDMD-NT protein band density, normalised to beta-actin, relative to the respective GSDMD band density. THP-1 cells treated with LPS & Nigericin were used as a positive control for pyroptosis and GSDMD-NT cleavage. Statistical analysis was performed using two-way ANOVA and Tukey's multiple comparison test. ns non significant, * p value < 0.05, ** p value < 0.01, *** p value < 0.001, **** p value < 0.0001.

Concentration	Doxorubicin (arbitrary units)	Doxorubicinol (arbitrary units)
Control (0 μM)	1 ± 0.25	1 ± 0.25
2.5 μM	0.64 ± 0.06	1.96 ± 0.48
5 μM	0.08 ± 0.03	1.86 ± 0.19
7.5 μM	0.06 ± 0.03	2.30 ± 0.23
10 μM	0.06 ± 0.03	2.35 ± 0.38
LPS & Nigericin	1.84 ± 0.86	

Table 6.1 Quantification of GSDMD band density in THP-1 cells following treatment with doxorubicin or doxorubicinol. The values are normalised to beta-actin and relative to the control group (N=3). The values correspond to the graph in Figure 6.3C. The values are mean ± standard errors of the mean.

Concentration	Doxorubicinol (arbitrary units)
2.5 μM	0.02 ± 0.01
5 μM	0.03 ± 0.01
7.5 μM	0.04 ± 0.01
10 μM	0.27 ± 0.150

Table 6.2 Quantification of GSDMD-NT band density in THP-1 cells following treatment with doxorubicinol. The values are normalised to beta-actin, relative to the respective GSDMD band density (N=3). The values correspond to the graph in Figure 6.3D. The values are mean ± standard errors of the mean.

Figure 6.3 A-B show a representative Western blot membrane of MCF-7 (A) and THP-1 cells (B) with their respective treatments (N=3). The housekeeping protein, beta-actin (B-actin), was similar in all samples, indicating equivalent loading.

In Figure 6.3A, a full-length Gasdermin D (GSDMD) band was not detected in the untreated and treated MCF-7 cells. Similarly, the N-Terminal of the Gasdermin D (GSDMD-NT) was not detected in any MCF-7 samples. In Figure 6.3B, a full-length GSDMD band was detected in the untreated THP-1 cells (lane 1). In doxorubicin-treated samples, the GSDMD band was detected at 2.5 μM doxorubicin but the GSDMD band diminished with increasing concentrations. The GSDMD-NT bands were not detected in doxorubicin-treated samples.

In doxorubicinol-treated samples, the GSDMD bands were detected. Interestingly, faint GSDMD-NT bands were detected in doxorubicinol-treated samples with increasing concentration (lanes 6-9). These faint GSDMD-NT bands were consistently detected in three biological experiments.

THP-1 cell was used as a positive control for the detection of cleaved GSDMD. In both Figure 6.3 A and B, full-length GSDMD was detected in the untreated as well as the LPS & Nigericin-treated THP-1 cells, as expected. The cleaved GSDMD-NT band was detected only in the LPS & Nigericin-treated THP-1 cells, confirming that cleaved GSDMD-NT could be detected when pyroptosis occurred.

Figures 6.3 C-D show the quantification of Gasdermin D, normalised to beta-actin, relative to the control group (C) and GSDMD-NT relative to GSDMD (D) in THP-1 cells. In doxorubicin-treated samples, there was a statistical difference observed in the expression of full-length GSDMD, particularly in 5 μM Doxorubicin and above. A significant statistical difference was also observed in the doxorubicinol-treated group with increasing concentration. Figure 6.3D shows there was statistically significant expression of GSDMD-NT in THP-1 cells treated with 10 μM doxorubicinol.

Overall, the graphs suggested that GSDMD expression in the doxorubicinol-treated THP-1 cells was higher than in doxorubicin-treated samples. The GSDMD-NT, albeit small, was detected with increasing concentration of doxorubicinol.

6.4.3 Western blot analysis on Caspase 3 processing in MCF-7 and THP-1 cells treated with doxorubicin and doxorubicinol

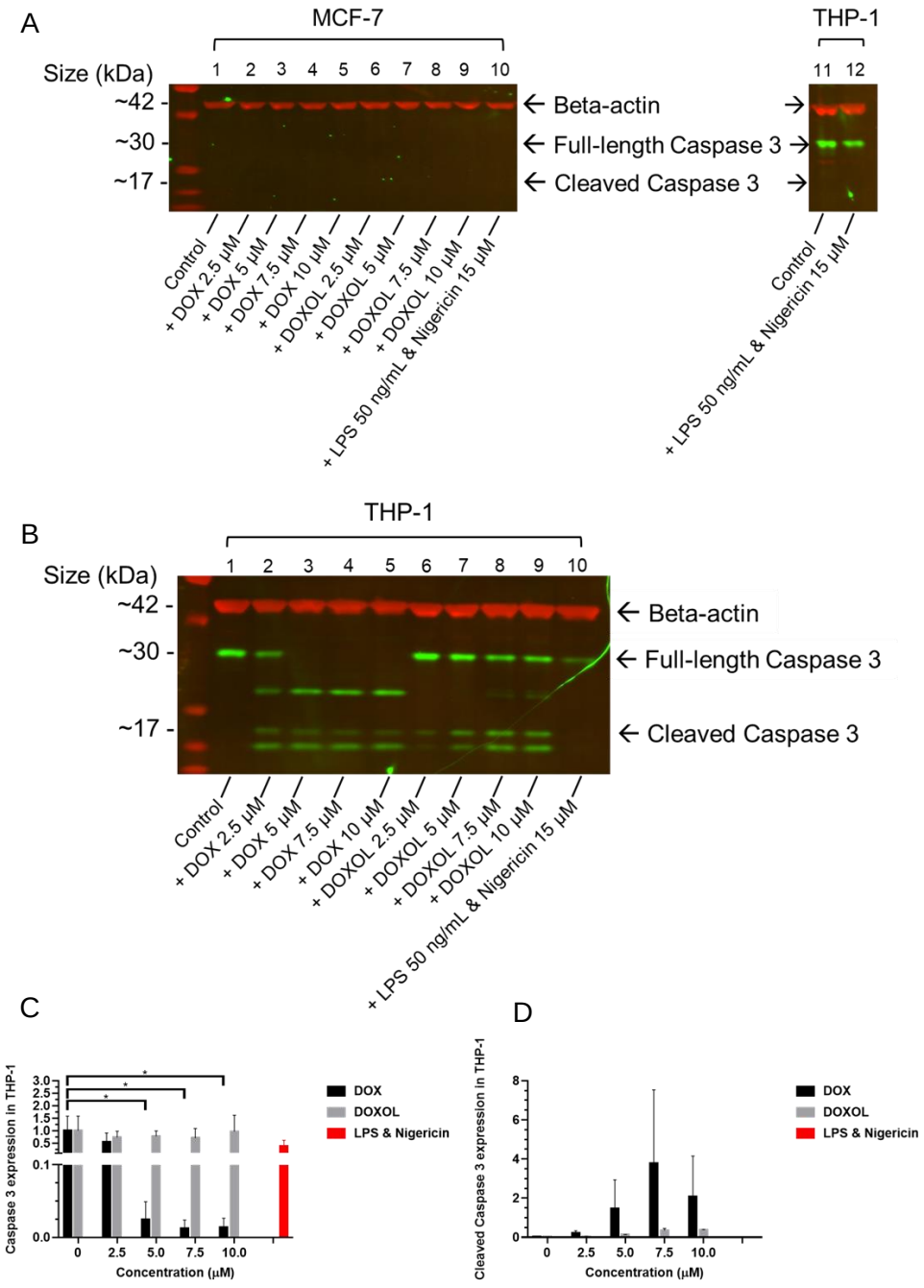

Figure 6.4 Western blot analysis of Caspase 3 in MCF-7 and THP-1 cell lines. **(A**,**B)** Representative immunoblots of MCF-7 (N=3) **(A)** and THP-1 (N=3) **(B)** cells that had been treated with doxorubicin (DOX) or doxorubicinol (DOXOL), probed for caspase 3 and beta-actin following treatment. Quantification of full-length and cleaved caspase 3 levels in THP-1 cell **(B)** is shown in **C-D** (N=3). The Y-axis in **(C)** showed the arbitrary unit quantification of the detected full-length caspase 3 protein band density, normalised to beta-actin, relative to the

control group. The Y-axis in **(D)** showed the arbitrary unit quantification of the detected cleaved caspase 3 protein band density, normalised to beta-actin, relative to the respective GSDMD band density. THP-1 cell treated with LPS & Nigericin was used as a negative control for apoptosis. Statistical analysis was performed using two-way ANOVA and Tukey's multiple comparison test. * p value < 0.05.

Concentration	Doxorubicin (arbitrary units)	Doxorubicinol (arbitrary units)
Control (0 μM)	1 ± 0.58	1 ± 0.58
2.5 μM	0.53 ± 0.37	0.72 ± 0.25
5 μM	0.03 ± 0.02	0.77 ± 0.22
7.5 μM	0.02 ± 0.01	0.70 ± 0.34
10 μM	0.02 ± 0.01	0.97 ± 0.65
LPS & Nigericin	0.37 ± 0.25	

Table 6.3 Quantification of full-length caspase 3 band density in THP-1 cells following treatment with doxorubicin or doxorubicinol. The values are normalised to beta-actin and relative to the control group (N=3). The values correspond to the graph in Figure 6.4C. The values are mean ± standard errors of the mean.

Concentration	Doxorubicin (arbitrary units)	Doxorubicinol (arbitrary units)
2.5 μM	0.22 ± 0.12	0.03 ± 0.02
5 μM	1.47 ± 1	0.12 ± 0.03
7.5 μM	3.77 ± 3.70	0.35 ± 0.11
10 μM	2.08 ± 2.01	0.37 ± 0.03

Table 6.4 Quantification of cleaved caspase 3 band density in THP-1 cells following treatment with doxorubicinol. The values are normalised to beta-actin, relative to the respective full-length caspase 3 band density (N=3). The values correspond to the graph in Figure 6.4D. The values are mean ± standard errors of the mean.

Figure 6.4 A-B show a representative Western blot membrane of MCF-7 (A) and THP-1 cells (B) with their respective treatments (N=3). The housekeeping protein, beta-actin (B-actin), was similar in all samples, indicating equivalent loading.

In the MCF-7 samples, the full-length caspase 3 was not detected in the untreated sample (lane 1) and all treated samples. Similarly, the cleaved caspase 3 was not detected in all samples. The full-length caspase 3 was detected in the

untreated as well as the LPS & Nigericin-treated THP-1 cell samples. As expected, cleaved caspase 3 was undetected in LPS & Nigericin-treated THP-1 cells.

In Figure 6.4B, full-length caspase 3 bands were detected in the untreated THP-1 cells (lane 1). As expected, the cleaved caspase 3 band was not detected in the control sample. In doxorubicin-treated samples, full-length caspase 3 band was only detected at 2.5 μM doxorubicin. Interestingly, cleaved caspase 3 bands were detected in all doxorubicin-treated samples.

Full-length caspase 3 bands along with cleaved caspase 3 were detected in doxorubicinol-treated THP-1 samples with increasing doxorubicinol concentration. Although full-length caspase 3 band was detected, cleaved caspase 3 was not detected in LPS & Nigericin-treated THP-1 cells.

Figures 6.4 C-D show the quantification of the full-length of caspase 3 protein expression, normalised to beta-actin, relative to the control group (C) and the expression of cleaved caspase 3 relative to full-length caspase 3 (D) in THP-1 cells. There was a statistical difference observed in the expression of full-length caspase 3 in THP-1 samples treated with increasing concentrations of doxorubicin. However, as Figure 6.4C shows a reduction in the full-length caspase 3, the expression of cleaved caspase 3 was notably increased in doxorubicin-treated groups as seen in Figure 6.4D. Doxorubicinol-treated samples also displayed a small expression of cleaved caspase 3 with increasing concentration.

Overall, the graphs suggested that the full-length caspase 3 in the doxorubicin group was detected and activated resulting in higher cleaved caspase 3 expression than in the doxorubicinol group.

6.5 Discussion

A summary of the results is as follows with further discussion of the results in the relevant subchapters.

Doxorubicin induced morphological changes in MCF-7 cells, which suggest the occurrence of apoptosis rather than pyroptosis. The fluorescent staining in doxorubicin-treated MCF-7 cells predominantly showed Annexin V binding, suggestive of early apoptotic injury. However, cleavage of caspase 3 was not detected in the Western blot experiment.

Doxorubicinol did not induce notable cellular changes in MCF-7 cells, with no fluorescent staining detected following treatment up to 10 μM.

In contrast to the effect on MCF-7 cells, doxorubicin induced morphological changes in THP-1 cells that resemble both apoptosis and pyroptosis injury. The fluorescent staining in doxorubicin-treated THP-1 cells showed co-staining of Annexin V binding and propidium iodide, suggestive of cells undergoing pyroptotic injury or mid-late apoptotic injury. The morphological alteration and fluorescent staining seen shared similar characteristics with THP-1 cells treated with LPS & Nigericin, a known inducer of pyroptosis. Both full-length GSDMD and caspase 3, were detected in THP-1 cells by Western blotting experiment following treatment with doxorubicin. Cleaved GSDMD-NT was not detected following treatment with doxorubicin, but cleaved caspase 3 was detected.

Doxorubicinol induced similar morphological changes and fluorescent co-staining on THP-1 cells as doxorubicin. Both full-length GSDMD and caspase 3 were detected in THP-1 cells by Western blot following doxorubicinol treatment. Both cleaved products, GSDMD-NT and cleaved caspase 3 were detected following treatment with doxorubicinol.

6.5.1 Doxorubicin and doxorubicinol concentration

The use of the doxorubicin and doxorubicinol concentration in this chapter has already been discussed in the previous chapter. In brief, the plasma concentration of doxorubicin up to 2.5 μM is clinically relevant, and a concentration between 5 μM to 10 μM may cover possible variations in the plasma concentration as well as clinical

profiles. As previously discussed, the same concentration was used for both doxorubicin and doxorubicinol to standardise the concentration range between the two treatment groups across different cell types.

6.5.2 MCF-7 microscope imaging, fluorescent staining, and Western blot analysis

The findings of the microscope images and fluorescent staining on treated MCF-7 suggest that the morphological changes caused by doxorubicin might be apoptotic changes.

Caspase 3 is a key executioner of apoptosis (Saraste *et al.*, 2000, Brentnall *et al.*, 2013, Movassagh *et al.*, 2008, Janicke *et al.*, 1998), and doxorubicin is known to induce apoptosis in tumour cells (Kerr *et al.*, 1994). Results from this research showed that apoptosis morphological alterations and Annexin V staining took place in the absence of caspase 3 protein when MCF-7 cells were treated with doxorubicin.

There have been some prior studies that investigated apoptotic cell death in MCF-7 cells treated with doxorubicin. For example, Ramazi *et al* conducted a flow cytometry assay to detect apoptosis using MCF-7 co-stained with Annexin V and PI after 24 h treatment with doxorubicin 2 μM and demonstrated that doxorubicin caused an increase in both apoptosis and necrosis (Ramazi *et al.*, 2023). They also showed that doxorubicin reduced viability in MCF-7 cells using an MTT assay in a dose-dependent and time-dependent manner. However, as discussed in the previous chapter, this assays mitochondrial activity as a surrogate of cell viability but not specific to apoptosis.

Ramazi *et al* also reported apoptotic morphological changes were similarly observed in my experiment. Cellular shrinkage and clusters appeared to be the predominant morphological changes observed in doxorubicin-treated cells. These changes shared some similar characteristics previously described in the literature (Häcker, 2000, Saraste *et al.*, 2000). Interestingly, plasma membrane blebbing was neither seen in MCF-7 in this study nor reported in Ramazi *et al*'s.

A possible explanation for the absence of plasma membrane blebbing was offered from an interesting study conducted by Jänicke *et al*, in which they found that MCF-7 cells were deficient in caspase 3 (Janicke *et al.*, 1998). They asserted that this deficiency was due to a 47-base pair deletion within exon 3 of the CASP-3 gene,

abrogating the translation of the CASP-3 mRNA. As a result, MCF-7 cells undergoing cell death did not exhibit some classic morphological characteristics of apoptosis such as membrane blebbing or shrinkage. This indicated that apoptosis still took place independent of caspase 3. Interestingly, the introduction of the CASP-3 gene into MCF-7 resulted in DNA fragmentation and membrane blebbing following TNF- or staurosporine-induced apoptosis.

In this research experiment, doxorubicinol did not show any notable morphological changes in MCF-7. There are limited studies that investigated the morphological changes induced by doxorubicinol on breast cancer cell lines such as MCF-7. Bains *et al* investigated cell viability using an MTT assay in a range of cell lines, including MCF-7 cell, following treatment with doxorubicin up to 150 μM or doxorubicinol up to 3000 μM for 48 h (Bains *et al.*, 2013). Bains *et al* found that doxorubicinol was less toxic than doxorubicin. Furthermore, they looked at the permeability of doxorubicin and doxorubicinol in MCF-7 cells following treatment of 1 μM over 24 h. They found that, during the first 24 h, the intracellular level of doxorubicin in doxorubicin-treated cells was significantly higher than the intracellular level of doxorubicinol in doxorubicinol-treated cells. Although doxorubicin and doxorubicinol share a relatively similar structure, the difference in the hydroxyl group on carbon-13 of doxorubicinol is likely to impede its influx.

Another study investigated the distribution of doxorubicin in MCF-7 cells (Xu *et al.*, 2014). They treated MCF-7 wild-type cells and MCF-7 drug-resistant cells with 5 μM doxorubicin over 24 h and assessed the distribution of doxorubicin and its conversion to doxorubicinol in the subcellular organelles. They found that, in MCF-7 wild type, doxorubicin was predominantly distributed in the nucleus and mitochondria. In drug-resistant MCF-7 cells, doxorubicin was predominantly in the cytoplasm. The conversion of doxorubicin to doxorubicinol was found to be higher in drug-resistant MCF-7 cells. Xu *et al* explained that this higher conversion is likely to be due to the presence of enzymes in the cytosol that are believed to be responsible for doxorubicin intracellular metabolism, such as aldo-keto reductase and carbonyl-reductase.

The Western blot results in this research did not detect caspase 3 and corroborated the findings from Jänicke *et al,* in which MCF-7 cells may be deficient in caspase 3 despite still being able to undergo apoptosis.

Furthermore, Pilco-Ferreto *et al* evaluated apoptosis through the expression of caspase 8, caspase 9, and caspase 3 gene and protein expression in three breast cancer cell lines; MCF-10F, MCF-7, and MDA-MB-231 (Pilco-Ferreto *et al.*, 2016). They treated these cell lines with 1 μM doxorubicin (MCF-10F and MDA-MB-231 cell lines) or 4 μM doxorubicin (MCF-7) for 48 h. Treatment caused a decrease in caspase 8 gene expression was downregulated in MCF-7 and MDA-MB-231 and its protein expression was upregulated in MCF-10F and MDA-MB-231 cell lines. However, caspase 8 was not detected in MCF-7. It has been proposed that caspase 8 accelerates apoptosis, presumably by the recruitment of other caspases such as caspase 9 and caspase 3 in B-lymphoid cells and breast cancer cells (Liu *et al.*, 2011). Similarly, Pilco-Ferreto *et al* found that the expression of caspase 9 was downregulated in MCF-7 when treated with doxorubicin but other studies suggested the caspase 9 expression was increased. For example, the expression of caspase 7 and 9 was increased in MCF-7 treated with an anti-neoplastic agent, neocarzinostatin, resulting in apoptosis in the absence of caspase 3 (Liang *et al.*, 2001).

In the context of caspase 3, Pilco-Ferreto *et al* found doxorubicin decreased gene expression in MCF-7 and MDA-MB-231 cell lines with the expression of caspase 3 protein in MCF-7 being detectable. On the contrary, a study conducted by Chen *et al* found that doxorubicin-resistant MCF-7 showed full-length caspase 3 and cleaved caspase 3 expression when treated with calcium ionophore and protein kinase C inhibitor staurosporine (Chen *et al.*, 2004). Chen *et al* explained that the activation of procaspase 3 was the first step observed in staurosporine-induced apoptosis in doxorubicin-resistant MCF-7 cells. Chen *et al* discussed that staurosporine-induced apoptosis followed a classic mitochondria-dependent pathway, as demonstrated by the loss of the mitochondrial membrane potential, cytochrome c release, and the cleavage of caspase 9.

Results in this research showed that apoptosis morphological alterations and Annexin V staining took place despite the absence of caspase 3 protein when MCF-7 cells were treated with doxorubicin. Different anti-caspase 3 antibodies may affect result, but, more importantly, a different source of MCF-7 cells also appears to influence result *(Osborne et al., 1987)*. Osborne *et al* investigated the MCF-7 cells sourced from the American Type Culture Collection (ATCC) and four MCF-7 sublines from different research laboratories. They found that there was a different growth rate,

oestrogen and progesterone receptor concentration among MCF-7 cell lines. Although these differences could be partly explained by different culture conditions, further karyotype analysis revealed that the MCF-7 cell line from ATCC was inherently different that other tested MCF-7 cell lines. Osborne *et al* demonstrated that the MCF-7 cell line from ATCC is derived from a different individual than the original source from the Michigan Cancer Foundation, hence the name MCF. Thus, the difference between the results in this research and other prior studies could be explained due to the origin of these cells.

6.5.3 THP-1 microscope imaging, fluorescent staining, and Western blot analysis

The findings of the microscope images and fluorescent staining on treated THP-1 cells suggest that the morphological changes might be pyroptotic changes with cellular and nuclear swelling following treatment with doxorubicin or doxorubicinol.

The changes induced by doxorubicin or doxorubicinol shared similarities to the morphological alterations induced by LPS and Nigericin, known inducers of pyroptosis. These morphological alterations were similar to what was described by Yu *et al* in their review article on pyroptosis (Yu *et al.*, 2021). Yu *et al* described pyroptotic process caused cellular swelling with pore formation, osmotic lysis, and loss of membrane integrity. Unlike apoptosis, the nucleus remains intact but can be swollen in pyroptosis. Co-staining of Annexin V and propidium iodide (PI) can be observed in pyroptotic cells.

Interestingly, apoptotic changes were also observed among doxorubicin-treated and doxorubicinol-treated cells with some cells displaying Annexin V-green fluorescence in the absence of PI-staining. It is possible that some cells are not triggered to undergo pyroptosis. However, the alternative stipulation is both pyroptosis and apoptosis occur concomitantly following treatment with doxorubicin or doxorubicinol, which will be discussed further below.

Western blot analysis was conducted to assess whether Gasdermin D (GSDMD) or caspase 3 processing took place in treated THP-1 cells. This analysis aims to further evaluate whether pyroptosis or apoptosis took place in the context of GSDMD or caspase 3 detections along with their respective cleaved or activated proteins. My Western blot was able to detect full-length GSDMD, full-length caspase 3 and cleaved caspase 3 with doxorubicin treatment. Full-length GSDMD, full-length

caspase 3 with their cleaved products were detected with doxorubicinol treatment. My findings suggested that both apoptosis and pyroptosis may be present in THP-1 cells with doxorubicin or doxorubicinol treatment.

Many studies in the literature have investigated apoptosis using THP-1 cells. For instance, apoptosis was investigated on THP-1 cells using a sub-lethal dose of doxorubicin 62.5 nM over 48 h (Bulut *et al.*, 2022). As part of their experiments, they found that, using Annexin V and flow cytometry, a sub-lethal dose of doxorubicin caused 30% of THP-1 cells to enter early apoptosis. Apoptosis was also observed when THP-1 cell was treated with other agents, such as artesunate which is used clinically as an antimalarial medicine but has been investigated to exert antineoplastic effects (Tan *et al.*, 2017). The result from observation in this research showed that doxorubicin and doxorubicinol treatment induced apoptotic morphology.

There have also been many studies of pyroptosis in haematological malignancies such as acute myeloid leukaemia. For instance, Zhou *et al* showed expression of GSDMD and cleaved GSDMD in THP-1 cells treated with 2 μM doxorubicin over 24 h (Zhou *et al.*, 2022a). They also found that genetically manipulated THP-1 cells lacking GSDMD, when treated with doxorubicin, did not display the pyroptotic morphology that was seen in wild-type cells. Their findings suggested that GSDMD was a key effector of pyroptosis in THP-1 cells treated with a chemotherapeutic agent. In the Western blot model of this research, the full-length GSDMD band was detected in 2.5 μM doxorubicin as well as in all doxorubicinol doses. GSDMD-NT bands were detected with the doxorubicinol group. Although the cleaved GSDMD-NT was not detected after doxorubicin treatment, this research study showed that the active metabolite of doxorubicin increased the expression of GSDMD and its cleaved GSDMD-NT.

Many studies investigated apoptosis or pyroptosis separately as described above. Findings from this doctoral research suggested that, specifically in THP-1 cells, both apoptosis and pyroptosis were observed occurring together.

There have been recent studies that found similar observations in THP-1 cells. Tabaazuing *et al* found that, in THP-1 cells deficient of GSDMD, treatment with 10 μg/mL LPS for 48 h followed by 20 μM Nigericin for 30 min resulted in apoptotic morphological changes and cleavage of PARP (Poly-ADP Ribose Polymerase), which

is mediated by activated caspase 3 (Taabazuing *et al.*, 2017). As expected, LPS and Nigericin treatment in wild-type THP-1 cell resulted in pyroptosis, as shown in the detection of full-length GSDMD and cleaved GSDMD in their immunoblot. In addition to pyroptotic changes, Tabaazuing *et al* also observed some apoptotic changes in wild-type THP-1 cells treated with LPS and Nigericin. Although doxorubicin was not used in their study, some findings of the experiment in this research suggested a similar observation of mixed apoptotic and pyroptotic changes. Future studies using the GSDMD knock-out variant with doxorubicin or doxorubicinol may wish to evaluate this further.

This research study further underlines the complexity in anthracycline-induced cytotoxicity. Anthracycline can induce different programmed cell death responses in cancer and non-cancer cells. Naturally, the cells need multitude of programme cell death signals to overcome pathogens or toxic substances in order to signal our immune system about potential dangers. The findings in the Western blot data of THP-1 cells in this research study were fascinating. Pyroptotic pathway was shown to be activated by doxorubicinol treatment in THP-1 acute myeloid leukaemia cells. This findings were different to the Western blot data in H9c2, HCAEC and HCMEC cells, where apoptotic pathway appeared to be the predominant programmed cell death pathway triggered by doxorubicin or doxorubicinol treatment. The potential clinical implication from these observations is a possibility to introduce a pyroptotic agonist drug in acute monocytic leukaemia patients without causing anthracycline-induced, apoptotic-driven cardiocytotoxicity.

6.6 Limitations

There are several limitations to be considered that may affect the result of this research experiment. The first limitation is related to the cell source. As mentioned previously, a frozen stock of MCF-7 cell line that was available at my laboratory was used in this experiment. It was not clearly documented how old or the passage number of this stock was. As far as this research study was concerned, the MCF-7 cell line used in this study was of a wild type and sourced from ATCC. However, while the MCF-7 has been the most investigated breast cancer cell line, different variants might be present resulting in mixed results across different laboratories (Osborne *et al.*, 1987,

Lee *et al.*, 2015). Similar consideration should be taken with the wild-type THP-1 cell line, which was provided by the Eastman Dental Institute.

Second, additional experiment methods could be used in the future to strengthen the findings of this research study. For instance, performing an assay of cell death such as the LDH cytotoxicity assay could complement the experiments carried out in this research. Sequencing the DNA or mRNA of inflammasome or apoptosome genes in the cell would validate whether there is a mutation in the cell that may affect their innate ability to subsequently express the respective proteins. In addition, flow cytometry could be to evaluate the proportion of cells undergoing early apoptosis and late apoptosis injury. This would be useful to provide quantitative data for the fluorescent staining experiments. Furthermore, the detection of other components of inflammasome or apoptosome, such as caspase 1, caspase 7, or ASC can further detect the cascade of inflammasome or apoptosome.

6.7 Conclusion

Tables 6.1 and 6.2 summarise the experiments in the human cancer cell lines, MCF-7 and THP-1, respectively. This chapter examined whether pyroptosis contributes to the anthracycline-induced cytotoxicity on MCF-7 and THP-1 treated with doxorubicin or doxorubicinol.

Findings from data analysis suggested that when treated with doxorubicin, MCF-7 human breast cancer cells underwent apoptosis with the fluorescent staining, suggesting early apoptosis in the absence of caspase 3 and its cleaved end product. On the contrary, doxorubicinol did not exert significant morphological changes to MCF-7 cells. Furthermore, the data suggested that THP-1 human monocytic acute myeloid leukaemia cells underwent both apoptotic and pyroptotic cellular alterations when treated with doxorubicin or doxorubicinol. This was further accompanied by the detection of full-length caspase 3 and GSDMD with its cleaved end products in doxorubicin and doxorubicinol, respectively.

The take-home message from this chapter is doxorubicin induced apoptotic changes in the absence of caspase 3 in MCF-7 cells. In addition, doxorubicin exerted predominantly apoptotic cell death in THP-1 cells, whereas doxorubicinol predominantly exerted pyroptotic cell death in THP-1 cells.

Assays	MCF-7 cell line	
	Doxorubicin	Doxorubicinol
Morphological changes	Apoptotic	Normal
Fluorescent staining	Annexin V green positive indicating early apoptosis	No fluorescent staining was detected
Western blot	Full-length GSDMD and caspase 3 were not detected GSDMD-NT and cleaved caspase 3 bands were not detected	Full-length GSDMD and caspase 3 were not detected GSDMD-NT and cleaved caspase 3 bands were not detected

Table 6.5 Table summary of MCF-7 experiments with doxorubicin and doxorubicinol.

Assays	THP-1 cell line	
	Doxorubicin	Doxorubicinol
Morphological changes	Predominantly apoptotic	Predominantly pyroptotic (cellular swelling with pore formation, osmotic lysis, and loss of membrane integrity)
Fluorescent staining	Annexin V green positive indicating apoptosis At higher concentrations, a mixture with propidium iodide positive stain, indicating permeability due to damaged plasma membrane in late apoptosis/necrosis/pyroptosis	Annexin V green positive indicating apoptosis At higher concentrations, a mixture with propidium iodide positive stain, indicating permeability due to damaged plasma membrane in late apoptosis/necrosis/pyroptosis
Western blot	Significant reduction in the detection of the full-length GSDMD with increasing concentration GSDMD-NT was not detected Significant reduction in the detection of the full-length caspase 3 with increasing concentration Increased detection of cleaved caspase 3 with increasing concentration	Significant increase in the detection of the full-length GSDMD with increasing concentration GSDMD-NT was detected with increasing concentration Reduction in the detection of the full-length caspase 3 with increasing concentration Cleaved caspase 3 band was detected with increasing concentration but was relatively smaller compared to those detected in the doxorubicin group

Table 6.6 Table summary of THP-1 experiments with doxorubicin and doxorubicinol.

Chapter 7 Conclusion

7.1 Research overview

This research studied whether pyroptosis plays a role in anthracycline-induced cytotoxicity. The research working hypothesis was that pyroptosis plays a role in anthracycline-induced cytotoxicity. *In vitro* experiments were conducted on five different cells with the immortalised rat ventricular cardiomyocyte H9c2 cell line, human coronary artery endothelial cell (HCAEC), human cardiac microvascular endothelial cell (HCMEC), human breast cancer cell (MCF-7), and human monocytic acute leukaemia cell (THP-1).

Following treatment with a range of doxorubicin or doxorubicinol concentrations over 18 h, the cell death response was evaluated with the LDH cytotoxicity assay. Cellular morphological alterations were assessed using microscope images, and fluorescent staining technique with Annexin V and propidium iodide. Furthermore, the detection of full-length GSDMD and caspase 3 with their cleaved end-products was evaluated as the hallmark of pyroptosis and apoptosis, respectively.

7.2 Summary of results

Tables 7.1 and 7.2 summarise the results in Chapters 4-6. Findings from the data analysis suggested that, when treated with doxorubicin or doxorubicinol, H9c2 rat ventricular cardiomyocytes underwent cell death by apoptosis in a dose-dependent manner. Doxorubicin exerted greater cytotoxicity to treated H9c2 cells resulting in late apoptosis or secondary necrosis, while doxorubicinol caused early apoptosis.

Similarly, doxorubicin and doxorubicinol were found to be likely to have induced cell death by apoptosis to a different extent in HCAEC or HCMEC cells, with HCAEC cells appearing to be more sensitive to anthracycline-induced cytotoxicity than HCMEC cells.

In MCF-7 cells, doxorubicin induced changes that were suggestive of apoptosis, even though caspase 3 cleavage was not detected.

Finally, doxorubicin caused predominantly apoptotic cell death in THP-1 cells, while doxorubicinol predominantly exerted pyroptotic cell death in THP-1 cells.

In conclusion, this doctoral study suggests that pyroptosis is not likely to play a major role in anthracycline-induced cytotoxicity. However, anthracycline-induced cytotoxicity is likely to cause an apoptotic injury.

Assays	Doxorubicin				
	H9c2	HCAEC	HCMEC	MCF-7	THP-1
LDH cytotoxicity assay	Significant cytotoxicity was detected at 10 μM after 18 h (12.3% ± 1.5%)	Significant cytotoxicity was detected at 2.5 μM after 18 h (29.9% ± 4%)	Significant cytotoxicity was detected at 2.5 μM after 18 h (20.9% ± 1.6%)	Not available	Not available
Morphological changes	Apoptotic	Apoptotic	Apoptotic	Apoptotic	Apoptotic
Fluorescent staining					
Annexin V fluorescence	No	Yes	Yes	Yes	Yes
Propidium Iodide fluorescence	Yes	Yes	No	No	Yes
Western blot					
Was full-length GSDMD detected?	Yes	Yes	No	No	Yes
Was cleaved GSDMD-NT detected?	No	No	No	No	No
Was full-length caspase 3 detected?	Yes	Yes	Yes	No	Yes
Was cleaved caspase 3 detected?	No	No	No	No	Yes

Table 7.1 Summary of doxorubicin treatment on rat cardiomyoblast H9c2, human vascular endothelial cells (HCAEC, HCMEC) and human cancer cell lines (MCF-7, THP-1).

Assays	Doxorubicinol				
	H9c2	HCAEC	HCMEC	MCF-7	THP-1
LDH cytotoxicity assay	Significant cytotoxicity was detected at 30 μM after 18 h (18.3% ± 2.6%)	Significant cytotoxicity was detected at 7.5 μM after 18 h (20.2% ± 5.6%)	No significant cytotoxicity was detected	Not available	Not available
Morphological changes	Apoptotic	Apoptotic	Apoptotic	Normal	Pyroptotic
Fluorescent staining					
Annexin V fluorescence	Yes	Yes	Yes	No	Yes
Propidium Iodide fluorescence	No	No	No	No	Yes
Western blot					
Was full-length GSDMD detected?	Yes	Yes	Yes	No	Yes
Was cleaved GSDMD-NT detected?	No	No	No	No	Yes
Was full-length caspase 3 detected?	Yes	Yes	Yes	No	Yes
Was cleaved caspase 3 detected?	No	No	No	No	Yes

Table 7.2 Summary of doxorubicinol treatment on rat cardiomyoblast H9c2, human vascular endothelial cells (HCAEC, HCMEC) and human cancer cell lines (MCF-7, THP-1).

7.3 Research contribution

Research in the field of anthracycline-induced cytotoxicity is growing with the advent of new findings. However, many unanswered questions are yet to be addressed. This doctoral research has hopefully contributed to fill in a lacuna in the field, developing our body of knowledge further. The research contribution of this thesis can be seen in three aspects.

First, this thesis studied and compared the cytotoxicity between doxorubicin and doxorubicinol, the supposedly active metabolite of doxorubicin, in five different cell types. There are only a few published studies, as far as this study is concerned, investigated the cytotoxicity between doxorubicin and doxorubicinol (Bains *et al.*, 2013, Reis-Mendes *et al.*, 2019, Zeng *et al.*, 2019).

Second, this thesis studied and compared apoptosis and pyroptosis within the same experiment model. As previously discussed, there have been studies which hypothesised whether apoptosis or pyroptosis drives anthracycline-induced cardiotoxicity (Kalyanaraman *et al.*, 2002, Michihiko *et al.*, 2006, Meng *et al.*, 2019). However, these studies tend to investigate apoptosis and pyroptosis separately. This PhD research study assessed both apoptosis and pyroptosis together over the same experiment design, offering insight into the predominant cell death pathway in anthracycline-induced cytotoxicity.

Third, the findings in the Western blot data of THP-1 cells in this research study were fascinating. Pyroptotic pathway was shown to be activated by doxorubicinol treatment in THP-1 acute myeloid leukaemia cells. This findings were different to the Western blot data in H9c2, HCAEC and HCMEC cells, where apoptotic pathway appeared to be the predominant programmed cell death pathway triggered by doxorubicin or doxorubicinol treatment. The potential clinical implication from these observations is a possibility to introduce a pyroptotic agonist drug in acute monocytic leukaemia patients without causing anthracycline-induced, apoptotic-driven cardiocytotoxicity.

7.4 Research limitations

It is important to underline that chemotherapy-induced cardiovascular injury is complex in its nature. The cocktail of chemotherapy used in clinical practice in addition

to the administration of radiotherapy reflects the multifaceted issues of cancer-therapy induced cardiovascular injury. Each common chemotherapy agent and radiotherapy pose a risk of cardiovascular injury. It is beyond the scope of this research to explore this. Thus, this research only focused on one chemotherapy agent.

Several considerations should be taken into account that may pose limitations in this research study. Limitations specifically related to the research methods have been discussed in respective chapters.

First, the whole of experiments in this research were conducted *in vitro*. Despite the efforts to conduct *in vitro* experiments as robust as possible, the results may not be transferrable to *in vivo* experiments. However, these *in vitro* results provide a good platform and further avenues to conduct *in vivo* experiments such as those attempting to reduce cardiomyocyte damage while preserving the cytotoxic effect on the cancer cells.

Second, the choice of cells in this study may have inherently affected the results and contributed to the variability seen in the literature. This particular limitation has been discussed thoroughly in each chapter. For instance, the difficulty in obtaining and culturing primary human cardiac myocytes means not all the cell sources in this study are of human origin. Using immortalised rat ventricular cardiomyocytes has certain advantages. One of which is that they have been widely used in anthracycline studies, which permits comparison to published results in the literature. However, immortalised rat ventricular cardiomyocytes may inherently be different to primary cardiomyocytes. In the limitations discussed in Section 4.6, an alternative approach using human pluripotent stem cell-derived cardiomyocytes (hPSC-CMs) treated with doxorubicin was explored (Maillet *et al.*, 2016). This innovative technique holds promise as a new avenue for studying anthracycline-induced cardiotoxicity through its use of more physiologically relevant human cardiac cells, potentially offering advantages over traditional models. Moreover, information on the specific human donor is invaluable for studies of human endothelial cells and cancer cell lines. However, these details can be difficult to trace, and as such may affect the results.

Third, the experiments in this study were carefully designed to assess acute or subacute anthracycline-induced cytotoxicity within a limited timeframe of my PhD. This study may not be suitable for assessing the chronic impact of anthracycline-induced

cytotoxicity. Similar *in vitro* studies usually administer doxorubicin based on our understanding of physiological plasma concentration in humans over 24 h. However, what has been overlooked by *in vitro* studies is the dose of doxorubicin is administered based on an individual's weight, and this may lead to variability in the plasma concentration. Conducting *in vivo* experiments with anthracycline may help elucidate this further as the dose of doxorubicin is usually tailored per animal's weight over a longer time duration. For instance, Gallan-Ariola *et al* administered five cycles of intracoronary injection of 0.45 mg/kg doxorubicin onto their pig model over eight-week periods and further total monitoring of sixteen weeks in their study to assess microcirculation damage induced by doxorubicin (Galan-Arriola *et al.*, 2021). Another example to illustrate this further in a rodent model is by Michihiko *et al* who administered 3 mg/kg doxorubicin through the tail vein weekly for five weeks before the rodents were sacrificed and the hearts were evaluated to assess for apoptosis pathway (Michihiko *et al.*, 2006).

7.5 Future studies

Following the findings obtained in this study, some recommendations for potential future research are outlined, but not limited to, as follows.

First, the use of human pluripotent stem cell-derived cardiomyocyte (hPSC-CM) may shed light on more physiologically relevant human cardiac cells and offer a comparative insight when considered with the result from the H9c2 cell line. In addition, using multiple cell stocks of different origins could improve the robustness of the data collected. Alternatively, repeating the experiment using isolated cardiac myocytes *ex vivo* may provide valuable information through comparison with these research findings. In addition, conducting genomic sequencing of relevant genes would be interesting to validate whether there is a mutation that affects their ability to express the respective proteins.

Second, additional research methods could be employed to further enhance the findings from this research. For instance, flow cytometry can help differentiate different stages of apoptosis objectively. Confocal microscopy may help assess the intracellular distribution of doxorubicin or doxorubicinol within the cell. By visualising their respective subcellular localisation, this technique could shed light on potential pharmacokinetic barriers that may contribute to doxorubicinol's reduced cytotoxicity.

Additionally, confocal microscopy might reveal differences in the affinity of each compound for specific cellular organelles, potentially elucidating distinct mechanisms of action and contributing to their varying cytotoxicity. Although the Western blot experiments carried out in this research did not detect cleaved caspase 3 despite the apoptotic morphological changes, it may be worthwhile to investigate whether other components of the apoptosis cascade are activated, such as caspase 7 or caspase 8.

Third, the findings from THP-1 cells experiment in this research illustrated the interesting possibility that anthracycline-induced cytotoxicity may potentially involve an overlap between apoptosis and pyroptosis. Findings in this research were unable to support that pyroptosis played a sole role in anthracycline-induced cytotoxicity. However, this research only looked at GSDMD-mediated pyroptosis. Some studies have suggested that Gasdermin E may play a role in both apoptosis and pyroptosis in a cell-specific manner depending on the level of expression (Wang *et al.*, 2017, Kovacs *et al.*, 2017). Thus, it may be valuable to assess Gasdermin E-mediated apoptosis or pyroptosis in future studies.

Fourth, the experiment in this research did not look at the off-target effect of anthracycline cytotoxicity. It would be interesting, for instance, to look at the impact of introducing a medium from doxorubicin or doxorubicinol-treated cancer cells into normal heart cells and assess whether the presence of cancer cell lysate induces accelerated cell death.

Fifth, conducting *in vivo* experiments to assess anthracycline-cytotoxicity on animal models such as rodents may provide valuable information and comparison with the *in vitro* data. *In vivo* experiments may also provide valuable information on the impact of chronic anthracycline cytotoxicity.

References

AHLMANN, M. & HEMPEL, G. 2016. The effect of cyclophosphamide on the immune system: implications for clinical cancer therapy. *Cancer chemotherapy and pharmacology,* 78**,** 661-671.

ARAI, M., YOGUCHI, A., TAKIZAWA, T.*, et al.* 2000. Mechanism of doxorubicin-induced inhibition of sarcoplasmic reticulum Ca2+-ATPase gene transcription. *Circulation research,* 86**,** 8-14.

ARCAMONE, F., CASSINELLI, G., FANTINI, G.*, et al.* 1969. Adriamycin, 14-hydroxydaimomycin, a new antitumor antibiotic from S. Peucetius var. caesius. *Biotechnology and bioengineering,* 11**,** 1101-1110.

ASNANI, A., MOSLEHI, J. J., ADHIKARI, B. B.*, et al.* 2021. Preclinical Models of Cancer Therapy-Associated Cardiovascular Toxicity: A Scientific Statement From the American Heart Association. *Circ Res,* 129**,** e21-e34.

AUNER, H., TINCHON, C., LINKESCH, W.*, et al.* 2003. Prolonged monitoring of troponin T for the detection of anthracycline cardiotoxicity in adults with hematological malignancies. *Annals of hematology,* 82**,** 218-222.

BACHETTI, T. & MORBIDELLI, L. 2000. Endothelial cells in culture: a model for studying vascular functions. *Pharmacological research,* 42**,** 9-19.

BACHOUR, N. R. 2002. Anthracyclines. *In:* BERTINO, J. R. (ed.) *Encyclopedia of Cancer.* 2nd edition ed.: Academic Press.

BAINS, O. S., SZEITZ, A., LUBIENIECKA, J. M.*, et al.* 2013. A correlation between cytotoxicity and reductase-mediated metabolism in cell lines treated with doxorubicin and daunorubicin. *Journal of Pharmacology and Experimental Therapeutics,* 347**,** 375-387.

BARISH, R., LYNCE, F., UNGER, K.*, et al.* 2019. Management of cardiovascular disease in women with breast cancer. *Circulation,* 139**,** 1110-1120.

BARTON, J. C. & BERTOLI, L. F. 2000. Transfusion iron overload in adults with acute leukemia: manifestations and therapy. *The American journal of the medical sciences,* 319**,** 73-78.

BORDERS, B., ROCHE, B., ROSS, J.*, et al.* 2013. Protein biomarkers of drug-induced cardiotoxicity in the isolated heart: Building a multi-scale approach. *Journal of Pharmacological and Toxicological Methods,* 1**,** e29.

BØTKER, H. E., HAUSENLOY, D., ANDREADOU, I.*, et al.* 2018. Practical guidelines for rigor and reproducibility in preclinical and clinical studies on cardioprotection. *Basic research in cardiology,* 113**,** 1-73.

BOUTAGY, N. E., FEHER, A., PFAU, D.*, et al.* 2020. Dual angiotensin receptor-neprilysin inhibition with sacubitril/valsartan attenuates systolic dysfunction in experimental doxorubicin-induced cardiotoxicity. *Cardio Oncology,* 2**,** 774-787.

BRENTNALL, M., RODRIGUEZ-MENOCAL, L., DE GUEVARA, R. L.*, et al.* 2013. Caspase-9, caspase-3 and caspase-7 have distinct roles during intrinsic apoptosis. *BMC cell biology,* 14**,** 1-9.

BULUT, I., LEE, A., CEVATEMRE, B.*, et al.* 2022. Dual LSD1 and HDAC6 inhibition induces doxorubicin sensitivity in acute myeloid leukemia cells. *Cancers,* 14**,** 6014.

BURGENER, S. S. & SCHRODER, K. 2020. Neutrophil extracellular traps in host defense. *Cold Spring Harbor perspectives in biology,* 12**,** a037028.

BURNETTE, W. 1981. Western blotting: electrophoretic transfer of proteins from SDS-polyacrylamide gels to unmodified nitrocellulose and radiographic detection with antibody and radioiodinated protein A. *Anal. Biochem,* 112**,** 195-203.

CAI, W., TENG, T., WANG, X.*, et al.* 2023. The protective effect of thiolutin on doxorubicin-induced H9c2 cardiomyocyte injury. *The Journal of Toxicological Sciences,* 48**,** 469-479.

CAI, Y., CHAI, Y., FU, Y.*, et al.* 2022. Salidroside ameliorates Alzheimer's disease by targeting NLRP3 inflammasome-mediated pyroptosis. *Frontiers in Aging Neuroscience,* 13**,** 809433.
CAPPETTA, D., ROSSI, F., PIEGARI, E.*, et al.* 2018. Doxorubicin targets multiple players: a new view of an old problem. *Pharmacological research,* 127**,** 4-14.
CARDINALE, D., BIASILLO, G. & CIPOLLA, C. M. 2016. Curing cancer, saving the heart: a challenge that cardioncology should not miss. *Current cardiology reports,* 18**,** 1-10.
CARDINALE, D., COLOMBO, A., BACCHIANI, G.*, et al.* 2015. Early detection of anthracycline cardiotoxicity and improvement with heart failure therapy. *Circulation,* 131**,** 1981-1988.
CARDINALE, D., IACOPO, F. & CIPOLLA, C. M. 2020. Cardiotoxicity of anthracyclines. *Frontiers in cardiovascular medicine,* 7**,** 26.
CARDINALE, D., SANDRI, M. T., COLOMBO, A.*, et al.* 2004. Prognostic value of troponin I in cardiac risk stratification of cancer patients undergoing high-dose chemotherapy. *Circulation,* 109**,** 2749-2754.
CERRETTI, D. P., KOZLOSKY, C. J., MOSLEY, B.*, et al.* 1992. Molecular cloning of the interleukin-1β converting enzyme. *Science,* 256**,** 97-100.
CHAMPOUX, J. J. 2001. DNA topoisomerases: structure, function, and mechanism. *Annual review of biochemistry,* 70**,** 369-413.
CHATTERJEE, K., ZHANG, J., HONBO, N.*, et al.* 2010. Doxorubicin cardiomyopathy. *Cardiology,* 115**,** 155-162.
CHAUDHARI, U., NEMADE, H., GASPAR, J. A.*, et al.* 2016. MicroRNAs as early toxicity signatures of doxorubicin in human-induced pluripotent stem cell-derived cardiomyocytes. *Archives of toxicology,* 90**,** 3087-3098.
CHEN, J. S., KONOPLEVA, M., ANDREEFF, M.*, et al.* 2004. Drug-resistant breast carcinoma (MCF-7) cells are paradoxically sensitive to apoptosis. *Journal of cellular physiology,* 200**,** 223-234.
CHEN, S., CAO, Z., PRETTNER, K.*, et al.* 2023. Estimates and Projections of the Global Economic Cost of 29 Cancers in 204 Countries and Territories From 2020 to 2050. *JAMA Oncology*.
CHEN, X., HE, W.-T., HU, L.*, et al.* 2016. Pyroptosis is driven by non-selective gasdermin-D pore and its morphology is different from MLKL channel-mediated necroptosis. *Cell research,* 26**,** 1007-1020.
CHEN, X., LIU, G., YUAN, Y.*, et al.* 2019. NEK7 interacts with NLRP3 to modulate the pyroptosis in inflammatory bowel disease via NF-κB signaling. *Cell death & disease,* 10**,** 906.
CHEN, Y., HUANG, T., SHI, W.*, et al.* 2020. Potential targets for intervention against doxorubicin-induced cardiotoxicity based on genetic studies: a systematic review of the literature. *Journal of Molecular and Cellular Cardiology,* 138**,** 88-98.
CHIUSA, M., HOOL, S.-L., TRUETSCH, P.*, et al.* 2012. Cancer therapy modulates VEGF signaling and viability in adult rat cardiac microvascular endothelial cells and cardiomyocytes. *Journal of molecular and cellular cardiology,* 52**,** 1164-1175.
CHRISTIDI, E. & BRUNHAM, L. R. 2021. Regulated cell death pathways in doxorubicin-induced cardiotoxicity. *Cell Death & Disease,* 12**,** 1-15.
CHU, T. F., RUPNICK, M. A., KERKELA, R.*, et al.* 2007. Cardiotoxicity associated with tyrosine kinase inhibitor sunitinib. *The Lancet,* 370**,** 2011-2019.
CHUNG, R., MAULIK, A., HAMARNEH, A.*, et al.* 2016. Effect of Remote Ischaemic Conditioning in Oncology Patients Undergoing Chemotherapy: Rationale and Design of the ERIC-ONC Study—A Single-Center, Blinded, Randomized Controlled Trial. *Clinical Cardiology,* 39**,** 72-82.
COOKSON, B. T. & BRENNAN, M. A. 2001. Pro-inflammatory programmed cell death. *Trends in microbiology,* 9**,** 113-114.
CREA, F., CAMICI, P. G. & BAIREY MERZ, C. N. 2014. Coronary microvascular dysfunction: an update. *European heart journal,* 35**,** 1101-1111.

CROWLEY, L. C., MARFELL, B. J., SCOTT, A. P.*, et al.* 2016. Quantitation of apoptosis and necrosis by annexin V binding, propidium iodide uptake, and flow cytometry. *Cold Spring Harb Protoc,* 2016**,** 953-957.
DALLONS, M., SCHEPKENS, C., DUPUIS, A.*, et al.* 2020. New Insights About Doxorubicin-Induced Toxicity to Cardiomyoblast-Derived H9C2 Cells and Dexrazoxane Cytoprotective Effect: Contribution of In Vitro (1)H-NMR Metabonomics. *Front Pharmacol,* 11**,** 79.
DEMCHENKO, A. P. 2013. Beyond annexin V: fluorescence response of cellular membranes to apoptosis. *Cytotechnology,* 65**,** 157-172.
DHALLA, N. S., TEMSAH, R. M. & NETTICADAN, T. 2000. Role of oxidative stress in cardiovascular diseases. *Journal of hypertension,* 18**,** 655-673.
DI MARCO, A. 1969. Adriamycin (NSC-123,127): a new antibiotic with antitumor activity. *Cancer Chemother Rep,* 53**,** 33-37.
DI MARCO, A., GAETANI, M., OREZZI, P.*, et al.* 1964. 'Daunomycin', a new antibiotic of the rhodomycin group. *Nature,* 201**,** 706-707.
DING, J., WANG, K., LIU, W.*, et al.* 2016. Pore-forming activity and structural autoinhibition of the gasdermin family. *Nature,* 535**,** 111-116.
DO CARMO, H., ARJUN, S., PETRUCCI, O.*, et al.* 2018. The caspase 1 inhibitor VX-765 protects the isolated rat heart via the RISK pathway. *Cardiovascular drugs and therapy,* 32**,** 165-168.
DOS SANTOS, D. S. & DOS SANTOS GOLDENBERG, R. C. 2018. Doxorubicin-induced cardiotoxicity: from mechanisms to development of efficient therapy. *Cardiotoxicity***,** 3-24.
DRUKER, B. J. & LYDON, N. B. 2000. Lessons learned from the development of an abl tyrosine kinase inhibitor for chronic myelogenous leukemia. *The Journal of clinical investigation,* 105**,** 3-7.
DRUMMOND, G. R., CAI, H., DAVIS, M. E.*, et al.* 2000. Transcriptional and posttranscriptional regulation of endothelial nitric oxide synthase expression by hydrogen peroxide. *Circulation research,* 86**,** 347-354.
DUBOST, M., GANTER, P., MARAL, R.*, et al.* 1963. UN NOUVEL ANTIBIOTIQUE'A PROPRI'ET'ES CYTOSTATIQUES: LA RUBIDOMYCINE. *CR Hebd Seances Acad Sci,* 257**,** 1813-1815.
EISENHAUER, E. A. & VERMORKEN, J. B. 1998. The taxoids: comparative clinical pharmacology and therapeutic potential. *Drugs,* 55**,** 5-30.
ELMORE, S. 2007. Apoptosis: a review of programmed cell death. *Toxicologic pathology,* 35**,** 495-516.
EWER, M. S., VON HOFF, D. D. & BENJAMIN, R. S. 2011. A historical perspective of anthracycline cardiotoxicity. *Heart failure clinics,* 7**,** 363-372.
FELKER, G. M., THOMPSON, R. E., HARE, J. M.*, et al.* 2000. Underlying causes and long-term survival in patients with initially unexplained cardiomyopathy. *New England Journal of Medicine,* 342**,** 1077-1084.
FRIEDLANDER, A. M. 1986. Macrophages are sensitive to anthrax lethal toxin through an acid-dependent process. *Journal of Biological Chemistry,* 261**,** 7123-7126.
FROST, B. M., EKSBORG, S., BJÖRK, O.*, et al.* 2002. Pharmacokinetics of doxorubicin in children with acute lymphoblastic leukemia: Multi-institutional collaborative study. *Medical and Pediatric Oncology: The Official Journal of SIOP—International Society of Pediatric Oncology (Societé Internationale d'Oncologie Pédiatrique,* 38**,** 329-337.
GALAN-ARRIOLA, C., VILCHEZ-TSCHISCHKE, J. P., LOBO, M.*, et al.* 2021. Coronary microcirculation damage in anthracycline cardiotoxicity. *Cardiovasc Res*.
GALÁN-ARRIOLA, C., VILLENA-GUTIÉRREZ, R., HIGUERO-VERDEJO, M. I.*, et al.* 2020. Remote ischaemic preconditioning ameliorates anthracycline-induced cardiotoxicity and preserves mitochondrial integrity. *Cardiovascular Research,* 117**,** 1132-1143.
GAO, H., CAO, M., YAO, Y.*, et al.* 2021. Dysregulated microbiota-driven gasdermin D activation promotes colitis development by mediating IL-18 release. *Frontiers in Immunology,* 12**,** 750841.

GAO, Y.-L., ZHAI, J.-H. & CHAI, Y.-F. 2018. Recent advances in the molecular mechanisms underlying pyroptosis in sepsis. *Mediators of inflammation,* 2018.
GHARANEI, M., HUSSAIN, A., JANNEH, O.*, et al.* 2013. Doxorubicin induced myocardial injury is exacerbated following ischaemic stress via opening of the mitochondrial permeability transition pore. *Toxicology and applied pharmacology,* 268**,** 149-156.
GILLERON, M., MARECHAL, X., MONTAIGNE, D.*, et al.* 2009. NADPH oxidases participate to doxorubicin-induced cardiac myocyte apoptosis. *Biochemical and biophysical research communications,* 388**,** 727-731.
GONG, A., MI, L., WEI, F.*, et al.* 2023. Downregulation of miR-137 Facilitates CD4+ T Cell Pyroptosis in Systemic Lupus Erythematosus via Stimulating AMPK Pathway. *Journal of Immunology Research,* 2023.
GREEN, D. R. & REED, J. C. 1998. Mitochondria and apoptosis. *science,* 281**,** 1309-1312.
GREENE, R. F., COLLINS, J. M., JENKINS, J. F.*, et al.* 1983. Plasma pharmacokinetics of adriamycin and adriamycinol: implications for the design of in vitro experiments and treatment protocols. *Cancer research,* 43**,** 3417-3421.
HÄCKER, G. 2000. The morphology of apoptosis. *Cell and tissue research,* 301**,** 5-17.
HADER, S. N., ZINKEVICH, N., NORWOOD TORO, L. E.*, et al.* 2019. Detrimental effects of chemotherapy on human coronary microvascular function. *Am J Physiol Heart Circ Physiol,* 317**,** H705-H710.
HAUSENLOY, D. J., MADDOCK, H. L., BAXTER, G. F.*, et al.* 2002. Inhibiting mitochondrial permeability transition pore opening: a new paradigm for myocardial preconditioning? *Cardiovascular research,* 55**,** 534-543.
HE, X., YANG, W., ZENG, Z.*, et al.* 2020. NLRP3-dependent pyroptosis is required for HIV-1 gp120-induced neuropathology. *Cellular & molecular immunology,* 17**,** 283-299.
HESCHELER, J., MEYER, R., PLANT, S.*, et al.* 1991. Morphological, biochemical, and electrophysiological characterization of a clonal cell (H9c2) line from rat heart. *Circulation research,* 69**,** 1476-1486.
HOFMARCHER, T., LINDGREN, P., WILKING, N.*, et al.* 2020. The cost of cancer in Europe 2018. *Eur J Cancer,* 129**,** 41-49.
HOLLER, N., ZARU, R., MICHEAU, O.*, et al.* 2000. Fas triggers an alternative, caspase-8–independent cell death pathway using the kinase RIP as effector molecule. *Nature immunology,* 1**,** 489-495.
HU, X., ZENG, Q., XIAO, J.*, et al.* 2022. Herpes simplex virus 1 induces microglia gasdermin D-dependent pyroptosis through activating the NLR family pyrin domain containing 3 inflammasome. *Frontiers in Microbiology,* 13**,** 838808.
HU, Y.-H., LIU, J., LU, J.*, et al.* 2020. sFRP1 protects H9c2 cardiac myoblasts from doxorubicin-induced apoptosis by inhibiting the Wnt/PCP-JNK pathway. *Acta Pharmacologica Sinica,* 41**,** 1150-1157.
ICHIKAWA, Y., GHANEFAR, M., BAYEVA, M.*, et al.* 2014. Cardiotoxicity of doxorubicin is mediated through mitochondrial iron accumulation. *The Journal of clinical investigation,* 124**,** 617-630.
IVANETICH, K. M. & SANTI, D. V. 1988. Thymidylate synthase and fluorouracil. *The Expanding Role of Folates and Fluoropyrimidines in Cancer Chemotherapy***,** 113-125.
JANG, Y. M., KENDAIAH, S., DREW, B.*, et al.* 2004. Doxorubicin treatment in vivo activates caspase-12 mediated cardiac apoptosis in both male and female rats. *FEBS letters,* 577**,** 483-490.
JANICKE, R. U., SPRENGART, M. L., WATI, M. R.*, et al.* 1998. Caspase-3 is required for DNA fragmentation and morphological changes associated with apoptosis. *Journal of Biological Chemistry,* 273**,** 9357-9360.
JIA, C., ZHANG, J., CHEN, H.*, et al.* 2019. Endothelial cell pyroptosis plays an important role in Kawasaki disease via HMGB1/RAGE/cathespin B signaling pathway and NLRP3 inflammasome activation. *Cell death & disease,* 10**,** 778.
KALIVENDI, S. V., KONOREV, E. A., CUNNINGHAM, S.*, et al.* 2005. Doxorubicin activates nuclear factor of activated T-lymphocytes and Fas ligand transcription: role of

mitochondrial reactive oxygen species and calcium. *Biochemical Journal,* 389**,** 527-539.
KALIVENDI, S. V., KOTAMRAJU, S., ZHAO, H.*, et al.* 2001. Doxorubicin-induced apoptosis is associated with increased transcription of endothelial nitric-oxide synthase: effect of antiapoptotic antioxidants and calcium. *Journal of Biological Chemistry,* 276**,** 47266-47276.
KALYANARAMAN, B., JOSEPH, J., KALIVENDI, S.*, et al.* 2002. Doxorubicin-induced apoptosis: implications in cardiotoxicity. *Molecular and cellular biochemistry,* 234**,** 119-124.
KASIBHATLA, S., BRUNNER, T., GENESTIER, L.*, et al.* 1998. DNA damaging agents induce expression of Fas ligand and subsequent apoptosis in T lymphocytes via the activation of NF-κB and AP-1. *Molecular cell,* 1**,** 543-551.
KAUSHAL, V., KAUSHAL, G. & MEHTA, P. 2004a. Differential toxicity of anthracyclines on cultured endothelial cells. Taylor & Francis.
KAUSHAL, V., KAUSHAL, G., MELKAVERI, S.*, et al.* 2004b. Thalidomide protects endothelial cells from doxorubicin-induced apoptosis but alters cell morphology. *Journal of Thrombosis and Haemostasis,* 2**,** 327-334.
KAYAGAKI, N., STOWE, I. B., LEE, B. L.*, et al.* 2015. Caspase-11 cleaves gasdermin D for non-canonical inflammasome signalling. *Nature,* 526**,** 666-671.
KERR, J. F., WINTERFORD, C. M. & HARMON, B. V. 1994. Apoptosis. Its significance in cancer and cancer therapy. *Cancer,* 73**,** 2013-2026.
KEUNG, E., TOLL, L., ELLIS, M.*, et al.* 1991. L-type cardiac calcium channels in doxorubicin cardiomyopathy in rats morphological, biochemical, and functional correlations. *The Journal of clinical investigation,* 87**,** 2108-2113.
KIMES, B. & BRANDT, B. 1976. Properties of a clonal muscle cell line from rat heart. *Experimental cell research,* 98**,** 367-381.
KISCHKEL, F. C., HELLBARDT, S., BEHRMANN, I.*, et al.* 1995. Cytotoxicity-dependent APO-1 (Fas/CD95)-associated proteins form a death-inducing signaling complex (DISC) with the receptor. *The EMBO journal,* 14**,** 5579-5588.
KOTAMRAJU, S., KONOREV, E. A., JOSEPH, J.*, et al.* 2000. Doxorubicin-induced apoptosis in endothelial cells and cardiomyocytes is ameliorated by nitrone spin traps and ebselen: role of reactive oxygen and nitrogen species. *Journal of Biological Chemistry,* 275**,** 33585-33592.
KOVACS, S. B. & MIAO, E. A. 2017. Gasdermins: effectors of pyroptosis. *Trends in cell biology,* 27**,** 673-684.
KROEMER, G., DALLAPORTA, B. & RESCHE-RIGON, M. 1998. The mitochondrial death/life regulator in apoptosis and necrosis. *Annual review of physiology,* 60**,** 619-642.
KUNO, A., HOSODA, R., TSUKAMOTO, M.*, et al.* 2022. SIRT1 in the cardiomyocyte counteracts doxorubicin-induced cardiotoxicity via regulating histone H2AX. *Cardiovascular Research*.
KUZNETSOV, A. V., JAVADOV, S., SICKINGER, S.*, et al.* 2015. H9c2 and HL-1 cells demonstrate distinct features of energy metabolism, mitochondrial function and sensitivity to hypoxia-reoxygenation. *Biochimica et Biophysica Acta (BBA)-Molecular Cell Research,* 1853**,** 276-284.
LEE, A. V., OESTERREICH, S. & DAVIDSON, N. E. 2015. MCF-7 cells—changing the course of breast cancer research and care for 45 years. *Journal of the National Cancer Institute,* 107**,** djv073.
LEE, B. L., STOWE, I. B., GUPTA, A.*, et al.* 2018. Caspase-11 auto-proteolysis is crucial for noncanonical inflammasome activation. *Journal of Experimental Medicine,* 215**,** 2279-2288.
LI, H., ZHU, H., XU, C.-J.*, et al.* 1998. Cleavage of BID by caspase 8 mediates the mitochondrial damage in the Fas pathway of apoptosis. *Cell,* 94**,** 491-501.
LIANG, Y., YAN, C. & SCHOR, N. F. 2001. Apoptosis in the absence of caspase 3. *Oncogene,* 20**,** 6570-6578.

LIM, C. C., ZUPPINGER, C., GUO, X., *et al.* 2004. Anthracyclines induce calpain-dependent titin proteolysis and necrosis in cardiomyocytes. *Journal of Biological Chemistry,* 279**,** 8290-8299.
LIU, D., ZENG, X., LI, X., *et al.* 2018. Role of NLRP3 inflammasome in the pathogenesis of cardiovascular diseases. *Basic research in cardiology,* 113**,** 1-14.
LIU, J., MAO, W., DING, B., *et al.* 2008. ERKs/p53 signal transduction pathway is involved in doxorubicin-induced apoptosis in H9c2 cells and cardiomyocytes. *American Journal of Physiology-Heart and Circulatory Physiology,* 295**,** H1956-H1965.
LIU, W.-H. & CHANG, L.-S. 2011. Fas/FasL-dependent and-independent activation of caspase-8 in doxorubicin-treated human breast cancer MCF-7 cells: ADAM10 down-regulation activates Fas/FasL signaling pathway. *The international journal of biochemistry & cell biology,* 43**,** 1708-1719.
LUCHNER, A., STEVENS, T. L., BORGESON, D. D., *et al.* 1998. Differential atrial and ventricular expression of myocardial BNP during evolution of heart failure. *American Journal of Physiology-Heart and Circulatory Physiology,* 274**,** H1684-H1689.
LUO, X., BUDIHARDJO, I., ZOU, H., *et al.* 1998. Bid, a Bcl2 interacting protein, mediates cytochrome c release from mitochondria in response to activation of cell surface death receptors. *Cell,* 94**,** 481-490.
LUU, A. Z., CHOWDHURY, B., AL-OMRAN, M., *et al.* 2018. Role of endothelium in doxorubicin-induced cardiomyopathy. *JACC: Basic to Translational Science,* 3**,** 861-870.
LYON, A. R., DENT, S., STANWAY, S., *et al.* 2020. Baseline cardiovascular risk assessment in cancer patients scheduled to receive cardiotoxic cancer therapies: a position statement and new risk assessment tools from the C ardio-O ncology S tudy G roup of the H eart F ailure A ssociation of the E uropean S ociety of C ardiology in collaboration with the I nternational C ardio-O ncology S ociety. *European journal of heart failure,* 22**,** 1945-1960.
MA, W., WEI, S., ZHANG, B., *et al.* 2020. Molecular mechanisms of cardiomyocyte death in drug-induced cardiotoxicity. *Frontiers in Cell and Developmental Biology,* 8**,** 434.
MACEDO, A. V., HAJJAR, L. A., LYON, A. R., *et al.* 2019. Efficacy of dexrazoxane in preventing anthracycline cardiotoxicity in breast cancer. *Cardio Oncology,* 1**,** 68-79.
MAILLET, A., TAN, K., CHAI, X., *et al.* 2016. Modeling doxorubicin-induced cardiotoxicity in human pluripotent stem cell derived-cardiomyocytes. *Scientific reports,* 6**,** 25333.
MAULIK, A., DAVIDSON, S. M., PIOTROWSKA, I., *et al.* 2018. Ischaemic preconditioning protects cardiomyocytes from anthracycline-induced toxicity via the PI3K pathway. *Cardiovascular drugs and therapy,* 32**,** 245-253.
MCGOWAN, J. V., CHUNG, R., MAULIK, A., *et al.* 2017. Anthracycline Chemotherapy and Cardiotoxicity. *Cardiovasc Drugs Ther,* 31**,** 63-75.
MCILWAIN, D. R., BERGER, T. & MAK, T. W. 2013. Caspase functions in cell death and disease. *Cold Spring Harbor perspectives in biology,* 5**,** a008656.
MEDINA-LEYTE, D. J., DOMÍNGUEZ-PÉREZ, M., MERCADO, I., *et al.* 2020. Use of human umbilical vein endothelial cells (HUVEC) as a model to study cardiovascular disease: A review. *Applied Sciences,* 10**,** 938.
MENG, L., LIN, H., ZHANG, J., *et al.* 2019. Doxorubicin induces cardiomyocyte pyroptosis via the TINCR-mediated posttranscriptional stabilization of NLR family pyrin domain containing 3. *Journal of molecular and cellular cardiology,* 136**,** 15-26.
MERTENS, A. C., LIU, Q., NEGLIA, J. P., *et al.* 2008. Cause-specific late mortality among 5-year survivors of childhood cancer: the Childhood Cancer Survivor Study. *Journal of the National Cancer Institute,* 100**,** 1368-1379.
METHANEETHORN, J., TENGCHAROEN, K., LEELAKANOK, N., *et al.* 2023. Population pharmacokinetics of doxorubicin: A systematic review. *Asia-Pacific Journal of Clinical Oncology,* 19**,** 9-26.
MICHIHIKO, U., YOSHIHIKO, K., KOH-ICHI, Y., *et al.* 2006. Doxorubicin induces apoptosis by activation of caspase-3 in cultured cardiomyocytes in vitro and rat cardiac ventricles in vivo. *Journal of pharmacological sciences,* 101**,** 151-158.

MINOTTI, G., MENNA, P., SALVATORELLI, E.*, et al.* 2004. Anthracyclines: molecular advances and pharmacologic developments in antitumor activity and cardiotoxicity. *Pharmacological reviews,* 56**,** 185-229.
MINOTTI, G., RECALCATI, S., MORDENTE, A.*, et al.* 1998. The secondary alcohol metabolite of doxorubicin irreversibly inactivates aconitase/iron regulatory protein-1 in cytosolic fractions from human myocardium. *The FASEB journal,* 12**,** 541-552.
MIRANDA, C. J., MAKUI, H., SOARES, R. J.*, et al.* 2003. Hfe deficiency increases susceptibility to cardiotoxicity and exacerbates changes in iron metabolism induced by doxorubicin. *Blood,* 102**,** 2574-2580.
MONTAIGNE, D., MARECHAL, X., BACCOUCH, R.*, et al.* 2010. Stabilization of mitochondrial membrane potential prevents doxorubicin-induced cardiotoxicity in isolated rat heart. *Toxicology and applied pharmacology,* 244**,** 300-307.
MORDENTE, A., MEUCCI, E., SILVESTRINI, A.*, et al.* 2009. New developments in anthracycline-induced cardiotoxicity. *Current medicinal chemistry,* 16**,** 1656-1672.
MOVASSAGH, M. & FOO, R. S.-Y. 2008. Simplified apoptotic cascades. *Heart failure reviews,* 13**,** 111-119.
MYERS, C. The role of iron in doxorubicin-induced cardiomyopathy. Seminars in oncology, 1998. 10-14.
NATIONAL CANCER REGISTRATION & ANALYSIS SERVICE AND CANCER RESEARCH UK. 2017. *"Chemotherapy, Radiotherapy and Tumour Resections in England: 2013-2014" workbook* [Online]. Available: http://www.ncin.org.uk/cancer_type_and_topic_specific_work/topic_specific_work/main_cancer_treatments [Accessed December 2021].
NICOLETTO, R. E. & OFNER III, C. M. 2022. Cytotoxic mechanisms of doxorubicin at clinically relevant concentrations in breast cancer cells. *Cancer Chemotherapy and Pharmacology,* 89**,** 285-311.
NOUSIAINEN, T., VANNINEN, E., JANTUNEN, E.*, et al.* 2002. Natriuretic peptides during the development of doxorubicin-induced left ventricular diastolic dysfunction. *Journal of internal medicine,* 251**,** 228-234.
OCTAVIA, Y., TOCCHETTI, C. G., GABRIELSON, K. L.*, et al.* 2012. Doxorubicin-induced cardiomyopathy: from molecular mechanisms to therapeutic strategies. *Journal of molecular and cellular cardiology,* 52**,** 1213-1225.
OLSON, R. D., MUSHLIN, P. S., BRENNER, D. E.*, et al.* 1988. Doxorubicin cardiotoxicity may be cause by its metabolite, doxorubicinol. *Proc Natl Acad Sci U S A,* 85**,** 3585-89.
OSBORNE, C. K., HOBBS, K. & TRENT, J. M. 1987. Biological differences among MCF-7 human breast cancer cell lines from different laboratories. *Breast cancer research and treatment,* 9**,** 111-121.
PALLE, J., FROST, B.-M., PETERSON, C.*, et al.* 2006. Doxorubicin pharmacokinetics is correlated to the effect of induction therapy in children with acute myeloid leukemia. *Anti-cancer drugs,* 17**,** 385-392.
PANJRATH, G. S., PATEL, V., VALDIVIEZO, C. I.*, et al.* 2007. Potentiation of doxorubicin cardiotoxicity by iron loading in a rodent model. *Journal of the American College of Cardiology,* 49**,** 2457-2464.
PATERSON, D. I., WIEBE, N., CHEUNG, W. Y.*, et al.* 2022. Incident cardiovascular disease among adults with cancer: a population-based cohort study. *Cardio Oncology,* 4**,** 85-94.
PIANTADOSI, C. A., CARRAWAY, M. S., BABIKER, A.*, et al.* 2008. Heme oxygenase-1 regulates cardiac mitochondrial biogenesis via Nrf2-mediated transcriptional control of nuclear respiratory factor-1. *Circulation research,* 103**,** 1232-1240.
PILCO-FERRETO, N. & CALAF, G. M. 2016. Influence of doxorubicin on apoptosis and oxidative stress in breast cancer cell lines. *International journal of oncology,* 49**,** 753-762.
POP, C., TIMMER, J., SPERANDIO, S.*, et al.* 2006. The apoptosome activates caspase-9 by dimerization. *Molecular cell,* 22**,** 269-275.

RAMAZI, S., SALIMIAN, M., ALLAHVERDI, A.*, et al.* 2023. Synergistic cytotoxic effects of an extremely low-frequency electromagnetic field with doxorubicin on MCF-7 cell line. *Scientific Reports,* 13**,** 8844.
RAUF, A., SHAH, M., YELLON, D. M.*, et al.* 2019. Role of Caspase 1 in Ischaemia/Reperfusion injury of the myocardium. *J Cardiovasc Pharmacol,* 74**,** 194-200.
RAWAT, P. S., JAISWAL, A., KHURANA, A.*, et al.* 2021. Doxorubicin-induced cardiotoxicity: An update on the molecular mechanism and novel therapeutic strategies for effective management. *Biomedicine & Pharmacotherapy,* 139**,** 111708.
REEVE, J. L., SZEGEZDI, E., LOGUE, S. E.*, et al.* 2007. Distinct mechanisms of cardiomyocyte apoptosis induced by doxorubicin and hypoxia converge on mitochondria and are inhibited by Bcl-xL. *Journal of cellular and molecular medicine,* 11**,** 509-520.
REIS-MENDES, A., CARVALHO, F., REMIÃO, F.*, et al.* 2019. The main metabolites of fluorouracil+ adriamycin+ cyclophosphamide (FAC) are not major contributors to FAC toxicity in H9c2 cardiac differentiated cells. *Biomolecules,* 9**,** 98.
REN, C., CHEN, J., CHE, Q.*, et al.* 2023. IL-37 alleviates TNF-α-induced pyroptosis of rheumatoid arthritis fibroblast-like synoviocytes by inhibiting the NF-κB/GSDMD signaling pathway. *Immunobiology,* 228**,** 152382.
RENART, J., REISER, J. & STARK, G. R. 1979. Transfer of proteins from gels to diazobenzyloxymethyl-paper and detection with antisera: a method for studying antibody specificity and antigen structure. *Proceedings of the National Academy of Sciences,* 76**,** 3116-3120.
RIDKER, P. M., THUREN, T., ZALEWSKI, A.*, et al.* 2011. Interleukin-1β inhibition and the prevention of recurrent cardiovascular events: rationale and design of the Canakinumab Anti-inflammatory Thrombosis Outcomes Study (CANTOS). *American heart journal,* 162**,** 597-605.
RISS, T., NILES, A., MORAVEC, R.*, et al.* 2019. Cytotoxicity assays: in vitro methods to measure dead cells. *Assay Guidance Manual [Internet]*.
ROTH, G. A., MENSAH, G. A., JOHNSON, C. O.*, et al.* 2020. Global Burden of Cardiovascular Diseases and Risk Factors, 1990–2019: Update from the GBD 2019 Study. *J. Am. Coll. Cardiol.,* 76**,** 2982-3021.
ROWINSKY, E. K., MCGUIRE, W., GUARNIERI, T.*, et al.* 1991. Cardiac disturbances during the administration of taxol. *Journal of Clinical Oncology,* 9**,** 1704-1712.
SAEKI, K., OBI, I., OGIKU, N.*, et al.* 2002. Doxorubicin directly binds to the cardiac-type ryanodine receptor. *Life sciences,* 70**,** 2377-2389.
SALVATORELLI, E., MENNA, P., CASCEGNA, S.*, et al.* 2006. Paclitaxel and docetaxel stimulation of doxorubicinol formation in the human heart: implications for cardiotoxicity of doxorubicin-taxane chemotherapies. *J Pharmacol Exp Ther,* 318**,** 424-33.
SANDHU, H. & MADDOCK, H. 2014. Molecular basis of cancer-therapy-induced cardiotoxicity: introducing microRNA biomarkers for early assessment of subclinical myocardial injury. *Clinical science,* 126**,** 377-400.
SANDRI, M. T., SALVATICI, M., CARDINALE, D.*, et al.* 2005. N-terminal pro-B-type natriuretic peptide after high-dose chemotherapy: a marker predictive of cardiac dysfunction? *Clinical Chemistry,* 51**,** 1405-1410.
SANTIN, A. D., BELLONE, S., ROMAN, J. J.*, et al.* 2008. Trastuzumab treatment in patients with advanced or recurrent endometrial carcinoma overexpressing HER2/neu. *International Journal of Gynecology & Obstetrics,* 102**,** 128-131.
SARASTE, A. & PULKKI, K. 2000. Morphologic and biochemical hallmarks of apoptosis. *Cardiovascular research,* 45**,** 528-537.
SARDÃO, V. A., OLIVEIRA, P. J., HOLY, J.*, et al.* 2009. Morphological alterations induced by doxorubicin on H9c2 myoblasts: nuclear, mitochondrial, and cytoskeletal targets. *Cell biology and toxicology,* 25**,** 227-243.

SBORGI, L., RÜHL, S., MULVIHILL, E.*, et al.* 2016. GSDMD membrane pore formation constitutes the mechanism of pyroptotic cell death. *The EMBO journal,* 35**,** 1766-1778.
SCHIFF, P. B., FANT, J. & HORWITZ, S. B. 1979. Promotion of microtubule assembly in vitro by taxol. *Nature,* 277**,** 665-667.
SHEPARD, H. M., LEWIS, G. D., SARUP, J. C.*, et al.* 1991. Monoclonal antibody therapy of human cancer: taking the HER2 protooncogene to the clinic. *Journal of clinical immunology,* 11**,** 117-127.
SHI, J., ZHAO, Y., WANG, Y.*, et al.* 2014. Inflammatory caspases are innate immune receptors for intracellular LPS. *Nature,* 514**,** 187-192.
SHI, Y. 2004. Caspase activation: revisiting the induced proximity model. *Cell,* 117**,** 855-858.
SHIGA, T. & HIRAIDE, M. 2020. Cardiotoxicities of 5-fluorouracil and other fluoropyrimidines. *Current treatment options in oncology,* 21**,** 27.
SIEGEL, R. M., KA-MING CHAN, F., CHUN, H. J.*, et al.* 2000. The multifaceted role of Fas signaling in immune cell homeostasis and autoimmunity. *Nature immunology,* 1**,** 469-474.
SMALL, H. Y., MONTEZANO, A. C., RIOS, F. J.*, et al.* 2014. Hypertension due to antiangiogenic cancer therapy with vascular endothelial growth factor inhibitors: understanding and managing a new syndrome. *Canadian Journal of Cardiology,* 30**,** 534-543.
SOLEM, L. E., HENRY, T. R. & WALLACE, K. B. 1994. Disruption of mitochondrial calcium homeostasis following chronic doxorubicin administration. *Toxicology and applied pharmacology,* 129**,** 214-222.
SOULE, H. D., VAZQUEZ, J., LONG, A.*, et al.* 1973. A human cell line from a pleural effusion derived from a breast carcinoma. *Journal of the national cancer institute,* 51**,** 1409-1416.
SOULTATI, A., MOUNTZIOS, G., AVGERINOU, C.*, et al.* 2012. Endothelial vascular toxicity from chemotherapeutic agents: preclinical evidence and clinical implications. *Cancer treatment reviews,* 38**,** 473-483.
SULIMAN, H. B., CARRAWAY, M. S., ALI, A. S.*, et al.* 2007. The CO/HO system reverses inhibition of mitochondrial biogenesis and prevents murine doxorubicin cardiomyopathy. *The Journal of clinical investigation,* 117**,** 3730-3741.
SUN, Z., SCHRIEWER, J., TANG, M.*, et al.* 2016. The TGF-β pathway mediates doxorubicin effects on cardiac endothelial cells. *Journal of molecular and cellular cardiology,* 90**,** 129-138.
SUNG, H., FERLAY, J., SIEGEL, R. L.*, et al.* 2021. Global cancer statistics 2020: GLOBOCAN estimates of incidence and mortality worldwide for 36 cancers in 185 countries. *CA: a cancer journal for clinicians,* 71**,** 209-249.
SUTER, T. M., PROCTER, M., VAN VELDHUISEN, D. J.*, et al.* 2007. Trastuzumab-associated cardiac adverse effects in the herceptin adjuvant trial. *Journal of clinical oncology,* 25**,** 3859-3865.
TAABAZUING, C. Y., OKONDO, M. C. & BACHOVCHIN, D. A. 2017. Pyroptosis and apoptosis pathways engage in bidirectional crosstalk in monocytes and macrophages. *Cell chemical biology,* 24**,** 507-514. e4.
TAN, M., RONG, Y., SU, Q.*, et al.* 2017. Artesunate induces apoptosis via inhibition of STAT3 in THP-1 cells. *Leukemia research,* 62**,** 98-103.
TAN, Y., CHEN, Q., LI, X.*, et al.* 2021. Pyroptosis: a new paradigm of cell death for fighting against cancer. *J Exp Clin Cancer Res,* 40**,** 153.
TAVAKOLI DARGANI, Z. & SINGLA, D. K. 2019. Embryonic stem cell-derived exosomes inhibit doxorubicin-induced TLR4-NLRP3-mediated cell death-pyroptosis. *American Journal of Physiology-Heart and Circulatory Physiology,* 317**,** H460-H471.
TEWEY, K., ROWE, T., YANG, L.*, et al.* 1984. Adriamycin-induced DNA damage mediated by mammalian DNA topoisomerase II. *Science,* 226**,** 466-468.
THORN, C. F., OSHIRO, C., MARSH, S.*, et al.* 2011. Doxorubicin pathways: pharmacodynamics and adverse effects. *Pharmacogenetics and genomics,* 21**,** 440.

THORNBERRY, N. A., BULL, H. G., CALAYCAY, J. R.*, et al.* 1992. A novel heterodimeric cysteine protease is required for interleukin-1βprocessing in monocytes. *Nature,* 356**,** 768-774.
TOLDO, S., MEZZAROMA, E., BUCKLEY, L. F.*, et al.* 2021. Targeting the NLRP3 inflammasome in cardiovascular diseases. *Pharmacology & therapeutics***,** 108053.
TOWBIN, H., STAEHELIN, T. & GORDON, J. 1979. Electrophoretic transfer of proteins from polyacrylamide gels to nitrocellulose INFECT. IMMUN. Downloaded from sheets: procedures and some applications. *Proc. Natl. Acad. Sci. USA,* 76**,** 43504354.
TSUCHIYA, K., NAKAJIMA, S., HOSOJIMA, S.*, et al.* 2019. Caspase-1 initiates apoptosis in the absence of gasdermin D. *Nature communications,* 10**,** 2091.
TSUCHIYA, S., YAMABE, M., YAMAGUCHI, Y.*, et al.* 1980. Establishment and characterization of a human acute monocytic leukemia cell line (THP-1). *International journal of cancer,* 26**,** 171-176.
VADUGANATHAN, M., HIRJI, S. A., QAMAR, A.*, et al.* 2019. Efficacy of neurohormonal therapies in preventing cardiotoxicity in patients with cancer undergoing chemotherapy. *Cardio Oncology,* 1**,** 54-65.
VAN ENGELAND, M., NIELAND, L. J., RAMAEKERS, F. C.*, et al.* 1998. Annexin V-affinity assay: a review on an apoptosis detection system based on phosphatidylserine exposure. *Cytometry: The Journal of the International Society for Analytical Cytology,* 31**,** 1-9.
VENTURA-CLAPIER, R., GARNIER, A. & VEKSLER, V. 2004. Energy metabolism in heart failure. *The Journal of physiology,* 555**,** 1-13.
VOGELSANG, T. W., JENSEN, R. J., HESSE, B.*, et al.* 2008. BNP cannot replace gated equilibrium radionuclide ventriculography in monitoring of anthracycline-induced cardiotoxity. *International journal of cardiology,* 124**,** 193-197.
VOLKOVA, M. & RUSSELL, R. 2011. Anthracycline cardiotoxicity: prevalence, pathogenesis and treatment. *Current cardiology reviews,* 7**,** 214-220.
VON HOFF, D. D., LAYARD, M. W., BASA, P.*, et al.* 1979. Risk factors for doxorubicin-lnduced congestive heart failure. *Annals of internal medicine,* 91**,** 710-717.
VOS, T., LIM, S. S., ABBAFATI, C.*, et al.* 2020. Global burden of 369 diseases and injuries in 204 countries and territories, 1990–2019: a systematic analysis for the Global Burden of Disease Study 2019. *The Lancet,* 396**,** 1204-1222.
WANG, J. C. 2002. Cellular roles of DNA topoisomerases: a molecular perspective. *Nature reviews Molecular cell biology,* 3**,** 430-440.
WANG, S., YUAN, Y.-H., CHEN, N.-H.*, et al.* 2019. The mechanisms of NLRP3 inflammasome/pyroptosis activation and their role in Parkinson's disease. *International immunopharmacology,* 67**,** 458-464.
WANG, Y., GAO, W., SHI, X.*, et al.* 2017. Chemotherapy drugs induce pyroptosis through caspase-3 cleavage of a gasdermin. *Nature,* 547**,** 99-103.
WILHELM, S. M., CARTER, C., TANG, L.*, et al.* 2004. BAY 43-9006 exhibits broad spectrum oral antitumor activity and targets the RAF/MEK/ERK pathway and receptor tyrosine kinases involved in tumor progression and angiogenesis. *Cancer research,* 64**,** 7099-7109.
WOJCIK, T., SZCZESNY, E. & CHLOPICKI, S. 2015. Detrimental effects of chemotherapeutics and other drugs on the endothelium: A call for endothelial toxicity profiling. *Pharmacological Reports,* 67**,** 811-817.
WU, S., KO, Y.-S., TENG, M.-S.*, et al.* 2002. Adriamycin-induced cardiomyocyte and endothelial cell apoptosis: in vitro and in vivo studies. *Journal of molecular and cellular cardiology,* 34**,** 1595-1607.
XIA, X., WANG, X., ZHENG, Y.*, et al.* 2019. What role does pyroptosis play in microbial infection? *Journal of cellular physiology,* 234**,** 7885-7892.
XU, J., SHENG, Y., XU, F.*, et al.* 2014. Quantitative subcellular study of transferrin receptor-targeted doxorubicin and its metabolite in human breast cancer cells. *European journal of drug metabolism and pharmacokinetics,* 39**,** 301-310.

YANG, F., TEVES, S. S., KEMP, C. J.*, et al.* 2014. Doxorubicin, DNA torsion, and chromatin dynamics. *Biochimica et Biophysica Acta (BBA)-Reviews on Cancer,* 1845**,** 84-89.
YU, P., ZHANG, X., LIU, N.*, et al.* 2021. Pyroptosis: mechanisms and diseases. *Signal transduction and targeted therapy,* 6**,** 128.
ZAMORANO, J. L., LANCELLOTTI, P., RODRIGUEZ MUÑOZ, D.*, et al.* 2016. 2016 ESC Position Paper on cancer treatments and cardiovascular toxicity developed under the auspices of the ESC Committee for Practice Guidelines: The Task Force for cancer treatments and cardiovascular toxicity of the European Society of Cardiology (ESC). *European Heart Journal,* 37**,** 2768-2801.
ZENG, X., CAI, H., YANG, J.*, et al.* 2019. Pharmacokinetics and cardiotoxicity of doxorubicin and its secondary alcohol metabolite in rats. *Biomedicine & Pharmacotherapy,* 116**,** 108964.
ZHANG, S., LIANG, Y., YAO, J.*, et al.* 2022. Role of pyroptosis in inflammatory bowel disease (IBD): From gasdermins to DAMPs. *Frontiers in Pharmacology,* 13**,** 833588.
ZHENG, X., ZHONG, T., MA, Y.*, et al.* 2020. Bnip3 mediates doxorubicin-induced cardiomyocyte pyroptosis via caspase-3/GSDME. *Life sciences,* 242**,** 117186.
ZHOU, B., RYDER, C. B., DUBYAK, G. R.*, et al.* 2022a. Gasdermins and pannexin-1 mediate pathways of chemotherapy-induced cell lysis in hematopoietic malignancies. *Science signaling,* 15**,** eabl6781.
ZHOU, L., HAN, Y., YANG, Q.*, et al.* 2022b. Scutellarin attenuates doxorubicin-induced oxidative stress, DNA damage, mitochondrial dysfunction, apoptosis and autophagy in H9c2 cells, cardiac fibroblasts and HUVECs. *Toxicology in Vitro,* 82**,** 105366.
ZHOU, Z., HE, H., WANG, K.*, et al.* 2020. Granzyme A from cytotoxic lymphocytes cleaves GSDMB to trigger pyroptosis in target cells. *Science,* 368**,** eaaz7548.
ZYCHLINSKY, A., PREVOST, M. C. & SANSONETTI, P. J. 1992. Shigella flexneri induces apoptosis in infected macrophages. *Nature,* 358**,** 167-169.